INFORMATION TO USERS

This manuscript has been reproduced from the microfilm master. UMI films the text directly from the original or copy submitted. Thus, some thesis and dissertation copies are in typewriter face, while others may be from any type of computer printer.

The quality of this reproduction is dependent upon the quality of the copy submitted. Broken or indistinct print, colored or poor quality illustrations and photographs, print bleedthrough, substandard margins, and improper alignment can adversely affect reproduction.

In the unlikely event that the author did not send UMI a complete manuscript and there are missing pages, these will be noted. Also, if unauthorized copyright material had to be removed, a note will indicate the deletion.

Oversize materials (e.g., maps, drawings, charts) are reproduced by sectioning the original, beginning at the upper left-hand corner and continuing from left to right in equal sections with small overlaps.

Photographs included in the original manuscript have been reproduced xerographically in this copy. Higher quality 6" x 9" black and white photographic prints are available for any photographs or illustrations appearing in this copy for an additional charge. Contact UMI directly to order.

ProQuest Information and Learning
300 North Zeeb Road, Ann Arbor, MI 48106-1346 USA
800-521-0600

Biosorption of Uranium and Cadmium on *Sargassum* Seaweed Biomass

Jinbai Yang

Department of Chemical Engineering
McGill University, Montreal, Canada

A thesis submitted to the Faculty of Graduate Studies and Research
in partial fulfillment of the requirements
of the degree of Doctor of Philosophy

National Library of Canada
Acquisitions and Bibliographic Services
395 Wellington Street
Ottawa ON K1A 0N4
Canada

Bibliothèque nationale du Canada
Acquisitions et services bibliographiques
395, rue Wellington
Ottawa ON K1A 0N4
Canada

Your file Votre référence

Our file Notre référence

0-612-64698-X

Canada

ABSTRACT

Biosorption is a property of certain types of inactive, dead biomass to bind and concentrate heavy metals from even very dilute aqueous solutions. It may be used for purification of metal-containing industrial waste effluents. The issues related to the biosorption process design and optimization were addressed by 1) equilibrium isotherm relationships, 2) biosorption process rate and 3) breakthrough time in a continuous-flow biosorption column. This work investigates these three aspects for the biosorption of the heavy metals uranium and cadmium on protonated *Sargassum fluitans* seaweed biomass.

Biosorption uptakes of uranium and cadmium were evaluated by determining their isotherms at different solution pH values. It was established that the state of uranium in aqueous solution and ion exchange play an important role in the biosorption of uranium. A new equilibrium biosorption isotherm model based on ion exchange of uranium complex ion species was developed. The new model is capable of predicting the effect of proton as an exchanged species and of the metal speciation on the biosorption uptake for a equilibrium batch biosorption system.

The end-point titration method was applied in the experimental determination of the biosorption uptake rates of uranium and cadmium at different pH levels. A one-dimensional intraparticle diffusion rate model reflected well the controlling step in the uranium and cadmium ion transport inside the biosorbent. The PDEs of this new model were solved numerically by the Galerkin Finite Element Method (GFEM).

Biosorption of uranium was examined in a continuous-flow fixed-bed column at the feed pH 2.5. The biomass binding capacity for the uranium before the breakthrough was as high as 105 mg /g biomass. The elution with diluted hydrochloric acid produced an overall uranium concentration factor of about 25-30. A mass transfer model based on the external and intraparticle diffusion was developed to describe the column sorption performance. The model equations were solved by the Orthogonal Collocation (OC) numerical method. The model-calculated breakthrough curves agreed well with the experimental ones, indicating the potential of the model for process design and optimization.

Résumé

La biosorption est définie comme la propriété de certains types de biomasse morte et innactive de lier et de concentrer les métaux lourds en solution. La biosorption peut être utilisée pour décontaminer les eaux usées contenant des métaux lourds, même en faible concentration. L'optimisation et le design des procédés de biosorption est caractérisée par 1) des relations d'isothermes à l'équilibre, 2) la vitesse du procédé de biosorption et, 3) le temps de perçage pour une colonne de biosorption en écoulement continu. Ces trois aspects de la biosorption de l'uranium et du cadmium par l'algue *Sargassum fluitans* protonée sont étudiés dans ce travail.

La rétention de l'uranium et du cadmium par le biosorbant a été évaluée à partir de leurs isothermes respectifs à différents pH. Il a été découvert que la spéciation de l'uranium en solution aqueuse et que l'échange d'ions jouent un rôle important dans la biosorption de l'uranium. Un nouveau modèle d'isotherme basé sur l'adsorption par échange d'ions du complexe d'uranium a été développé. Ce nouveau modèle peut prédire l'effet des protons (en tant qu'espèces échangeables) et l'effet de la spéciation du métal en solution sur la rétention de métal par biosorption.

La titration a été appliquée pour déterminer expérimentalement la rétention de l'uranium et du cadmium à différents pH en fonction du temps. Un modèle de cinétique de diffusion intraparticulaire à une-dimension reflète bien l'étape limitante dans le transport d'ions de l'uranium et du cadmium dans le biosorbant. Les EDPs de ce nouveau modèle ont été résolues numériquement par la méthode des élements finis de Galerkin.

La biosorption de l'uranium a été étudiée dans une colonne à lit fixe en écoulement continu à un pH 2.5. La capacité de la biomasse de retenir l'uranium avant le point de percage est très élevée, soit 105 mg U/g biomasse. L'élution par de l'acide chlorydrique diluée a produit un facteur de concentration d'environ 25-30. Un modèle de transfert de masse intégrant les paramètres de diffusion intraparticulaire et de diffusion externe a été développé pour décrire les performances de la colonne de biosorption. Les équations de ce modèle ont été résolues par la méthode numérique de Collocation Orthogonale (OC). Les courbes de percage calculées par le modèle sont en accord avec

les courbes expérimentales, ce qui indique que le modèle est fiable et peut être utilisé pour l'optimisation et le design des procédés.

ACKNOWLEDGMENTS

I enjoyed the education I obtained under Prof. Volesky's supervision in the Department of Chemical Engineering at McGill University during the past few years. I would like to thank Prof. Volesky for his help in critical evaluation of the research work and in written and oral presentations of the research results are appreciated very much. In addition, my thanks to Prof. Volesky and the Department for providing me with the scholarship that made it all possible.

Then thanks to all friendly staff in the Chemical Engineering department, especially to Mr. Ed Siliauskas and Mr. Lou Cusmich for their help with laboratory analyses.

I would like to express my appreciation to my colleague Mr. Thomas Davis who proof read my thesis and corrected many grammatical and presentational errors. Thanks to Dr. Eric Fourest for his help in proof reading French Résumé. Special thanks are due to other colleagues in my research group. I appreciated the discussions of biosorption and other general chemical engineering topics with them. The help and support I received from them always moved my heart.

TABLE OF CONTENTS

LIST OF FIGURES

Chapter 1

Chapter 2

Chapter 3

Chapter 4

LIST OF TABLES

SYMBOLS & ABBREVIATIONS

[ ]	representative of concentration for the bracketed species (mmol/L)
A, AR	the first order axial and radial discretizing matrix in
$[A^-]$	concentration of anions in the solution (mM)
	Orthogonal Collocation method
a	specific surface area of particle (cm^{-1})
$a_{X/Y/Z/H}$	activity for the specified ion (mM)
B, BR	second order axial and radial discretizing matrix in Orthogonal
	Collocation method (in Section 4.3)
B	representative of free biomass binding sites (in Section 4.1)
Bo	$\frac{K_f R}{D_e}$ (dimensionless)
C, $\overline{C}$	dimensionless metal concentration inside the particle and in bulk solution
C_0	initial metal concentration in bulk solution (mmol/L)
C_b	instant metal concentration in bulk solution (mmol/L)
C_r	metal concentration in the fluid in the pore of the biosorbent (mmol/L)
$C_{des.}$	metal concentration in the eluting solution (mmol/L)
C_i, C_f	Initial or final metal concentration (mmol/L)
$\vec{C}$	solution vector at present time
$\vec{C}^{old}$	solution vector at previous time
$\vec{C}_N$	solution vector in the boundary element at present time
$\vec{C}_N^{old}$	solution vector in the boundary element at previous time
C_r	metal concentration in bulk solution at position r and time t (mg/L)
C_t	total concentration of binding sites on the biomass (mmol/g)
D	dilution ratio of the sample
D_e	effective intraparticle diffusion coefficient (cm^2/sec)

D_L, D_R	axial and radial dispersion coefficients in the column (cm^2/s)
D_m	molecular diffusion coefficient (cm^2/sec)
E	measuring tolerance in analysis (in Equation 4.1-1)
F_i	weighted residual vector in GEFM method
$f(c)$	isotherm expression relationship
$[H]$	proton concentration (mmol/L)
I	ionic strength (mM)
K	Langmuir equilibrium constant (mmol/L)
$\bar{\bar{K}}$	stiffness matrix
K_f	mass transfer coefficient across the fluid-particle interface (cm/s)
K_h	equilibrium formation constant of proton and biomass in Equation 4.1-8 (L/mol)
K_x	equilibrium formation constant of UO_2^{2+} and biomass in Equation 4.1-9 (L/mol)
K_y	equilibrium formation constant of $(UO_2)_2(OH)_2^{2+}$ and biomass in Equation 4.1-10 (L/mol)
K_z	equilibrium formation constant of $(UO_2)(OH)^+$ and biomass in Equation 4.1-11 (L/mol)
K^a_{ey}	hydrolysis equilibrium constant in Equation 4.1-4
K^a_{ez}	hydrolysis equilibrium constant in Equation 4.1-5
K_{ey}	apparent hydrolysis equilibrium constant in Equation 4.1-6
K_{ez}	apparent hydrolysis equilibrium constant in Equation 4.1-7
K_w	water equilibrium constant
k	Freundlich frequency model parameters
$\bar{\bar{M}}$	coefficient matrix
$[M]$	metal concentration (mmol/L)
n	total number of experimental points
N	number of elements (in Section 4.2.6)
p	Freundlich exponential model parameters
P	sensitivity of the analytical instrument (in Equation 4.1-1)
pK	logarithms of the hydrolysis equilibrium constant in aqueous solution

q	metal uptake biomass (mmol/g)
$q_{des.}$	eluted metal content per gram of biomass (mmol/g)
q_{exp}	experimental value of metal uptake (mmol/g)
q_H	uptake of proton on biomass (mmol/g)
q_m	Langmuir maximum uptake (mmol/g)
q_{model}	model-calculated value of metal uptake (mmol/g)
q_t	total metal uptake biomass (mmol/g)
q_U	uptake of uranium on biomass (mmol/g)
R	half thickness of the biomass particle (cm)
R_a	spatial variable in column radial direction (cm)
r	arbitrary position coordinate (cm)
S_t	total surface area of biomass particles (cm^2)
t	dimensionless time, ($t = \frac{D_e}{R^2}\theta$ in Section 4.3.6)
Δt	time difference
U_s	fluid superficial velocity (cm/s)
u	dimensionless concentration in bulk stream, ($u = \frac{C_b}{C_{in}}$ in Section 4.3.6)
u_j	approximate value of u at the j^{th} axial collocation point
V	solution volume (L)
v	dimensionless concentration in bulk stream ($v = \frac{C_r}{C_{in}}$ in Section 4.3.6)
v_{ik}	approximate value of v at the j^{th} axial collocation point and the k^{th} radial collocation point
W	weight of biosorbent (g)
X	representative of UO_2^{2+}
x	dimensionless arbitrary position coordinate (cm)
x_j	coordinate of the i^{th} axial collocation point
Y	representative of $(UO_2)_2(OH)_2^{2+}$
y_{il}	coordinate of the l^{th} radial collocation point and the i^{th} axial point
Z	representative of $(UO_2)(OH)^+$
Z_i	electrical charge of an ion in solution

α	D_e / R^2, (sec^{-1})
β	$(1-\varepsilon)\gamma$ (in Section 4.3.6)
γ	$\frac{D_e L}{U_s R^2}$ (dimensionless)
γ_1	$\rho\, q_m / C_0$, (dimensionless)
γ_2	K / C_0 , (dimensionless)
γ_i	activity coefficient for an ion in the solution
$\gamma_{HX/YZ}$	activity coefficient for the specified ion
γ_t	overall activity coefficient
γ_α	overall activity coefficient (Equation 4.1-7)
γ_α	overall activity coefficient (Equation 4.1-8)
ω	$V / (S_t R)$, (dimensionless)
ε, ε_p	bed porosity and intraparticle porosity
ϕ_i	linear base function in GFEM method
φ	objective function for curve fitting
$\lambda(v)$	function expression, $\lambda(v) = \varepsilon_p + \rho \frac{\partial f}{\partial c}(c_{in}\ v)$
ρ	density of biomass g/(1000 cm^3)
θ	corrected time, $\tau - \frac{\varepsilon z}{Us}$ (sec)
τ	time (sec)
$\tilde{\tau}$	time related to the intraparticle diffusion (sec)
μ	the volume ratio of total biomass particles and the bulk solution. V_p / V

GFEM	Galerkin Finite Element Method
HIEM	Hydrolyzed Ion Exchange Model
OC	Orthogonal Collocation
ODE	Ordinary Differential Equation
PDE	Partial Differential Equation
TSS	Total Suspension Solid

1 Introduction

1.1 Heavy metal pollution in industry

It has been recognized and confirmed in toxicological studies that heavy metals pose a severe threat to human health, animals and plants alike. The different types of heavy metal toxic effects vary. Some heavy metals tend to replace other elements in biological molecules and thus render them disfunctional, whereas others denature proteins or inhibit enzymatic catalysis. Once absorbed, heavy metals may persist in tissues for a long time. In the environment, heavy metals are accumulated by bio-magnification in the food chain, which further increases the danger to humans.

As humans uncover and use increasing amounts of heavy metals in industrial application, increasing amounts of these metals find their way into the environment. There are many sources in industry. Mining and milling industries release large amounts of heavy metals every day in the form of acid mine drainage. In Canada, 113 million cubic meters of contaminated water are produced annually from mining waste management areas (Kratochvil, 1997). Generally, metal-bearing waste water is discharged from various industrial sources at flowrates between 4 – 1200 m^3/day and contamination levels vary from parts per million to grams per liter (Gazea, et al., 1996). The processing costs for remediation of mine sites in Canada were estimated to cost CDN $ 4 billion over the next twenty years (Filion, 1990). As high-grade ores are gradually exhausted, low-grade ores will become more extensively used in the mining industry. The processing of the latter will produce more liquid waste for the same amount of metal produced. Therefore, the amount of heavy metal pollution will likely further increase.

Another main source of heavy metals is the surface finishing industry. This includes electroplating, anodizing, chromating and electrolytical plating operations. The sources for the effluents generated are mainly from rinse waters and spent plating bath liquids. An investigation of the surface finishing industry in Canada conducted in 1983

revealed that 275 companies in Canada (128 in Quebec) discharged 1,364 m^3 of waste water containing heavy metals. The average heavy metal concentration levels in those effluents varied from less than ten to hundreds of parts per million, as shown in Table 1.1. This is approximately 20 times higher than values allowed for according to Federal Guidelines (see Table 1.2; EPS, 1987). More than 85% of these waste waters enter municipal sewage processing systems while the remainder runs off directly into fresh water bodies and the ocean. The heavy metals contained within this portion of the waste water accumulates in the ocean and posses a serious environmental hazard.

Table 1.1 Composition of waste water from surface finishing industries (EPS, 1987)

Pollutant	Average concentration (mg/L)
Cu	0 - 36
Zn	0 - 40
Cd	0 – 6.2
Cr	0 - 50
Ni	0 - 12
TSS*	2 -440
pH	5.5 – 9.5

*TSS: Total Suspend Solid

Table 1.2 Federal guidelines for metal finishing liquid effluents (EPS, 1987)

Pollutant	Average concentration (mg/L)
Cu	1.0
Zn	2.0
Cd	1.5
Cr	1.0
Ni	2.0
TSS	20.0

Uranium is one of the most threatening heavy metals due to its high toxicity and radioactivity. Uranium mill tailings are a source of low-level radiation, typically in the range of 0.1 – 1.0 mR/h. Radioactive isotopes originate from nuclear industrial operations, and may be found downstream of these locations. The utilization of nuclear isotopes in fission reaction fuel rods and military weapons in addition to losses sustained from recovery protocols all contribute to increasing uranium waste (Benedict, et al., 1981). Uranium contamination also poses a threat to some surface reservoirs and groundwater aquifers (Laul, 1992; White, 1983).

Cadmium is used in a wide variety of industrial processes, such as alloy preparation, metal plating and electronic manufacturing. Cadmium is well recognized to be one of the three most toxic heavy metals threatening the environment and human health today. Cadmium has a half-life of 10 – 30 years in humans and may cause serious kidney damage and bone disease.

1.2 Treatment of heavy metal-containing waste water in industries

Treatment of heavy metal-containing industrial effluents is mainly based on precipitation, ion exchange and activated carbon adsorption. During precipitation, base is mixed with waste water that contains heavy metals. The resulting heavy metal hydroxide precipitates are typically insoluble or have very low solubility. Another alternative is the introduction of hydrogen sulfide gas (H_2S) into the waste water to convert the heavy metals into insoluble metal sulfides (Ku, 1987). The precipitated solid hydroxides or sulfides may then be separated by various solid-liquid separation techniques such as sedimentation or decantation. In some cases more expensive filtration is required, and this results in a dramatic reduction of the heavy metal concentration in the supernatant. Precipitation can be carried out in a batch or a continuous-flow scheme. It is recommended that the treated volume or flowrate is large and the concentration of pollutant(s) is/are high. Many mining effluents are currently being treated by precipitation. However, there are serious limitations to the precipitation method. One example is the formation rate of solid metal hydroxides. When the concentration of the contaminant is low, the precipitation reaction is correspondingly very slow. As a result, very large mixing and decanting tanks are required. In addition, effective dewatering of

dilute sludges is often required which increases the cost of sludge disposal. Furthermore, the final disposal of sludge (labelled as 'hazardous substances') is becoming more strictly regulated and corresponding disposal costs are increasing very rapidly. Safe methods for detoxification and/or final disposal of high-metal containing sludge are still being sought.

Activated carbon adsorption has become a standard engineering practice in waste water detoxification and treatment over the past 20 years (Tien, 1994). The process is mainly used for the removal of organic components and it may also be applied for the removal of heavy metals from aqueous solution. Ku and Peters (Ku, 1987) reported that activated carbon treatment was used as a polishing step following either metal hydroxide or metal sulfide precipitation in the removal of residual zinc and cadmium from plating waste waters. Granular activated carbon columns may also be used to remove lead and cadmium and reach low ppm levels (Periasamy and Namasivayam, 1994; Reed and Berg, 1993). An activated carbon system for mercury decontamination was implemented and reported to be effective (Rigo and Chandler, 1994).

Similar to carbon sorption, the ion exchange process is a polishing step in the remediation of waste water. Ion exchange is usually implemented in a continuous-flow continuous flow column packed with special polymer resins. This is particularly effective for processing high volumes of effluents with low metal concentrations. During the exchange process, heavy metal cations replace the cations or protons originally present on the ion exchange sites. Since the equilibrium metal uptake for most heavy metals at low pH is very low, the bound heavy metal cations may be simply eluted from the resin using a low-pH wash (Greene, et al., 1987; Guibal, et al., 1992; Treen-Sears, et al., 1984; Tsezos, 1980). The dependence of metal uptake is a function of solution pH and is illustrated in Figure 1.1.

An advantage of using ion exchange is that heavy metals may be sequestered from waste water selectively when the appropriate resin is chosen. Many ion exchange resins are commercially available for removal of various metals (Kratochvil, 1997). Such selectivity is especially useful when precious or strategically important heavy metals are to be recovered. Despite this, there are several limitations to the application of ion exchange resins. First, in some situations, the resin may become 'poisoned' by the irreversible deposition of undesirable metals. The regeneration of the resin therefore

becomes more difficult or even impossible. Second, if a significant level of organics are present in the waste water, the resins are further prone to fouling (Harland, 1994). Finally, the most serious limitation of ion exchange is the cost incurred in large scale projects. These resins are expensive; their prices ranging from $ 30 – 60 USD per kilogram of resin (on a dry weight basis).

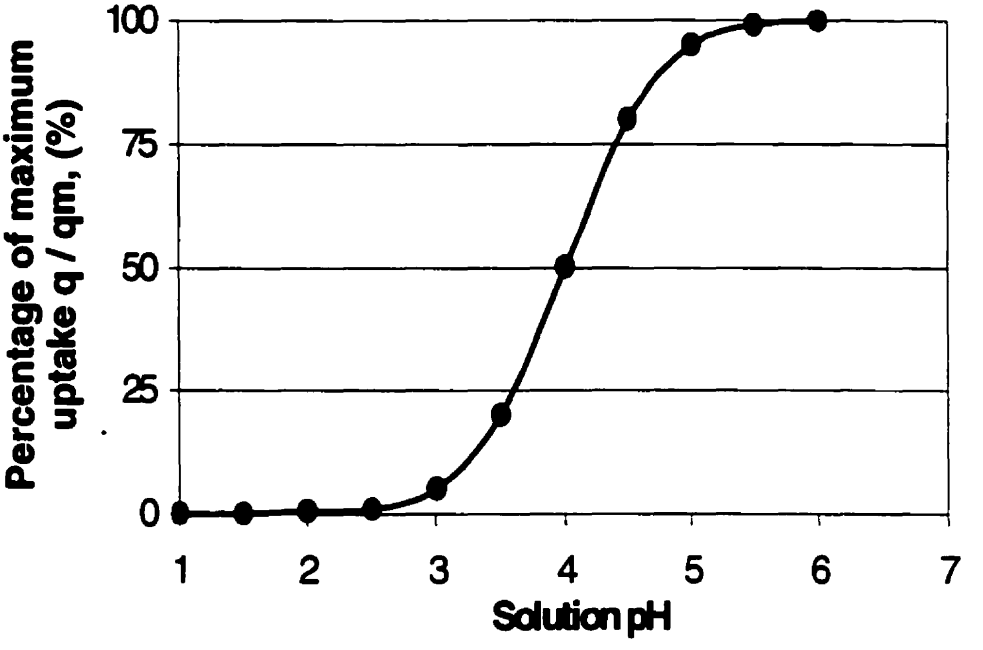

Figure 1.1: Influence of solution pH on the metal uptake in ion exchange

The use of biological treatment systems is also a popular practice in heavy metal decontamination. Municipal sewage may be processed relatively efficiently with activated sludge technology which is used in most industrial countries. However, the resulting bio-sludge is highly toxic and this makes safe sludge disposal more difficult. This toxicity prevents the use of such sludge as agricultural fertilizers. Disposal by incineration constitutes another form of pollution in addition to further increasing sludge disposal cost.

1.3 Possible application of biosorption technology

Biosorption is a process whereby certain types of inactive, dead biomass may bind and concentrate heavy metals from aqueous solution. In contrast to the passive nature of biosorption, *bioaccumulation* occurs in living cells and is metabolically driven. Many types of biomass including bacteria and fungi, from seaweed to higher plants, possess the ability to sequester significant quantities of metals from aqueous solution. In particular, it is the cell wall structure that is principally responsible for this phenomenon.

Large scale application of biosorption in industry is ultimately the impetus for biosorption research. Some proprietary biosorption technologies have been developed in recent years. For instance, process of gold sorption by *Sargassum* seaweed has been patented and the immobilized biosorbents AlgaSORB and AMT-BIOCLAIM have been marketed (Kuyucak, 1990).

There are several advantages to using biosorption technology for waste water treatment. First of all, the efficiency of biosorption removal of toxic heavy metals is high. Metal levels can be decreased from the 1 - 100 ppm range to drinking water levels of 0.01 - 0.1 mg/L in continuous flow biosorption columns. Second, biosorption may be implemented over a wide range of operating solution pH, pressures and temperatures. In addition, the regeneration of the biosorbent and the recovery of the metals deposited in the biomass can also be achieved relatively easily by acid elution. Thus no sludge is produced as in the precipitation process. The main advantage is the lower cost of the biosorbent, since it may be derived from various cheap raw materials. These include waste biomass from the fermentation industry and naturally abundant marine algae that are ubiquitous. Furthermore, recent studies revealed that only minimum pre-treatment such as acid washing may be necessary to use naturally beach dried raw *Sargassum* seaweed effectively in a continuous flow column (Kratochvil, 1995).

The potential application of biosorption can be carried out in a continuous flow column that is filled with properly selected and treated biomass. Figure 1.2 demonstrates biosorption and desorption cycles that take place alternately. It would be desirable to evaluate the performance of biosorption column operation and prediction of metal binding capacity under different processing conditions. A computerized process

simulation could effectively and economically provide the necessary information for process design and optimization. For this purpose, effective mathematical models need to be established. A well defined binding mechanism is helpful in establishing a mathematical model.

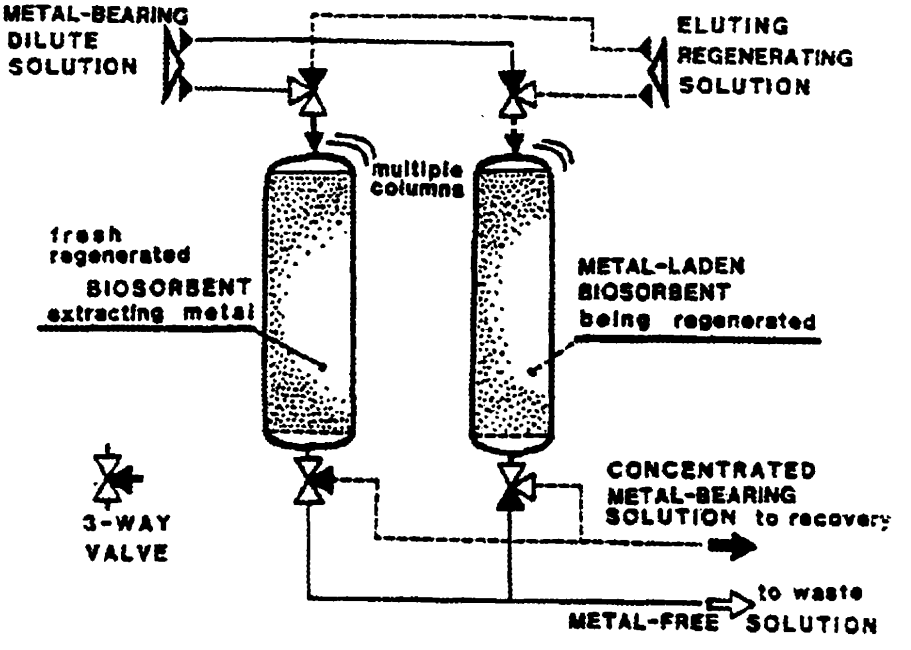

Figure 1.2: Flow sheet of possible biosorption application (Volesky, 1990)

1.4 Objectives

This work investigates the equilibrium, batch dynamics and continuous column operation for the biosorption of uranium and cadmium by the protonated brown algal biomass *Sargassum fluitans*. The detailed objectives are as follows:

Equilibrium

- Determine the equilibrium uptake of uranium and cadmium by *Sargassum* brown algal biomass.
- Elucidate the biosorption mechanism for uranium binding at various pH values.
- Develop a mathematical model describing the uranium equilibrium binding to pre-protonated algal biomass over a wide range of equilibrium uranium concentrations in solution. The solution pH must be incorporated into the model equation as an independent variable.
- Determine optimal conditions for the desorption of uranium and cadmium from metal-laden biomass.

Biosorption dynamics in the batch system

- Develop a suitable mathematical model describing the biosorption rate.
- Solve the partial differential model equations and determine the model parameters.
- Determine the rate of biosorption under selected experimental conditions.

Biosorption column

- Evaluate the performance of uranium biosorption in a continuous flow column packed with *Sargassum* brown algal biomass.
- Develop and apply a mass transfer model to continuous-flow sorption column operation which uses *Sargassum* biomass as the biosorbent.
- Solve the partial differential model equations and determine the model parameters.

2 Literature review

2.1 Biosorption technology

2.1.1 Overview of biosorption technology

Biosorption has received considerable attention as in recent years. As early as 1935, Adams and Holmes (1935) used the tannin resins of black wattle bark (*A. mollissima*) to bind calcium and magnesium ions from waste water on to woody fibers. It was their work that pioneered the field of ion exchange which eventually lead us to the field of biosorption. In recent years, removal of toxic heavy metal contaminants from industrial waste water by biosorption has been proposed as a safe and cost effective process for the treatment of high volumes of low concentration metal-bearing solutions. This could be combined with metal recovery by a desorption process (Brierley, 1990). Volesky and Holan (1995) compiled a list of different types of biomass and metals that have been tested for biosorption. Research on biosorption has revealing that it is a complex phenomenon whereby the metallic species are bound by the solid biosorbent through different sequestering processes. These include chelation, complexation and ion exchange. Muzzarelli et al. (1980) considered that chelation was the main mechanism for cupric ions binding to chitosan membranes. Darnall et al. (1986), Kuyucak and Volesky (1989a) and Sharma and Forster (1994) attributed the biosorption of heavy metals to chemical sorption. Treen-Sears et al. (1984) presented evidence for the ion exchange of the uranyl ion by *Rhizopus* fungal biomass. Crist et al. (1993; 1988; 1992) and Schiewer and Volesky (1995) confirmed that ion exchange played an important role in biosorption of heavy metals on to brown algal biomass.

2.1.2 Biosorption of uranium and cadmium

Biosorption of dangerous elements from aqueous nuclear waste has attracted significant attention in recent years (Ashley and Roach, 1990; Macaskie, 1991). Various non-living biomass types including those of the filamentous fungi, such as *Asperillus*

niger, *Rhizopus oryzae*, and *Penicillium* species; bacteria such as *Pseudomonas aeruginosa* and *Zoogloea ramigera*; actinomycetes such as *Streptomyces lonwoodensis*; and yeast such as *Saccharomyces cerevisiae* have been reported to bind uranium with high sorption uptakes in excess of 150 mg/g of dry biomass (Guibal, et al., 1992; Hu, et al., 1996; Macaskie, et al., 1992; Munroe, et al., 1993; Volesky and Tsezos, 1981). Fresh water algae such as *Chlorella regularis* and *vulgaris*, have also demonstrated good uranium sorption performance (Byerley, et al., 1987 ; Horikoshi, et al., 1979). Despite the fact that live marine algae are capable of biologically concentrating radionuclides such as radium, thorium and uranium (Edgington, et al., 1970), the biosorption of uranium by non-living marine algae has not be significantly investigated.

Cadmium can be sorbed by various types of microorganisms (Mann 1990; Volesky 1990). However, the brown algae *Sargassum fluitans* has been found to be particularly effective in the binding of gold, cadmium, copper and zinc. (Volesky and Holan, 1995; Kuyucak and Volesky, 1990). The easy regeneration of this algal biomass by acid elution makes this substrate particularly favorable to implementation in the biosorption process. (Aldor, et al., 1995; Leusch, et al., 1995). Particularly interesting was a report on the maximal equilibrium cadmium binding capacity by *Sargassum* biomass which exceeds 100 mg Cd/g (dry biomass). Such a high level enables serious consideration of this biomass type for industrial application (Volesky and Schiewer. 1999).

2.2 Properties of *Sargassum* biomass

The brown algae *Sargassum*, can be readily collected from the oceans or else where they accumulate along the intra coastal environment. For example, large quantities of *Sargassum* biomass has been observed along the coast of Cuba, Puerto Rico and Florida. This biomass type serves as a basis for the metal biosorption process. It can accumulate in excess of 25% of its dry weight when sequestering the heavy metals: Pb, Cd, U, Cu, Zn and Cr (present as the anionic group $Cr_2O_7^{2-}$).

2.2.1 Occurrence and structure of *Sargassum*

Sargassum is a brown marine algae. Marine algae proliferate in the littoral zones of world's oceans where they are stable and fast growing. *Sargassum* is extensively distributed in tropical and subtropical waters (Bold and Wynne, 1985). It grows either floating on the ocean surface or attached to the ocean floor in the tidal and sub-tidal zone (Lee, 1989b). The species *Sargassum fluitans* and *Sargassum natans* occur as huge tangled floating masses in the Caribbean, the Gulf of Mexico, the Gulf Stream and Sargasso Sea (Chapman, 1963). The Sargasso Sea represents the most significant source of *Sargassum* from which it derives its name. *Sargassum* algae have stem-like stipes with fronds on them. The structure of typical *Sargassum* biomass is shown in Figure 2.1.

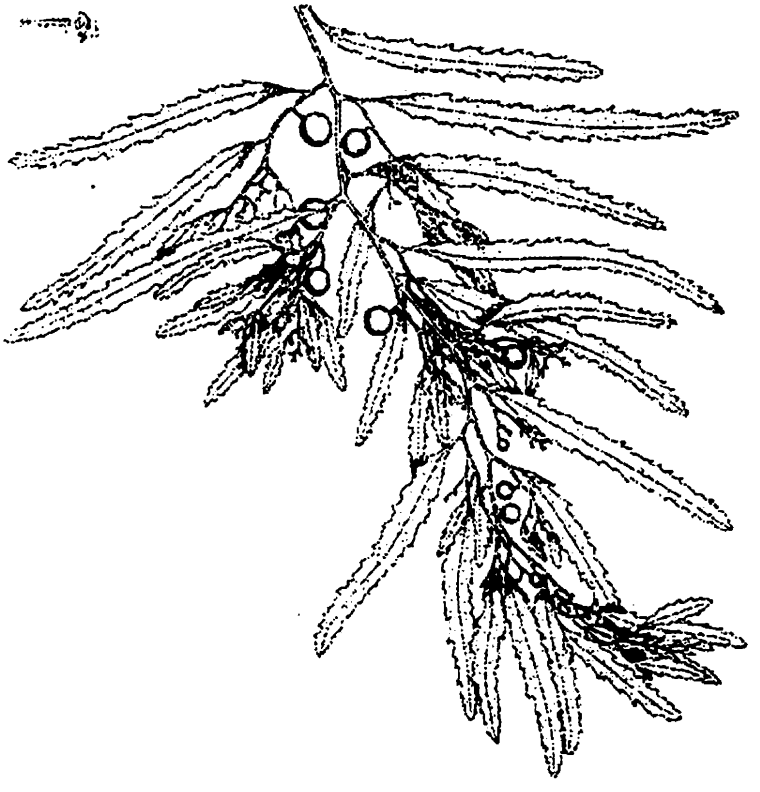

Figure 2.1: A sketch of *Sargassum fluitans* (Taylor, 1960).

Typically the dimensions of *Sargassum* are on the order of decimeters and its fronds are approximately 1.5 – 8.0 centimeters in length and approximately 2 - 8

centimeters in width (Chapman, 1963). The air bladders, which measure several millimeters in diameter, are attached to the stipe and allow the algae to float. The algal tissue consists of several layers of cells. Extra-cellular polysaccharides form a protection layer that prevent desiccation (South and Whittick, 1987). There are two different layers in the algal cell wall. The outer one is an amorphous embedding matrix and the inner one consists of a fibrillar skeleton which provides the structural framework for the cell (Lee, 1989).

2.2.2 Main chemical composition of *Sargassum* biomass

Polysaccharides make up a large portion (up to 65%) of the overall dry weight of the algal cell (Bold and Wynne, 1985). The most common polysaccharides in the brown algae are cellulose (β-1,4-D-glucose), laminarin (mainly D-glucose), alginic acid (a family of linear polysaccharides containing 1,4-linked β-D-mannuronic (M) and α-L-guluronic (G) acids) and fucoidan (mainly L-glucose and sulfate esters) (O'Colla, 1962; Percival and McDowell, 1967b). Cellulose is the main component of the cell wall. It provides a rigid fibrillar skeletal structure that supports the whole cell. Laminarin mainly functions as a long term storage product. Alginic acid and fucoidan are mainly present in the cell wall and, to a lesser extent, in the intercellular mucilage (Lee, 1989a). Fucoidan is also located in the cell wall structure where it is described as a viscous, water soluble and hygroscopic compound. Among the polysaccharides, alginic acid and fucoidan possess functional groups of interest to biosorption. Specifically, alginic acid carries the carboxyl group R-COOH, and fucoidan carries the sulfate group ($R\text{-}OSO_3H$). Both carboxyl and sulfate groups can be deprotonated and are responsible for metal sorption (Fourest and Volesky, 1997). Crist et al. (1992) have also found the carboxylate and sulfate groups to be the active functional groups in metal biosorption by marine algae.

Alginic acid

Alginic acid is found in all brown algae where it constitutes between 10 – 40% of the dry cell weight (Kreger, 1962; Percival and McDowell, 1967b; Fourest and Volesky, 1996). It contains two constituent monomer blocks: β-1,4-D-mannuronic acids (M) and α-1,4-L-guluronic acids (G) (Chapman, 1963; Lewin, 1974). Usually, the alginic acid

polymer is comprised of block which may be either exclusively $(M)_n$, exclusively $(G)_n$ or a third heterogenous type with alternating M and G unites $(MG)_n$ (Percival and McDowell, 1967b). The ratio and sequence of the two saccharide units, mannuronic acid and guluronic acid (termed the M:G ratio), in a particular brown alga may vary with specie, growth phase and the area of growth (Haug, et al., 1974). Each segment of the monomer chain may contain between 20 –30 M or G monomers where the total chain length may reach 80 monomer units (Chapman, 1980). The M:G ratio typically varies between 0.5 – 3 and it was found to be approximately 1.2 for *Sargassum fluitans* (Fourest and Volesky, 1997). The chemical structure of alginic acid is depicted in Figure 2.2.

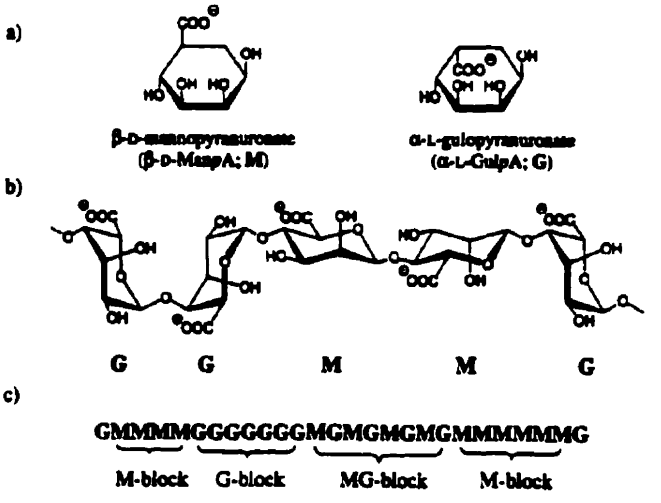

Figure 2.2: The chemical structure of alginic acid (after Smidsrod and Draget, 1996). G: guluronic acid; M: mannuronic acid.

(a) molecular structure; (b) configuration; (c) monomer blocks.

In algal biomass, alginic acid exists in the salt form (alginate) typically as salts of sodium, potassium, magnesium and calcium. Alginates contribute to structural rigidity while at the same time imparting flexibility to the cell wall (Smidsrod and Haug, 1996). The salt may be extracted from the cell matrix at elevated pH and temperature and is stable at low pH in the insoluble form. The dissociation constants (pK_a) for the carboxylic groups of mannuronic and guluronic acids are 3.38 and 3.65, respectively (Percival and McDowell, 1967a).

Fucoidan

Brown algae may contain up to 16% of fucoidan (Volesky, 1970). Fucoidan is a branched polysaccharide sulfate ester with L-fucose building blocks as the major component which are predominantly α(1→2)-linked. Branches occur as (1→3) or (1→4)-linkages (Lobban, et al., 1985; Mackie and Preston, 1974b; O'Colla, 1962). The chemical structure is illustrated in Figure 2.3.

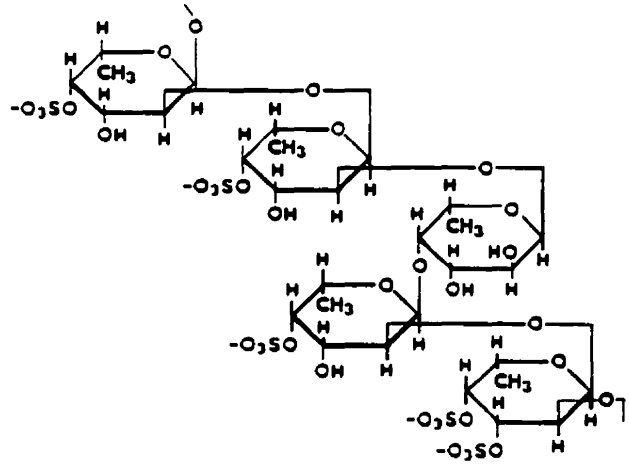

Figure 2.3: The chemical structure of fucoidan (Percival and McDowell, 1967c)

The sulfate ester and fucose components constitute about 40% and 60%, respectively, of the fucoidan mass (Percival and McDowell, 1967c). The sulfate ester groups ($R\text{–}OSO_3^-$) are strongly acidic with a *pKa* range of 2 – 2.2 depending on the extractant source. The fact that the brown algae demonstrate a high sorption capacity at low solution pH may be attributed to the low *pKa* value of sulfate groups in fucoidan. Veroy et al. (1980) also indicated that the dissociated sulfate groups are capable of binding metals.

2.3 Biosorption equilibrium

Usually, the biosorption of heavy metal has been evaluated by deriving relevant sorption equilibrium isotherms. Langmuir (1918) and Freundlich (1926) models are used most extensively. They are defined, respectively, as follows:

Langmuir isotherm:

$$q = \frac{q_{max}[M]}{K + [M]} \tag{2.1}$$

where q and $[M]$ are equilibrium metal uptake and concentration, respectively. q_m is the maximum uptake and K is the Langmuir sorption equilibrium constant.

Freundlich isotherm:

$$q = k[M]^{1/p} \tag{2.2}$$

where k and p are empirically determined constants. k is related to the maximum binding capacity and p to the affinity between sorbent and sorbate.

Both isotherms have been used successfully to describe equilibrium biosorption (Holan and Volesky, 1994; Prasetyo, 1992; Tsezos and Volesky, 1981). Although both models are empirical for biosorption application, the Langmuir model constants are more easily interpretable. The Langmuir model was originally derived for the adsorption of gas on to activated carbon with the assumption of formation of a mono-layer. Its two parameters reflect the maximum gas uptake and the affinity of the gas component on the sorbent. For the biosorption of heavy metals, initially the uptake increases in a linear fashion with rising equilibrium concentration. Uptake is eventually limited by the fixed number of active sites and a resulting plateau can be observed. This phenomenon is depicted well by Langmuir isotherms. The maximum metal uptake and the affinity of the metal ion for the biosorbent may well be described by the two empirically regressed Langmuir parameters, q_m and K. It is further well known that protons play a crucial role in biosorption by brown algal biomass (Crist, et al., 1988; Marinsky, 1987; Schiewer and Volesky, 1995). Proton concentration is not taken into account in either of the above mathematical models. The common practice is to determine a series of separate sorption isotherms for different pH values (Ho, et al., 1995; Huang, et al., 1991; Xue and Sigg, 1990). This methodology is a necessity when the pH-insensitive Langmuir or Freundlich

models are used. It is difficult to quantitatively evaluate the effect of the solution pH or the presence of another light metal ion on sorption performance. As a result, it is the convention that isotherms be determined at various constant pH values.

Since the biosorption of heavy metals by algal biomass is largely an ion exchange process (Crist, et al., 1990; Kuyucak and Volesky, 1989a), the use of ion exchange constants is only natural. However, the complex nature of the biomass material makes it difficult to process it in the same way as is done with relatively simple synthetic ion exchange resins. Furthermore, it is difficult to determine the activity coefficients of the various species inside the bulk biomass (Shallcross et al., 1988; Mehablia et al., 1994). If the approach of using ion exchange constants is used, a tedious iteration procedures is required for the calculation of equilibrium metal binding and the explicit expression between metal uptake and equilibrium metal concentration can not be established. In many applications, such as the modeling of biosorption dynamics, an explicit relationship (in the form of an equation) is necessary. The incorporation of the proton concentration into the isotherm model equation was proposed by Schiewer and Volesky (1995). They used an isotherm equation for biosorption of cadmium, copper and zinc, in which the proton concentration functioned as an independent variable. The prediction of biosorption uptake at various solution pH levels becomes an explicit relationship and is easily solvable. However, the Schiewer-Volesky model neglected the possible hydrolysis of metal ions in aqueous solution. For some metals, such as cadmium and zinc, the ionic species are simply hydrated over a wide range of metal concentrations and pH. The effect of hydrolysis is therefore negligible. For other metals, such as uranium, hydrolysis takes place under most biosorption experimental conditions. The existence of these hydrolyzed ions plays an important role in the biosorption of those complexes. Guibal et al. (1992) and Hu et al. (1996) discussed qualitatively the effect of uranium hydrolysis on the biosorption by the filamentous fungus *Mucor meihei* and *Pseudomonas aeruginosa* strain CSU, respectively. It therefore seems appropriate to develop a proper model equation that would be able to quantitatively describe the biosorption of different hydrolyzed metal species in solution.

Desorption is another important aspect for the application of biosorption since regeneration of biomass is crucial for cost effectiveness. In this process, toxic heavy

metals bound on the biomass may be eluted. Aldor et al. (1995) investigated equilibrium cadmium desorption from protonated *Sargassum fluitans* by various eluants. It was established that the mineral acids, particularly 0.1 N HCl or H_2SO_4, are efficient and biomass damage was limited.

2.4 Biosorption rate mechanism and dynamics in a batch system

For any practical application, process design or operation control, the sorption process rate and dynamic behavior of the system are very important factors. A mathematical model is a very desirable tool which must describe a fair representation of the behavior of all relevant metals that are sorbable by the particular biosorbent considered. In order to do this the model must incorporate dynamic process parameters which include the rate controlling aspects. There are four types of rate control mechanisms: external mass transfer (or film diffusion), pore diffusion, surface diffusion and intrinsic chemical reactions. Since diffusion in the bulk liquid phase can be easily accelerated by agitation, it is not considered to be the rate controlling step. Models other than those based on the mass transfer rate controlling step have also been used by some investigators. For example, Lo and Leckie (1993) adapted a two-stage rate model in order to determine the internal diffusion coefficient for cadmium and zinc ions in porous aluminium oxides. The model assumption includes a rapid initial stage and a much slower secondary stage which controls the process and was based on an empirical formula. The calculated values of the cadmium diffusion coefficient were lower than the molecular diffusivity of cadmium ions in water by one to two orders of magnitude and thus were not considered reasonable.

External mass transfer takes place when the sorbate material passes through the thin layer surrounding the external surface of the sorbent particle. Allen et. al (1992) used a singular external mass transfer rate in order to model the sorption of heavy metal ions by peat moss. Leusch and Volesky (1995) tested a single external mass transfer resistance model for the biosorption of cadmium on the *Sargassum fluitans* biomass. However, the experimental data showed that the effect of internal mass transfer on the

overall rate of the biosorption process could not be neglected. Internal diffusion includes both diffusion through the internal surfaces of the porous biomass particles and diffusion in the static liquid that fills the micro-pores of the particles. For the seaweed biomass, internal diffusion takes place through the alginate gel phase of the particles. Thomas (1951), Rosen (1952) and Hand et al. (1984) proposed that surface diffusion was the only rate controlling step. On the other hand, Hall et al. (1966) and Hashimoto et al. (1975) proposed that pore diffusion was the sole intraparticle mass transfer resistance. Jang et al. (1990) used the Shrinking Core (SC) model, with single-resistance intraparticle diffusion as the controlling step to describe the biosorption of Cu^{2+} by calcium-alginate beads. Chen et al. (1993) showed that the SC model-calculated diffusion coefficient for copper ions in a series of increasingly dense calcium alginate gel beads was not plausible. They proposed the Linear Adsorption (LA) model to describe the process of metal binding to sorbent particles. The effective diffusion coefficient within a matrix should be less than the molecular value due to tortuosity and porosity of the solid phase (Helfferich, 1962; Westrin and Axelsson, 1991). However, the LA model-calculated values of the copper diffusion coefficient in calcium alginate beads were greater than the molecular diffusion coefficient of copper ion in water.

Apel and Torma (1993) studied metal ion diffusion of Cd^{2+}, Ba^{2+} and UO_2^{2+} in Ca-alginate beads. Although they assumed that sorption rate was controlled by intraparticle diffusion they did not use diffusion equations. Instead they used a hyperbolic enzyme reaction rate equation at steady state conditions. This described the experimental data adequately but is not compatible with their assumption of intraparticle diffusion control. Furnas (1932), Klinkenberg (1954) and Goldstein (1953a; 1953b) provided a solution for a system in which external and surface diffusion controlled sorption rate. Tsezos et al. (1988) applied a two-resistance mass transfer model for uranium sorption in a batch reactor by inactive immobilized *Rhizopus arrhizus* particles. The overall film diffusion coefficient and intraparticle diffusion coefficient were then regressed from a set of experimental data of concentration *versus* time simultaneously. It should be noted that there may be more than one set of multiple parameters matching the regression criteria.

2.5 Fixed-bed column operation and mathematical model

The most common sorption option for industrial waste water treatment application is the fixed-bed column system (Stenzel, 1993). In general removal of metal ions by biomass is similar to ion exchange (Trujillo et al., 1991). The design and optimization of a fixed-bed sorption column requires a knowledge of the equilibrium and mass transfer relationships inside the sorbent particles as well as the fluid flow properties in the column. Based on conservation of mass, the general mathematical equation that describes macroscopic fluid flow is as follows:

$$\varepsilon\frac{\partial C_b}{\partial \tau}+U_s\frac{\partial C_b}{\partial z}-D_L\frac{\partial^2 C_b}{\partial z^2}-D_R\left(\frac{1}{R_a^2}\frac{\partial}{\partial R_a}(R_a^2\frac{\partial C_b}{\partial R_a})\right)+\rho(1-\varepsilon)\frac{\partial \bar{q}}{\partial \tau}=0 \qquad (2.3)$$

where D_L and D_R are the axial and radial dispersion coefficients in the column, respectively. R_a is a spatial variable for radial direction of the column. Other symbols can be found in the notation list.

Usually, radial dispersion in a continuous flow column is negligible. The role axial dispersion plays in the column operation have been investigated by many researchers. According to Levenspiel (1972), the particle Peclet number for a fixed-bed is almost constant over a wide range of Reynolds numbers. Crittenden et al. (1978a; 1978b) and Crittenden and Weber (1978) concluded that the effect of axial dispersion on the operation of activated carbon column adsorbers could be neglected when a relatively large column length was employed. Furthermore, Liu and Weber (1981) reported that axial dispersion is negligible for very short columns. Thus, a plug flow assumption was adopted and used for most of the mathematical models describing sorption columns.

The last term of Equation (2.3) represents the average sorption rate for the sorbent particle. It is dependent on the dynamic mechanisms that control the overall sorption rate in the sorbent particle, as described in Section 2.4. In addition, Thomas (1944) proposed a second order reaction to describe the rate controlling step for the ion exchange of calcium for sodium by zeolite columns. Weber and Crittendden (1975) also adopted a second order reaction, the Langmuir rate kinetics equation, in their MADAM-I model for

activated carbon columns. Although the single resistance mechanism is simpler and the model equations on which it is based are easily solvable, it was necessary to introduce a more complicated two-resistance model in many instances. Weber and Liu (1980; 1981) proposed a column model where both external and surface diffusion were equally significant. Rosen (1954), Amundson (1956) and Fleck (Fleck, 1973) investigated how the external and pore fluid diffusion controlled the overall sorption rate in the column. Masamune and Smith (1965), Fleck (1973), Hall et al. (1966) proposed, respectively, a more general rate mechanism for column models which include together film diffusion, surface diffusion and pore diffusion. However, as indicated by Keinath and Weber (1968), each development for the three-resistance models used for the fixed-bed column requires a simplifying assumption regarding a solute equilibrium distribution relationship.

The solution of the model equations is an essential step in the modeling of fixed-bed columns. As early as 1944, Thomas (1944) obtained an analytic solution for a fixed-bed sorption column model equation which adopted a second-order rate and the Langmuir sorption isotherm. Later, Heister and Vermeulen (1952) and Vermeulen (Vermeulen, 1958) verified that the fixed-bed column model with no matter what single resistance rate control, external, solid diffusion or pore diffusion could be approximated well by the Thomas analytical solution (1944). Various numerical techniques were developed for the solution for the more complicated column model equations. For instance, the Finite Difference Method and the Orthogonal Collocation were used by Weber and Crittenden (1975). Kratochvil and Volesky (1998) used the Finite Element method to solve the column equations successfully. The details of various numerical methods were covered well by Lapidus and Pinder (1982). The application of the Orthogonal Collocation Method to fixed-bed adsorption calculations was investigated by Villadsen and Michelsen (1978).

Several models have been suggested for the modelling of biosorption columns. Prasetyo (1992), Muraleedharan et al (1994) and Jansson-Charrier et al. (1996) used the conventional Bohart-Adams sorption model to analyze the performance of biosorption columns. The Bohart and Adams model (1920) was originally developed for sorption on granulated activated carbon and it assumes the sorption zone in the column approximates a constant pattern, or in other words the breakthrough curves obtained from different

positions for a given column have the same shape. Although the model equations could be solved easily and the model provided a simple and fast evaluation of the column performance, its validity was limited by its oversimplified assumptions which are related to the range of conditions used in specific experiments (Faust and Aly, 1987).

Kratochvil (1997) applied the Equilibrium Column Model (EBC), developed by Klein et al.(1967) and Tondeur and Klein (1967) for multicomponent ion exchange, to biosorption of heavy metal by *Sargassum* biomass. The model assumes a negligible mass transfer resistance for ions diffusing in and out of the biomass particle, thus considering a homogeneous metal concentration inside the biomass in equilibrium with the biomass uptake. The EBC model succeeded in predicting the minimum usage of biomass for the column, the elution order of ions from the saturated column, the occurrence of effluent concentration overshoots and the maximum overshoot concentrations at the column outlet. The drawback of this model is that it failed to predict the exact column service time and the shape of the model-calculated breakthrough curves could not be confirmed by the experimental results. More successful was the application of the Tan-Spinner mass transfer model (1994) by Kratochvil (1997). The effect of dispersion on column dynamics was included in the model and sorption rate was assumed to be proportional to the difference between the equilibrium uptake and the average uptake. The mass transfer resistance due to external and intraparticle diffusion was combined into the proportionality coefficient. The model-calculated column service time and the shape of breakthrough curves agreed well with the experimental results. On the other hand, the lumped mass transfer coefficient is not accurate and may depend on specific experimental conditions.

The difficulty of applying mathematical model (which include intraparticle diffusion) to biosorption columns is that the assumption of uniform spherical particles is not held for the brown algal biomass since it displays a variable plant-like morphology. Since the thickness of the seaweed biomass is much smaller than the particle length, a one-dimensional diffusion should be applicable for intraparticle diffusion in either batch or column applications. When a correct model is used engineers may select the appropriate experimental conditions necessary for pilot experiments when scaling-up of the biosorption process is performed. A good mathematical process model will assist in

guiding experimental work and the further evaluation of experimental results obtained from column operation.

2.6 Section summary

Biosorption refers to the binding and concentration of heavy metals from dilute solutions to certain types of inactive, dead biomass. Biomass of the brown marine algae *Sargassum fluitans* has been proven to be an effective heavy metal biosorbent. The alginic acid and fucoidan biopolymers of this biomass are the key functional groups which are mainly responsible for heavy metal sequestration by the cell wall. A higher solution pH is preferable for metal binding to the biomass.

Traditionally, biosorption performance has been evaluated through the use of simple sorption isotherm relationships such as the Langmuir or Freundlich models. However, neither model is able to predict the effect of solution pH on biosorption performance and the determination of a series of isotherms at different solution pH values is necessary. Based on ion exchange and binding to free sites, the Schiewer-Volesky model incorporates proton concentration in to the sorption isotherm equations. However, for some metals, such as uranium, the effect of hydrolysis in aqueous solution may dramatically affect biosorption performance. Up until this point, discussion of hydrolysis has mainly been qualitative and a mathematical model including the hydrolysis constants of metallic species is necessary and will follow.

Biosorption dynamics is an important factor in process design and control. External diffusion resistance, surface diffusion resistance and the kinetics of intrinsic chemical reactions at biomass binding sites all are potential rate controlling steps in the sorption process. Practical application of sorption for the separation and purification of heavy metals is most commonly carried out by a fixed-bed column system. Normally dispersion in the column, in addition to external and intraparticle diffusion of the particles are factors that may affect a column's sorption performance. However, in this case, dispersion has been shown to be negligible for most column operations. Various mathematical models for conventional sorption that combine macroscopic fluid flow equations with sorption rate dynamics have been proposed and solved by analytical and

numerical methods. The application of these models to the biosoption of heavy metals have not been tested rigorously yet.

3. Material and Methods

3.1 Chemicals used

For sections 4.1, 4.2 and 4.3, the stock solutions were prepared by dissolving various metal salts, $UO_2(NO_3)_2 \cdot 6H_2O$ (JT Baker Chemical), $UO_2SO_4 \cdot 3H_2O$ (Fisher Scientific), $Cd(NO_3)_2 \cdot 4H_2O$ (Fisher Scientific) in distilled water. $CaCl_2$ (Fisher Scientific) was dissolved in distilled water and used in preparing calcium loaded biomass. The 0.05 - 0.1 N LiOH solutions used in sections 4.1, 4.2 were prepared from $LiOH \cdot 2H_2O$ (Fisher Scientific). The 0.1 N HCl solution being used as an eluant was diluted from concentrated HCl (Fisher Scientific).

3.2 Biomass preparation

3.2.1 Biomass for equilibrium and column

A batch of beach-dried *Sargassum fluitans* biomass, collected in Naples, FL, was reacted with 0.1 N HCl (10 g biomass / L) for 3 hours to standardize the biomass by eliminating the light metal cations such as calcium and magnesium originally bound by the algae. The biomass was then rinsed with the same volume of deionized water many times until a stable solution pH 4.0 was reached for the wash. The biomass was dried in an oven at 40 - 60^{o}C overnight. The natural shape and leafy structure of the algae was not destroyed during the acid protonation treatment and the material was stored for later use.

3.2.2 Biomass for batch dynamics

The biomass used was the same as in the previous section and was first ground by a homogenizer and sieved to different size fractions. The batch of biomass with particle sizes ranging between 1.0 - 1.4 mm was selected for further protonation. The elimination of salts bound by the biomass was carried out as in the previous section by rinsing. In order to guarantee that different size particles of biomass were of uniform composition, biomass particles of size (0.5 - 0.7) mm and (0.84 -1.0) mm were prepared

from manually cut identical biomass parts. All biomass particles were of the same thickness (approximately 0.2 - 0.5 mm). Unless specified otherwise, the biomass particle size used in the latter experiments was (1.0 - 1.4) mm.

The biomass can be reinforced by cross-linking with formaldehyde. In the cross-linking process, the biomass was prepared in the same way as the protonated one except that a mixture of 0.1 N HCl and 1.0 M formaldehyde was used for cross-linking and acidification. A more detailed description of the cross-linking procedure can be found in Leusch, et al. (1995).

3.3 Metal concentration analysis

Dissolved metal concentrations in solution were determined by a flame atomic absorption spectrophotometer (AAS, Thermo Jarrel Ash, Model Smith-Hieftje II) and inductively coupled plasma atomic emission spectrophotometer (ICP-AES, Thermo Jarrel Ash, Model TraceScan). Multiple metals were analyzed simultaneously by ICP-AES. The characteristic wavelengths used in AA and ICP-AES analysis for various metals are listed in Table 3.1. The calibration of four points and two points were used for the AAS and the ICP, respectively. The concentration range of the standard solution is between 0 – 20 mg/L for uranium and 0 – 10 mg/L for other metals, which are in the linear range of the instruments. Five and ten ppm standards were used produce a calibration curve for the linear region of metal emission. When these standards were re-tested for reproducibility, the analyses displayed a deviation not exceeding 3%.

Table 3.1: The characteristic wavelengths used by AA and ICP-AES for various metals

Elements	Analysis	Wavelength (nm)	Mode	Detection Limit (mg/L)
Uranium	ICP-AES	409.014	Emission	0.01
Cadmium	AA	228.8	Absorption	0.01
Lithium	ICP-AES	367.8	Emission	0.01
Calcium	ICP-AES	422.7	Emission	0.01

Experimental samples were filtered or centrifuged before they were introduced into the ICP-AES system. Preliminary tests for sorption of dissolved metals on the filter assembly were conducted and no detectable sorption by the filter was observed under the experimental conditions.

3.4 Sorption equilibrium experiments

3.4.1 Concentration difference method

A sorption dynamics methodology (described later in the next section) was used to establish that 2 - 4 hours of contact was necessary for the attainment of sorption equilibrium. A series of 50 ml solution samples with different uranium or cadmium nitrate concentrations were mixed with 0.1 g of biomass in 150 ml Erlenmeyer flasks. The suspensions were agitated on a rotary shaker at 2-3 Hz at room temperature. The suspension pH was adjusted to the desired values with 0.1 N LiOH or 0.1 N HCl. When the sorption equilibrium was reached, 3 hours after the suspension pH stabilized at the desired value, the suspension was filtered or centrifuged. The supernatant was diluted with distilled water as required for metal concentration analysis by the ICP-AES. The recovered biomass was soaked and rinsed with deionized water several times (no biosorbed metal loss was detected) before drying it at 40-60°C in an oven overnight. The dried metal-loaded biomass was then used in desorption experiments. The parallel control samples contained no biomass and were processed with the same protocol.

The metal uptake was calculated from the concentration difference which is based on the mass balance as follows (Volesky and Holan. 1995):

$$q_U = \frac{C_i V_i - C_f V_f}{W} \tag{3.1}$$

with V_i and V_f being the initial and final solution volume, respectively. W is the weight of biosorbent. C_i and C_f are the initial and final metal concentrations, respectively. While C_i corresponds to the control samples, C_f was for the supernatant solution after the sorption contact. Both of them were determined by AA or ICP-AES after proper dilutions.

3.4.2 Acid elution method

When the concentration difference between the initial and the equilibrium metal concentration is relatively small, it may not be possible to determine the metal uptake (using the conventional method) accurately. In conventional equilibrium experiments, W grams of biomass are mixed with L liters of metal ion solution under controlled pH conditions. The solution metal concentrations before and after the sorption process, as determined by ICP-AES or AA analysis, are C_i and C_f, respectively. If the sensitivity of the analysis instrument is P, which is the minimum concentration difference that the instrument can distinguish, and the acceptable measuring tolerance is E, then the following condition holds:

$$\frac{P}{(C_i - C_f)/D} << E \qquad (3.2)$$

where D is the dilution ratio of the sample. Taking L as the approximation of the solution volume, V_i and V_f, in Equation (3.1), we combine Equations (3.1) and (3.2) :

$$\frac{W}{L} >> \frac{P\,D}{q\,E} \qquad (3.3)$$

Equation (3.3) represents the limitation imposed by the instrument sensitivity in the conventional concentration difference method. At high sorption pH values, the metal uptake q is large enough to produce a metal concentration difference which can be detected directly by an ICP-AES or AA analysis. But when uptake q is low, as in the case of acidic conditions, even at higher equilibrium concentrations (resulting in high dilution P), a high ratio of biomass weight to solution volume is required to achieve a satisfactory degree of accuracy. In turn, the ratio of biomass weight to liquid volume is limited by the mixing conditions and swelling properties of the biomass. Thus the conventional concentration difference method was not suitable and the acid elution method should be applied instead.

In this method, 0.1 g of dry metal-loaded biomass was mixed with 50 ml 0.1 N HCl in a 150 ml Erlenmeyer flask. After 3-4 hours, the metal was eluted from the biomass and the metal concentration of the desorbing solution was determined using the same protocol as in the previous sorption equilibrium experiments. No pH adjustment was required since the change of proton concentration caused by the elution of uranium metal ions was negligible compared with the eluant pH. The amount of metal eluted from the biomass can be calculated as follows:

$$q_{des} = \frac{C_{des} V}{W} \tag{3.4}$$

where q_{des} is the (eluted) metal content per gram of biomass, and C_{des} is the metal concentration of the HCl eluant solution.

The preliminary experimental results established that the use of 0.1 N HCl was sufficient to complete remove heavy metals from the biomass. When the pH of the solution is between 3.0 and 4.0 the difference obtained by the two methods is negligible (within 2% deviation).

3.5 Sorption dynamics in a batch system

End-point titration was used to study the dynamics of the batch sorption process. 0.1 gram of biomass was mixed in 50 ml distilled water in a magnetically stirred vessel with baffles for 1.0 hour. From this point on the computer-driven autotitrator (PHM82 pH meter, TTT80 Titrator and ABU80 AutoBurette, Radiometer, Copenhagen, Denmark) followed the progression of the reaction in end-point titration mode. The pH value of the solution was maintained (e.g. pH 4.0) by the autotitrator through the addition of a 0.05 N LiOH solution to the vessel with an internal high-speed pump and a burette. When sorption equilibrium was reached, 1.0 ml of concentrated heavy metal (nitrate or sulphate) solution was added into the well stirred vessel which initiated the metal sorption process. An initial metal concentration of approximately 200 – 250 mg/L was used. The pH value and the volume of the added base *versus* contacting time were recorded by the computer system. A series of 0.2 ml samples of solution were removed

from the vessel at pre-defined time intervals. After appropriate dilution, the samples were analyzed for metal concentration by either AA or ICP-AES.

In order to determine the biosorption rate at a constant solution pH, the protons released from *Sargassum* biomass must be neutralized instantly. In the end-point titration experiment, the response time of the pH probe and the speed of base solution addition are of crucial importance. When the solution pH decreased below the predefined pH value due to proton release, the internal burette of the autotitrator was activated and delivered LiOH solution into the reactor instantly until the solution pH was restored to the designed level. The performance of the autotitrator was examined first. Computer recorded data demonstrated that the autotitrator read the solution pH as fast as 1 - 8 times every second and the delivery speed of the internal burette was fast and adjustable up to 0.1 ml/sec. From the titration results (in Figure 4.2.1 and 4.2.2 for uranium and cadmium, respectively), a stable solution pH was observed. The pH values fluctuated only within a very narrow range of 0.05 – 0.1 unit except during the first 30 seconds at which time a larger pH fluctuation of 0.2 unit was observed. This indicates that the response of the pH probe is adequate.

3.6 Sorption and desorption in a continuous flow column

The sorption column (the diameter is 3 cm and the length = 45 cm) was uniformly packed with 22.64 g (dry basis) of protonated biomass. The continuous-flow experimental arrangement is illustrated in Figure 3.1. In sorption operation mode, an aqueous solution containing ~238 mg/L (1 mM) of uranium at feed pH was continuously pumped upward through the column at a constant flowrate (e.g. 340 ml/h). The samples were collected from the outlet of the column with a fraction collector (Gilson 205) at pre-set time intervals and were analyzed for uranium concentration with ICP-AES. The pH value of the outlet solution was recorded by a computer. When the biomass in the column was saturated with metal, the column feed was switched to distilled water for several hours and then followed by a 0.1 N HCl acid solution in order to elute the uranium. The collection and analysis of the elution outlet samples was the same as for the sorption protocol.

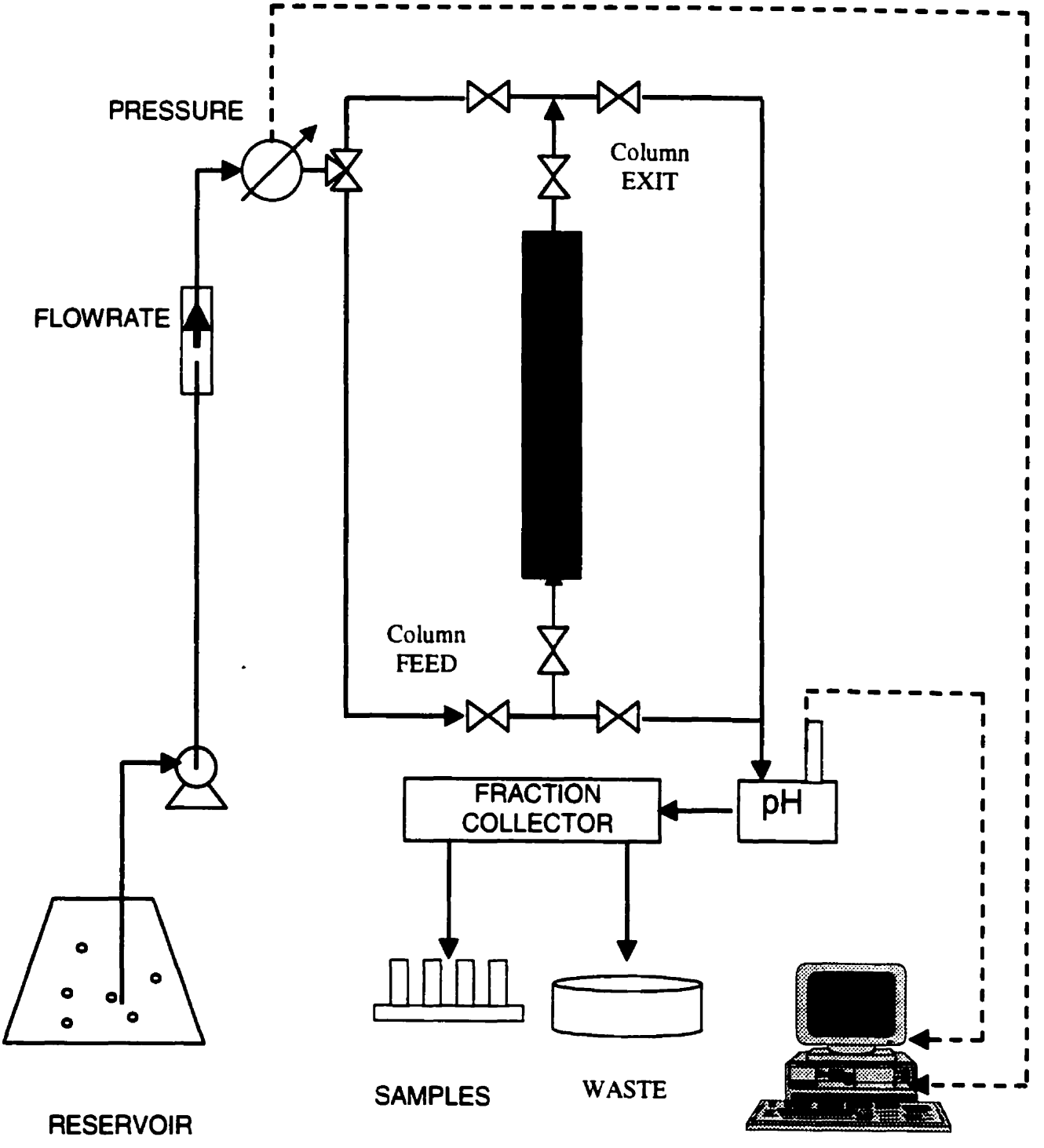

Figure 3.1: The experimental arrangement of the continuous flow biosorption column.

3.7 Experimental temperature

All the equilibrium, dynamic and column biosorption experiments described in the above sections (3.4, 3.5 and 3.6) were performed at room temperature (20 – 22 ^{o}C, maintained by a central air conditioning system).

4. Results and Discussion

4.1 Biosorption equilibrium

In this section, *Sargassum* biomass biosorption performance for the uptake of uranium or cadmium was evaluated by determining the respective sorption isotherms for different pH values. The conventional Langmuir sorption model was used initially. Eventually, the ion exchange characteristics and the influence of uranium hydrolysis was investigated in solution. A new equilibrium isotherm model based on the ion exchange of hydrolyzed uranium complexes was developed.

4.1.1 Effect of solution pH on metal sorption isotherms

The solution pH played a significant role in the biosorption process. The effect of solution pH on metal biosorption is represented by a series of experimental sorption isotherms in which the pH was either 2.5, 3.0, 3.5 or 4.0 and the biosorbent was *Sargassum fluitans* as shown in Figure 4.1.1 for uranium and in Figure 4.1.2 for cadmium. The points represent the experimental data and the solid curves were calculated with the conventional Langmuir sorption isotherm model (Equation 2.1). The model parameters were obtained through a non-linear regression using KaleidaGraph™ software and are listed in Table 4.1.1 for uranium and cadmium at various solution pH values. q_m is the maximum uptake capacity and K is the equilibrium constant. When the equilibrium metal concentration is increased, the metal uptake at a specific solution pH increases correspondingly. In the range of pH 2.5 – 4.0, an increased metal uptake was observed with increasing pH for the same equilibrium metal concentration. The pH dependency of biosorption performance is clearly seen when plotting the Langmuir model parameters *versus* the solution pH, as demonstrated in Figure 4.1.3. The q_m and the affinity parameter b (reciprocal of the Langmuir equilibrium constant K) increased with increasing solution pH values.

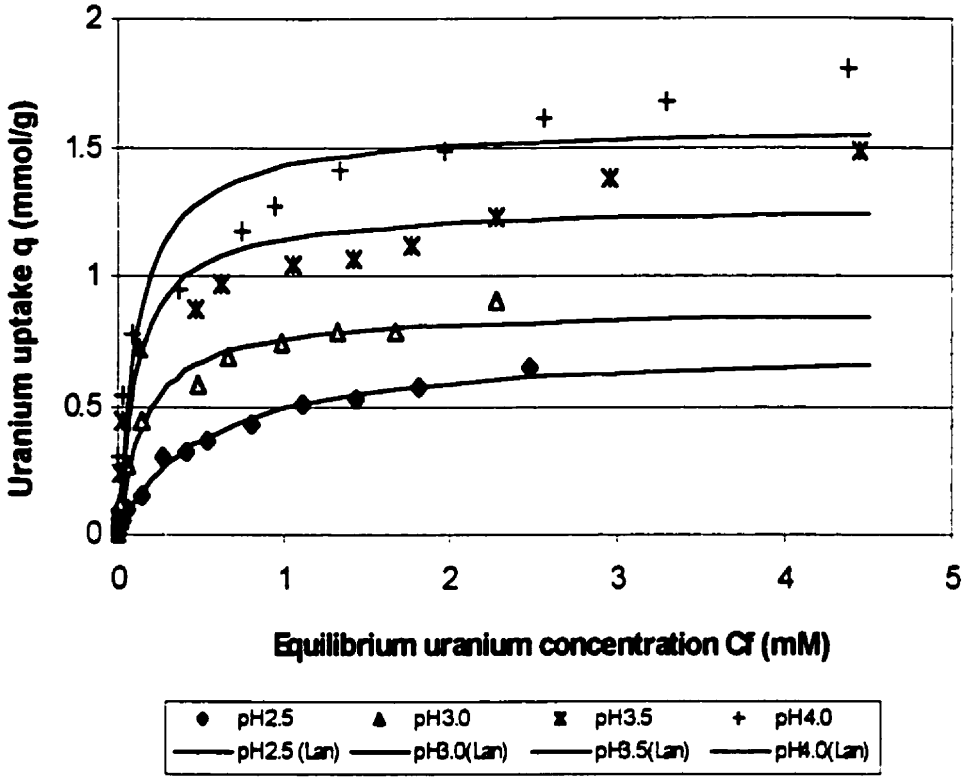

Figure 4.1.1: Influence of solution pH on uranium biosorption isotherms.

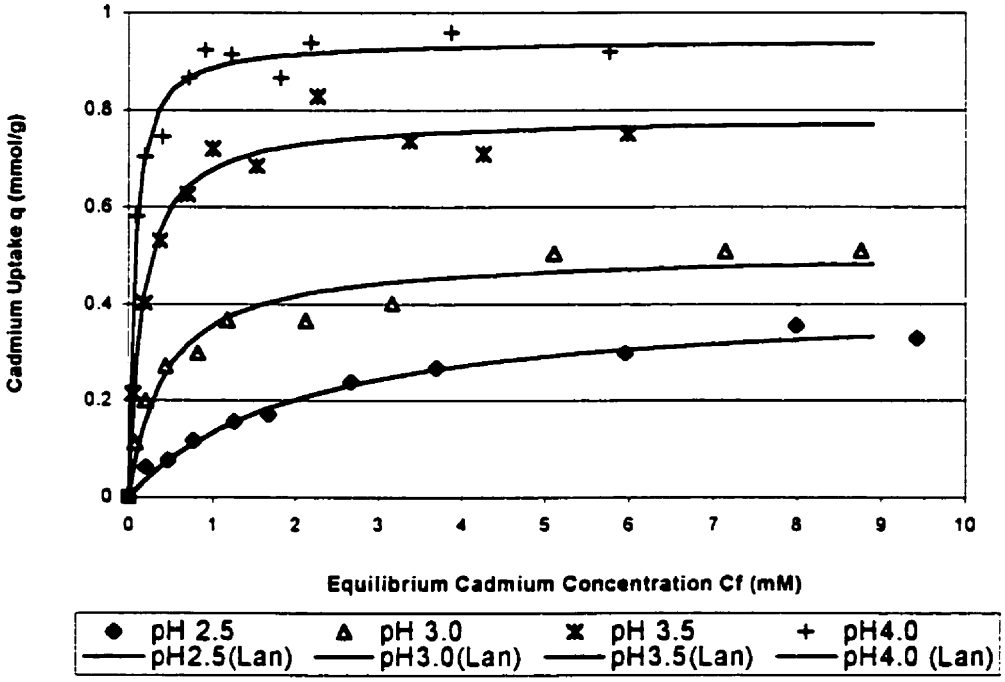

Figure 4.1.2: Influence of solution pH on cadmium biosorption isotherms.

Table 4.1.1 Langmuir model parameters

	Parameter	pH 2.5	pH 3.0	pH 3.5	pH 4.0
Uranium	K (mmol/L)	0.48	0.15	0.11	0.11
	q_m (mmol/g)	0.73	0.87	1.27	1.59
	Correlation coefficient	0.996	0.993	0.976	0.960
Cadmium	K (mmol/L)	2.1	0.43	0.16	0.06
	q_m (mmol/g)	0.41	0.51	0.78	0.94
	Correlation coefficient	0.993	0.978	0.988	0.993

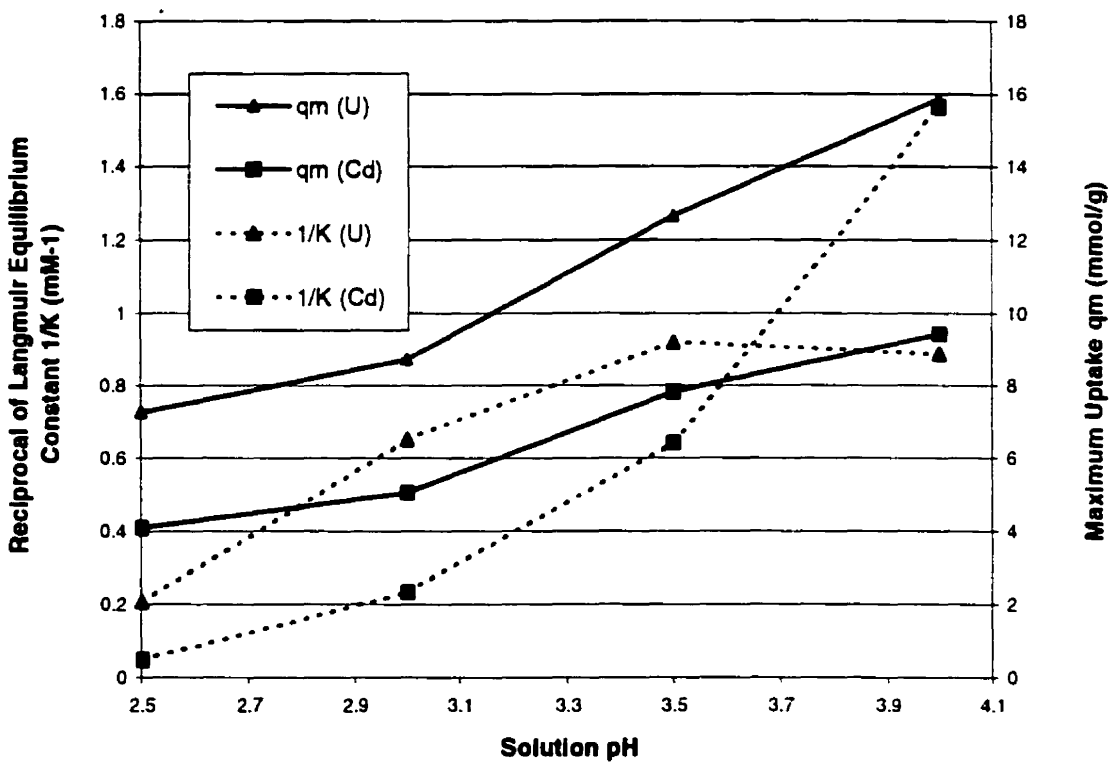

Figure 4.1.3: Influence of solution pH on the Langmuir model parameters for uranium and cadmium biosorption.

Figures 4.1.1 and 4.1.2, illustrate that the Langmuir isotherm model fits well for cadmium at all pH levels but it produces a relatively large deviation for uranium isotherms at pH 3.5 and pH 4.0. Although the trend of isotherms at pH 3.5 and pH 4.0 agree with the experimental data, trend analyses of residuals, described by Himmelblau (1970), shows that the Langmuir model can not fit the data well at pH 3.5 and pH 4.0. In later sections 4.1.4 - 4.16, a more accurate isotherm model will be developed for uranium biosorption equilibrium. It has been well established that sorption of various metal species, such as Cd^{2+}, Cu^{2+}, Zn^{2+}, Pb^{2+}, Ni^{2+}, Mn^{2+}, Al^{3+} and Co^{2+} increases with increasing solution pH whereby metal hydroxides generally become thermodynamically favored over the divalent species. (Ferguson and Bubela, 1974; Holan, et al., 1993; Ramelow, et al., 1992; Darnall, et al., 1986; Greene, et al., 1987; Kuyucak and Volesky, 1989a; Tsezos and Volesky, 1981; Greene, et l., 1986a; Tobin, et al., 1984). Only a few metal ions such as Ag^{+} , Au^{+} and Hg^{2+}, in aqueous solution either form negatively charged complexes or have a strong tendency to sorb by forming covalent bonds. In those cases, the increase in solution pH would decrease the sorption uptake or would not affect the sorption at all (Ramelow, et al., 1992; Greene, et al., 1986b; Greene, et al., 1987).

There are several possible ways in which the solution pH can influence metal biosorption. First of all, the state of the active binding sites on the biomass may change at different pH values. For *Sargassum* biomass, the binding groups are acidic and the availability of free sites is dependent on the solution pH. At low pH, protons would compete for active binding sites with metal ions (Greene, et al., 1986a; Tobin, et al., 1984). The protonation of active sites thus tends to decrease the metal sorption. At a low enough pH, all the binding sites may be protonated, thereby desorbing all originally bound metals from the biomass (Aldor, 1995). Second, extreme pH levels, such as those usually employed in the process of biosorbent regeneration, may cause structural damage of the sorbent material. The degree of damage depends on the type of biomass material used. Under acidic conditions, the pre-protonated *Sargassum* biomass demonstrated stability (no visible structure damage and only slight weight loss). However, under base conditions, extraction of alginate from *Sargassum* biomass decreased the binding capacity significantly. (Fourest and Volesky, 1997). Last but not least, the solution pH

may significantly influence the ionic speciation of some types of metals, such as uranium. At lower solution pH, the metal ion is the predominant form in the solution. But metal hydrolysis occurs at higher solution pH whereby these hydroxide complexes represent a significant percentage of the overall speciation. The hydrolysis of the uranyl ions in aqueous solution is significant at higher solution pH value, such as pH 4.0. Numerous hydroxides of U(VI) are known, and $(UO_2)_2(OH)_2^{2+}{\cdot}H_2O$ is the stable specie in the presence of water at 25°C (Base and Mesmer, 1976a). An illustration for the distribution of the uranium hydrolysis products at 0.1 M and 10^{-5} M uranium concentration in the aqueous solution over a pH range is shown in Figure 4.1.4. At 0.1 M concentration, the percentage of UO_2^{2+} decreases while those for $(UO_2)_2(OH)_2^{2+}$ and $(UO_2)_3(OH)_5^{2+}$ increase with an increase in solution pH. At pH 4.0, the concentration of $(UO_2)_2(OH)_2^{2+}$ can constitute approximately 60% of the total uranium concentration.

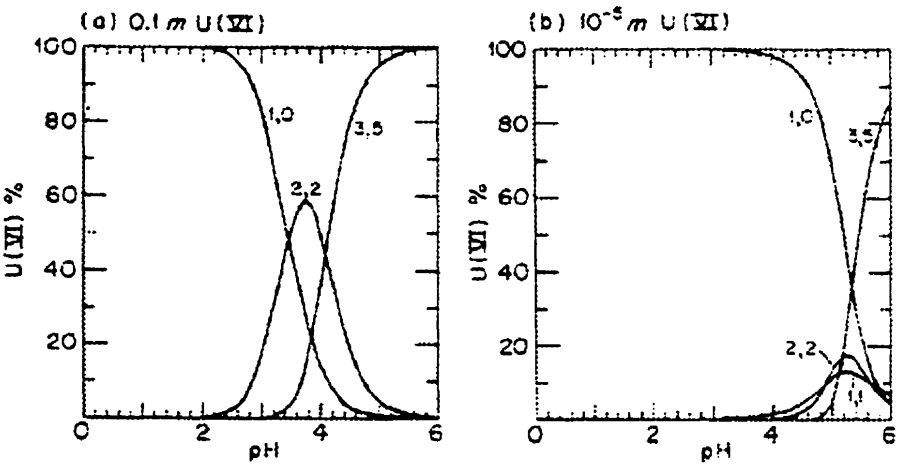

Figure 4.1.4 Distribution of uranium hydrolysis products (reproduced from Base and Mesmer, 1976a). (1, 0): UO_2^{2+}; (2, 2): $(UO_2)_2(OH)_2^{2+}$; (3, 5): $(UO_2)_3(OH)_5^{2+}$.

The uranium concentration in this study ranges from 0 – 6.0 mM. Both diagrams in Figure 4.1.4 do not well depict the distribution of the ionic composition for this concentration range. An extensively used chemical equilibria calculation program, MINEQL+ (Schecher, 1991) is applied in order to obtain the uranium ionic composition

distribution in aqueous solution in the uranium concentration range of 0 – 4.0 mM under pH 4.0. The results are illustrated in Figure 4.1.5. The hydrolyzed uranium complex ions, especially $(UO_2)_2(OH)_2^{2+}$, contributes 10 – 40% of the total uranium concentration within the range of 0.5 – 4.0 mM at pH 4.0. The uranium complexes may have even higher affinity for the biomass binding sites in some instances which results in an enhancement of biosorption performance at higher solution pH (Baes and Mesmer, 1976c; Morel, 1983; Stumm and Morgan, 1970). The binding of the hydrolyzed uranium complex ions may drive the hydrolysis reaction toward to the formation of hydrolyzed complex ions. The quantitative calculation of the binding of the hydrolyzed ions will be discussed later in section 4.1.5. The much higher uranium biosorption uptakes that occur at pH 3.5 and 4.0 compared to those of cadmium may be attributed to the influence of this hydrolysis since the binding of hydrolyzed ions results in more uranium bound by the biomass.

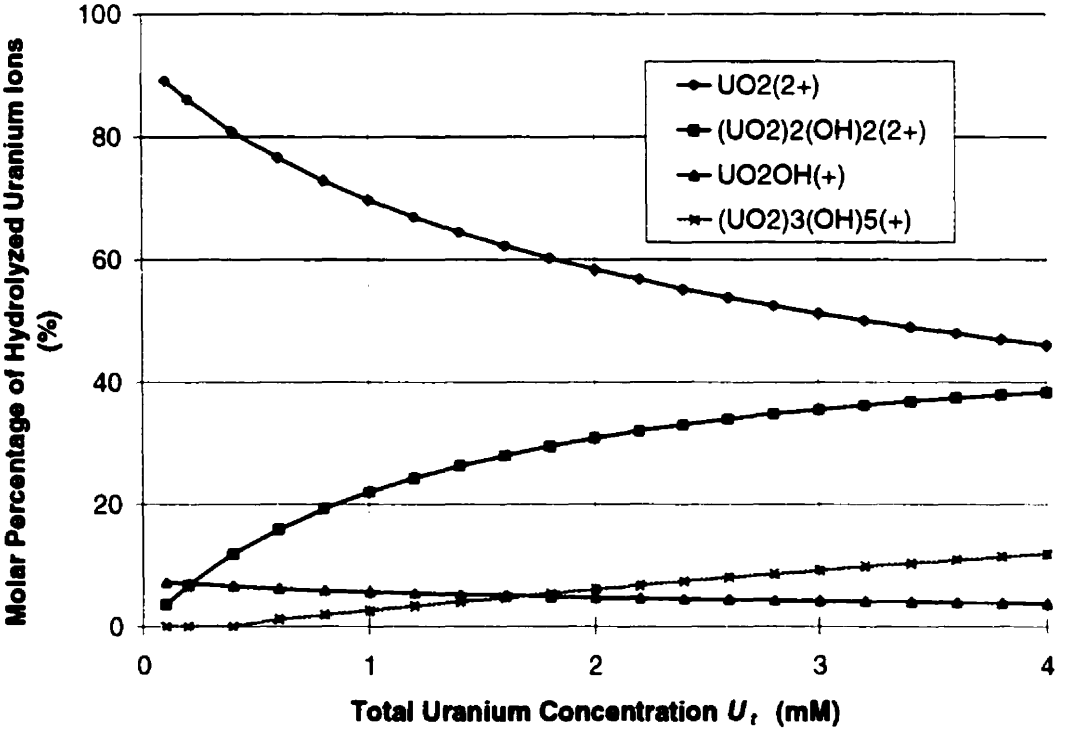

Figure 4.1.5. Ionic composition of hydrolyzed uranium ions at pH 4.0.

(Obtained from running program MINEQL$^+$ (Schecher, 1991), $UO_2^{2+} + NO_3^- + H_2O + H^+$ system, pH 4.0, multiple run for total concentration.)

4.1.2 Influence of anions and light metals

The sulphate group (SO_4^{2-}) is present in authentic uranium-containing waste water and the influence of this anion on the biosorption of uranium was also investigated. The biosorption uptake was investigated using uranyl nitrate and uranyl sulphate for a fixed initial uranium concentration at a pH of 2.5 4.0. The results are illustrated in Table 4.1.2.

Table 4.1.2 Influence of sulphate group (SO_4^{2-}) on the uranium uptake

Uranium uptake (mg/g) at pH 2.5				Uranium uptake (mg/g) at pH 4.0			
U_0 (ppm)	UO_2SO_4	$UO_2(NO_3)_2$	E (%)	U_0 (ppm)	UO_2SO_4	$UO_2(NO_3)_2$	E (%)
30	12.1	11.9	-1.7	30	14.8	14.9	0.8
100	33.9	34.6	2.1	150	72.7	73.9	1.6
200	70.7	70.0	-1.0	250	125.1	123.5	-1.3
400	104.9	103.7	-1.1	400	185.8	187.1	0.7
600	124.9	126.9	1.7	550	227.9	230.9	1.4

U_0 is the initial uranium concentration. E is the deviation.

No significant difference in uranium biosorption uptake was observed for both anionic groups at various solution pH values and initial uranium concentrations. Hu et al (1996) investigated inhibition by sulphate on the uranium biosorption of *P. aeruginosa* biomass. Its uranium uptake was not affected significantly by the presence of sulphate even at concentrations as high as 30,000 mg/L. Schiewer (1995) reported that the effect of light metals, such as Na, Mg and Ca, on the heavy metal uptakes can be ignored. Since the light metals were in chloride salt, this also means that the effect of chloride on the heavy metal uptake is minor too. Therefore the influence of anions on the biosorption of uranium and cadmium can be ignored.

LiOH was added to the heavy metal solution in order to maintain a constant pH value during the sorption process. Similar to other light metals, Li^+ cations can not

compete with heavy metal cations for biomass binding sites. Lithium uptake as measured during uranium biosorption is illustrated in Table 4.1.3. The lithium concentration was determined by ICP-AES (wavelength 367.8 nm) simultaneously with the uranium analyses. The lithium uptake compared to uranium binding was less than 0.2% for different lithium concentrations used in the batch sorption experiments. For this reason, interference by lithium was neglected in the biosorption of uranium.

Table 4.1.3 Influence of Li^+ concentration on the uranium uptake

C_L (ppm)	C_U (ppm)	q_L (mg/g)	q_U (mg/g)	q_L / q_U	pH
6.4	77.4	0.18	116.6	0.15%	2.8
7.2	6.2	0.08	52.4	0.15%	3.2
13.6	40.2	0.08	136.7	0.05%	3.0
26.5	17.2	0.29	201.2	0.14%	3.9
35.3	97.7	0.32	235.2	0.14%	4.0
45.7	143.5	0.39	247.2	0.16%	4.0

4.1.3 Desorption of bound metal from biomass

In order to apply biosorption technology for industrial effluent treatment, the desorption of bound metals and the subsequent regeneration of the biosorbent should be investigated. The desorption process may not only eliminate potential secondary pollution produced by metal-bearing biomass sludge but also may improve process economics by reusing the biosorbent in multiple uptake-desorption cycles. The diluted mineral acids H_2SO_4, HNO_3 and HCl were effective in desorption of bound uranium and cadmium from *Sargassum* biomass and the damage to the biomass caused by the exposure to the acid was negligible. Figure 4.1.6 demonstrates the elution of the uranium from the uranium-laden biomass with 0.1 N HCl solution, where the elution efficiency is plotted *versus* initial uranium loading.

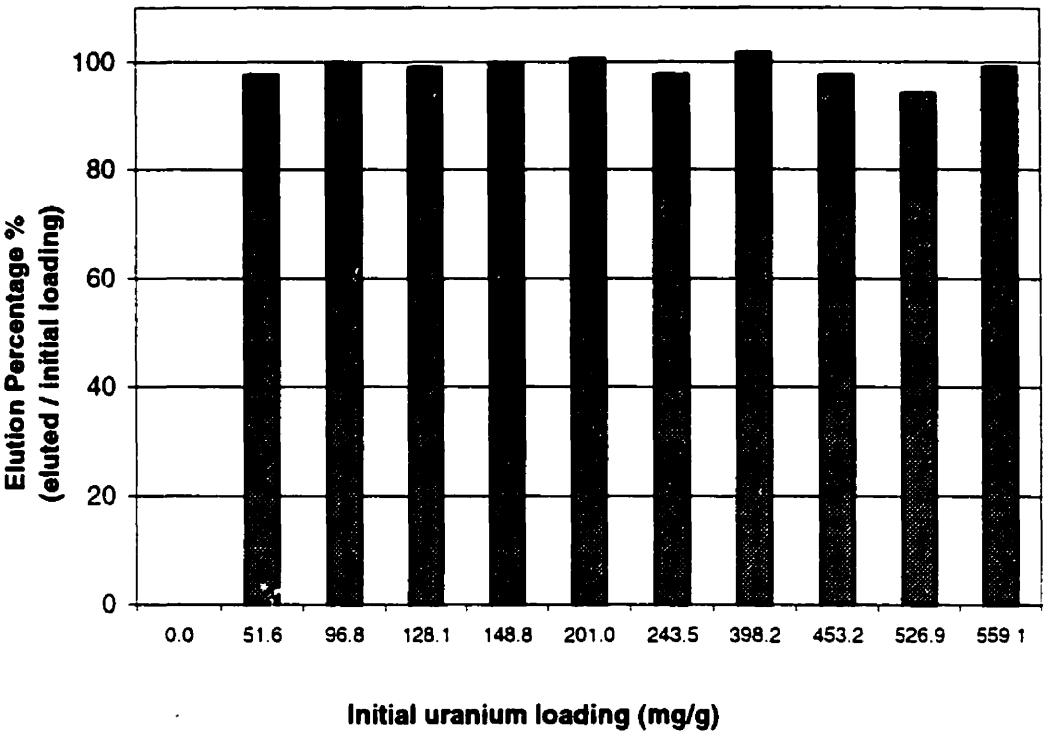

Figure 4.1.6: Uranium elution with 0.1 N HCl

The biomass weight loss during the acidic desorption process was observed to be relatively small (around 4%). The experimental data for the eluted uranium was corrected for biomass weight loss. It can be noticed that the elution efficiency is always close to unity, indicating that the elution with 0.1 N HCl was complete. The higher than unity elution efficiency is within the analytical error.

The desorption of cadmium with 0.1 N HCl yielded results similar to those for uranium as shown in Figure 4.1.6. When the cadmium uptake under acidic conditions (0.1 N HCl) was determined quantitatively, it yielded only a very flat isotherm shown in Figure 4.1.7. Over a wide concentration range, the cadmium isotherm displayed a nearly linear pattern, with less than 0.08 mmol/g cadmium uptake even at very high equilibrium concentration of 80 mM.

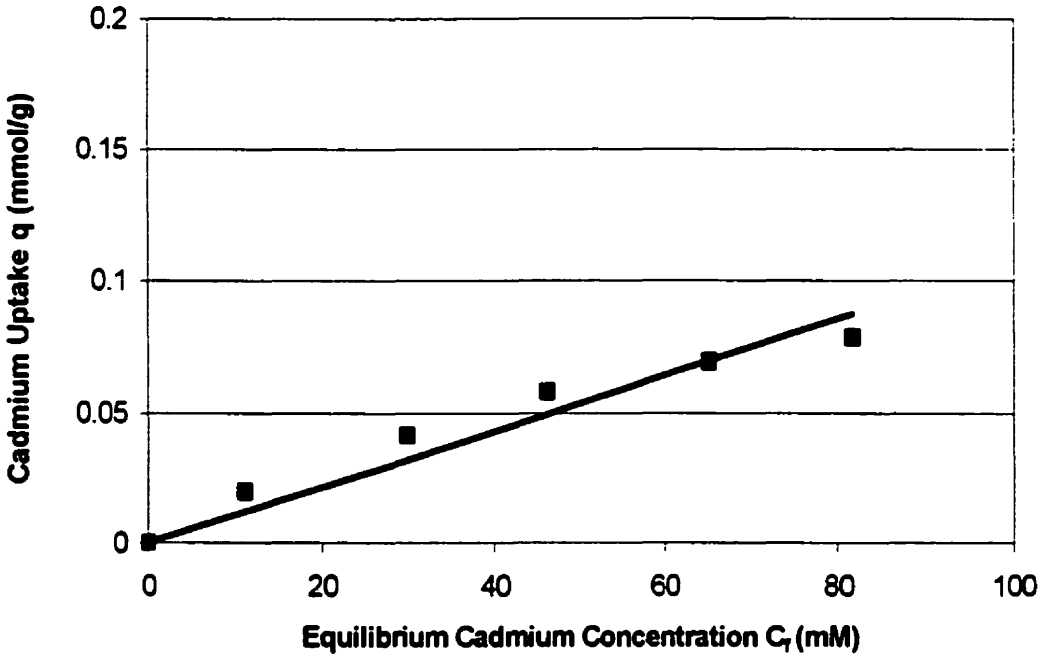

Figure 4.1.7: Cadmium isotherm under acidic conditions (0.1 N HCl).

Hydrochloric acid has been recognized as an effective eluant (Brooks, 1991; Goto et al., 1993; Holan et al., 1993). The desorption of heavy metals from biomass was the result of a competition between protons and heavy metal ions under acidic conditions. Active site protonation is favored at low solution pH levels and the competition between protons and metals has been documented by many researchers (Brooks, 1991; Crist et al., 1990; Fourest and Roux, 1992). In addition to the mineral acids, many other elution agents, such as $NaHCO_3$, Na_2CO_3, $(NH_4)_2SO_4$, were also used for desorption of bound heavy metals from various types of biomass. Carbonate and bicarbonate have proven to be effective for the desorption of uranium from fungal biomass (Tsezos, 1984). Ammonium ions may also act as competing cations or a cadmium complexing agent (Muzzarelli, 1972). The high elution efficiency, low biomass damage and low-cost make diluted mineral acid elution appropriate for further application. An additional advantage of using acid for desorption is that the biomass becomes protonated at the same time and is ready for the next run of metal biosorption.

4.1.4 Sorption stoichiometry for different pH values.

The biosorption of heavy metals on to protonated *Sargassum* biomass was always accompanied by the release of protons from the biomass, which would normally cause a decrease in the solution pH. In order to maintain constant solution pH values, a LiOH solution was added into the sorption system. Since the sorption of lithium on to the biomass was negligible (Table 4.1.3), the added LiOH was mainly consumed for the neutralization of released protons. Uranium or cadmium uptakes were proportional to the amount of LiOH added to the solution and the ratio of moles of the uranium or cadmium sorption to that of LiOH consumption was approximately 1 : 2. Figure 4.1.8 demonstrates this linear relationship for uranium biosorption at various solution pH values. The result for cadmium was similar and is not shown.

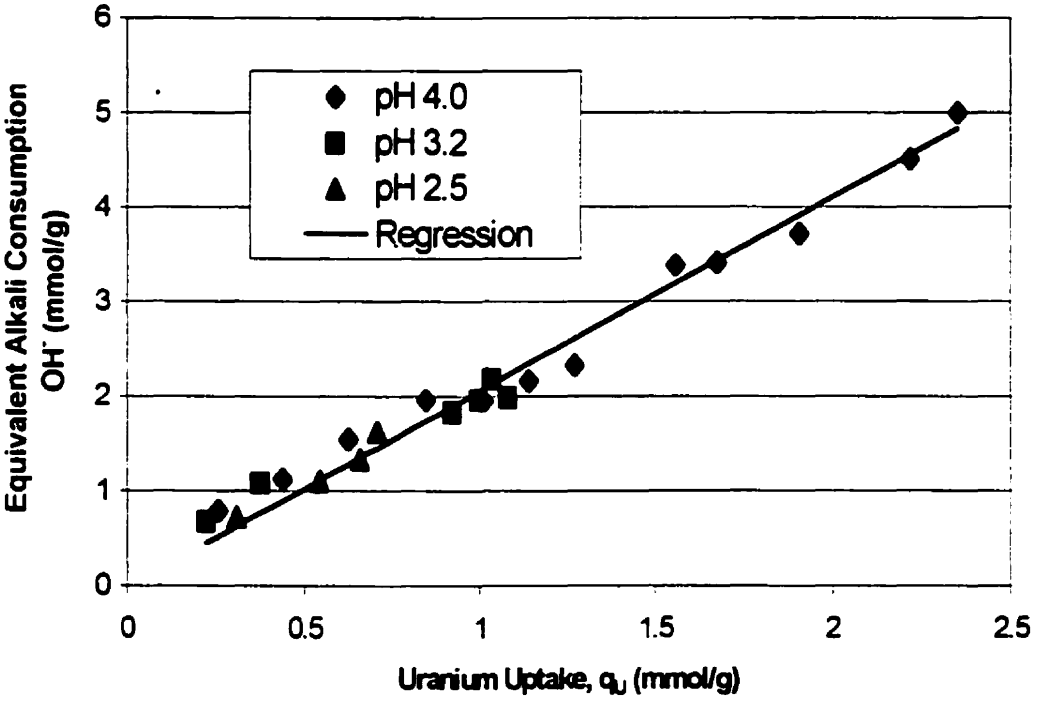

Figure 4.1.8: Comparison of uranium uptake and LiOH consumption.

Ion exchange was considered to play an important role in the metal sequestration mechanism of algal biomass (Crist, et al., 1993; Crist, et al., 1988; Schiewer and

Volesky, 1995). 1:2 linear sorption stoichiometry is an indication of ion exchange taking place between the divalent uranyl ions (UO_2^{2+}) and cadmium ions with monovalent protons on the biomass. The specific biosorption mechanism for uranium and cadmium are quite different. For cadmium, the free Cd^{2+} ions are the predominant form at the experimental pH and concentration ranges where no other speciation of cadmium ions occurs. The ion exchange between cadmium and protons was stoichiometric. The maximum experimental cadmium uptake, 1.95 meq/g (0.975 mmol/g), is close to the concentration of biomass binding sites, 2.25 meq/g, which was determined by acid-base titration of the *Sargassum* biomass (Schiewer, et al., 1995, Fourest et al., 1996). For uranium biosorption, the maximum experimental uptake values at pH 3.5 and pH 4.0 are 2.97 and 3.60 meq/g, respectively. Both values exceed the amount of the biomass binding sites. The control samples demonstrated that very high uranium uptake could not be attributed to micro-precipitation. This phenomenon could not be explained by the ion exchange between UO_2^{2+} and protons either. The hydrolysis of uranium ions in aqueous solution must be taken into consideration.

4.1.5 HIEM model for uranium biosorption isotherm

It would be helpful and time-saving to have a mathematical model capable of predicting the final uranium metal uptake at a given equilibrium condition. The solution pH plays an important role in the biosorption process in which ion exchange between metal ions and protons occurs. However, conventional sorption models, (e.g. the Langmuir or Freundlich), can not predict sorption as a function of proton concentration. The ion exchange based Schiewer model is generally able to do so. However, it does not successfully describe uranium uptake which exceeds stoichiometric biomass binding capacity. In this section, a new equilibrium sorption isotherm model, the Hydrolysed Ion Exchange Model (HIEM), which is based on ion exchange and hydrolysis of uranium complex ions, is developed. The model assumptions are as follows:

1. In the range of acidic to near neutral pH values, the uranyl cation UO_2^{2+} is hydrolysed in an aqueous solution. The four major products of uranium hydrolysis are the complex ions, UO_2^{2+}, $(UO_2)_2(OH)_2^{2+}$, UO_2OH^+ and $(UO_2)_3(OH)_5^+$, that

exist in hydrolysis equilibrium. The speciation of hydrolysed uranium depends on the solution pH and on the total uranium concentration in the solution.

2. The ion exchange reaction takes place between various hydrolysed uranium ions and protons of the biomass binding sites and equilibrium is reached for all forms of complex uranium ions. Carbonate and sulphate functional groups are treated identically for simplicity.
3. Total uranium uptake is attributed to the binding of all forms of hydrolysed uranium ions by the biomass.

The hydrolysis equilibria of uranium metal ions obeys the following stoichiometric relationships (Baes and Mesmer, 1976b):

$$2\,UO_2^{2+} + 4H_2O \leftrightarrow (UO_2)_2(OH)_2^{2+} + 2\,H_3O^+ \qquad pK = 5.62 \qquad (4.1\text{-}1)$$

$$UO_2^{2+} + 2H_2O \leftrightarrow UO_2OH^+ + H_3O^+ \qquad pK = 5.80 \qquad (4.1\text{-}2)$$

$$3UO_2^{2+} + 10H_2O \leftrightarrow (UO_2)_3(OH)_5^+ + 5H_3O^+ \qquad pK = 15.63 \qquad (4.1\text{-}3)$$

where *pK*s are the negative logarithms of the equilibrium constants.

As indicated by the *pK* value in Equation (4.1-3), the contribution of the uranium complex ion $(UO_2)_3(OH)_5^+$ to the overall uranium biosorption can be neglected in the model development. The hydrolysis equilibrium constants for equations (4.1-1) and (4.1-2) are expressed with activities of the ions in the following manner:

$$K_{eq}^a = \frac{a_Y a_H^2}{a_X^2} = \left(\frac{\gamma_Y \gamma_H^2}{\gamma_X^2}\right)\left(\frac{[Y][H]^2}{[X]^2}\right) = 10^{-5.62} \qquad (4.1\text{-}4)$$

$$K_{eq}^a = \frac{a_Z a_H}{a_X} = \left(\frac{\gamma_Z \gamma_H}{\gamma_X}\right)\left(\frac{[Z][H]}{[X]}\right) = 10^{-5.80} \qquad (4.1\text{-}5)$$

where K^a_{ey} and K^a_{ez} are the equilibrium constants for equations (4.1-1) and (4.1-2), respectively. *X*, *Y* and *Z* represent ionic species UO_2^{2+}, $(UO_2)_2(OH)_2^{2+}$ and $(UO_2)(OH)^+$, respectively. The a_i and γ_i represent activity and activity coefficients of *X*, *Y*, and *Z*, respectively.

Rewriting the above equations (4.1-4) and (4.1-5), we obtain:

$$K_{ey} = \frac{K^a_{ey}}{\left(\frac{\gamma_Y \gamma_H^2}{\gamma_X^2}\right)} = \frac{K^a_{ey}}{\gamma_\alpha} = \frac{[Y][H]^2}{[X]^2} \qquad (4.1\text{-}6)$$

$$K_{ez} = \frac{K^a_{ez}}{\left(\frac{\gamma_Z \gamma_H}{\gamma_X}\right)} = \frac{K^a_{ez}}{\gamma_\beta} = \frac{[Z][H]}{[X]} \qquad (4.1\text{-}7)$$

where K_{ey} and K_{ez} are the apparent equilibrium constants for equations (4.1-1) and (4.1-2), respectively. The parameters γ_α and γ_β are the overall activity coefficients, which can be calculated from the activities of the individual ions in the solution.

$$\gamma_\alpha = \frac{\gamma_Y \gamma_H^2}{\gamma_X^2} \qquad (4.1\text{-}8)$$

$$\gamma_\beta = \frac{\gamma_Z \gamma_H}{\gamma_X}. \qquad (4.1\text{-}9)$$

The activity coefficients for the individual ions in equations (4.1-8) and (4.1-9) can be evaluated using Davies equation and will be discussed later in section 4.1.6.

The binding of divalent cations to alginic acid was described by Rees and co-workers (1981). Alginates are thought to adopt an ordered solution conformation, through dimerization of the polyguluronic sequences in the presence of calcium or other divalent cations of similar size. The rigid and buckled shape of the poly-L-guluronic sections results in an alignment of two chain sections yielding an array of coordination sites with cavities suitable for calcium (and other metal cations or complexes). These

cavities are favorable to ionic species because they are lined with carboxylate and other electronegative oxygen atoms. This description is known as the "egg-box" model (Morris et al., 1980; Rees, 1981). Distances between the chains are flexible (Grant et al., 1973, Morris et al., 1978) and therefore alginic acid based biomass can easily accommodate many kinds of metal cations or metal complexes.

Based on the assumption of ion exchange between all forms of uranium ions and protons on the biomass binding sites, the following equilibrium equations are proposed:

$$H^+ + B \leftrightarrow HB, \qquad K_h = [HB] / [H] [B] \qquad (4.1\text{-}10)$$

$$X + 2B \leftrightarrow 2X_{0.5}B \qquad K_x = [X_{0.5}B]^2 / [X] [B]^2 \qquad (4.1\text{-}11)$$

$$Y + 2B \leftrightarrow 2Y_{0.5}B \qquad K_y = [Y_{0.5}B]^2 / [Y] [B]^2 \qquad (4.1\text{-}12)$$

$$Z + B \leftrightarrow ZB \qquad K_z = [ZB] / [Z] [B] \qquad (4.1\text{-}13)$$

where K_h, K_x, K_y and K_z are the equilibrium formation constants for the binding of hydrolyzed ions on to the biomass. The formulation for the complex divalent uranium ionic groups and biomass binding sites was chosen to be $2M_{0.5}B$ instead of M_2B. This is meant to emphasize not only the role of electrostatic attraction in metal binding but also that of complexation since two bonds have to be broken between the metal ion and the biomass (Buffle, 1988; Schiewer and Volesky, 1995).

The total number of binding sites on the biomass is distributed among all the bound forms of hydrolyzed uranium ions and protons as well as with residual free sites:

$$C_t = [B] + [HB] + [X_{0.5}B] + [Y_{0.5}B] + [ZB] \qquad (4.1\text{-}14)$$

where C_t and $[B]$ are the concentrations of the total and free binding sites, respectively.

Upon substituting of equations (4.1-10) - (4.1-13) into equation (4.1-14), the concentration of free binding sites in the equilibrium system is obtained as follows:

$$[B] = \frac{C_t}{1+K_h[H]+\sqrt{K_x[X]}+\frac{[X]}{[H]}\left(\sqrt{K_{cy}K_y}+K_{cz}K_z\right)} \quad (4.1\text{-}15)$$

Substituting equation (4.1-15) into equations (4.1-10), (4.1-11), (4.1-12) and (4.1-13), respectively, we obtain:

$$q_H = [HB] = \frac{C_t K_h[H]}{1+K_h[H]+\sqrt{K_x[X]}+\frac{[X]}{[H]}\left(\sqrt{K_{cy}K_y}+K_{cz}K_z\right)} \quad (4.1\text{-}16)$$

$$[X_{0.5}B] = \frac{C_t \sqrt{K_x[X]}}{1+K_h[H]+\sqrt{K_x[X]}+\frac{[X]}{[H]}\left(\sqrt{K_{cy}K_y}+K_{cz}K_z\right)} \quad (4.1\text{-}17)$$

$$[Y_{0.5}B] = \frac{C_t \frac{[X]}{[H]}\sqrt{K_{cy}K_y}}{1+K_h[H]+\sqrt{K_x[X]}+\frac{[X]}{[H]}\left(\sqrt{K_{cy}K_y}+K_{cz}K_z\right)} \quad (4.1\text{-}18)$$

$$[ZB] = \frac{C_t \frac{[X]}{[H]}K_{cz}K_z}{1+K_h[H]+\sqrt{K_x[X]}+\frac{[X]}{[H]}\left(\sqrt{K_{cy}K_y}+K_{cz}K_z\right)} \quad (4.1\text{-}19)$$

Equation (4.1-16) may be used for the calculation of proton sorption on the biomass at any given uranium concentration level and solution pH. The total uranium uptake q_U is calculated as the summation of all the bound forms of uranium ions, i.e.:

$$q_U = 0.5\,[X_{0.5}B] + (2\text{x}0.5)\,[Y_{0.5}B] + [ZB] \quad (4.1\text{-}20)$$

$[X_{0.5}B]$, $[Y_{0.5}B]$ and $[ZB]$ were substituted from equations (4.1-17) - (4.1-19) into equation (4.1-20) and the following equation was obtained:

$$q_U = \frac{C_t\left(0.5\sqrt{K_x[X]}+\frac{[X]}{[H]}\left(\sqrt{K_{cy}K_y}+K_{cz}K_z\right)\right)}{1+K_h[H]+\sqrt{K_x[X]}+\frac{[X]}{[H]}\left(\sqrt{K_{cy}K_y}+K_{cz}K_z\right)} \qquad (4.1\text{-}21)$$

From equation (4.1-21), the uranium uptake may be calculated from the solution pH, or proton concentration *[H]* and the concentration of the free uranyl ion UO_2^{2+}, *[X]*. Although the mathematical form of equation (4.1-21) is similar to that of the multicomponent Langmuir sorption isotherm as adapted by Hill (1977), its underlying assumption is completely different. The HIEM model considers ion exchange in addition to simple competition for free binding sites whereby no reverse reaction takes place. In equation (4.1-21), the concentration of the free uranium ion *[X]* is not necessarily the same as the total uranium concentration for the solution since hydrolysis takes place. In other words, *[X]* can not be measured directly and it must be evaluated from the measurable parameter (the total uranium concentration) through a hydrolysis equilibrium calculation. Normally this may be done using a computer program such as MINEQL$^+$ (Schecher, 1991), which is a software used for chemical equilibria calculations. However, it would be more useful to derive a formula that expresses the concentration of the complexion ions as an explicit function of the measurable total uranium concentration and the pH value.

The total uranium concentration U_t in the solution consists of free ions and all the major hydrolyzed ions:

$$\begin{aligned} U_t &= [UO_2^{2+}] + 2[(UO_2)_2(OH)_2^{2+}] + [(UO_2)(OH)^+] \\ &= [X] + 2[Y] + [Z] \end{aligned} \qquad (4.1\text{-}22)$$

Substituting [*Y*] from the hydrolysis equilibrium equation (4.1-4) and [*Z*] from equation (4.1-5) into equation (4.1-22), the following mass balance results:

$$U_t = [X] + 2K_{cy}[X]^2/[H]^2 + K_{cz}[X]/[H] \qquad (4.1\text{-}23)$$

When LiOH is added to the system to maintain solution pH, the electroneutrality condition is given by:

$$[NO_3^-] + [OH^-] + [A^-] = [H^+] + [Li^+] + 2[UO_2^{2+}] + 2[(UO_2)_2(OH)_2^{2+}] + [(UO_2)(OH)^+]$$
$$= [H^+] + [Li^+] + 2[X] + 2[Y] + [Z] \quad (4.1\text{-}24)$$

where nitrate appears in the solution as a co-ion released from uranyl nitrate and its concentration $[NO_3^-]$ remains constant in the system. $[A^-]$ is the concentration of other anions in the solution.

Based on water equilibrium constant K_w, we can express the concentration of hydroxide as:

$$[OH^-] = 10^{-14} / [H^+] \quad (4.1\text{-}25)$$

Substituting the above water equilibrium equation (4.1-25) and hydrolysis equilibrium equations (4.1-6) and (4.1-7) into charge-balance equation (4.1-24), we obtain:

$$[NO_3^-] + [A^-] + 10^{-14} / [H^+] = [H^+] + [Li^+] + 2[X] + 2K_{cy}[X]^2/[H^+]^2 + K_{cz}[X]/[H^+] \quad (4.1\text{-}26)$$

Equation (4.1-26) can be solved for $[X]$ which represents the uranyl concentration:

$$[X] = \frac{[H]^2\left\{\sqrt{\left(\frac{K_{cz}}{[H^+]}+2\right)^2 + \frac{8K_{cy}}{[H^+]^2}\left([NO_3^-]+[A^-]+\frac{10^{-14}}{[H^+]}-[H^+]-[Li^+]\right)} - \left(\frac{K_{cz}}{[H^+]}+2\right)\right\}}{4K_{cy}} \quad (4.1\text{-}27)$$

If there are no impurities in the solution and lithium is added as base LiOH to maintain the solution pH, the term $[A^-]$ in the above equation is zero. Therefore, equation (4.1-27) can serve for calculation of the uranyl concentration $[X]$ from the concentrations

of nitrate, lithium and protons in the solution. Consequently, the uranium uptake can also be calculated from those concentrations using equations (4.1-21) and (4.1-27). A complication arises when other non-determined ionic impurities are present in the system. These unknown species, both cations and anions, would have to be accounted for in the charge balance, which would bring them into equation (4.1-27).

Since the relationship between the metal uptake and the equilibrium metal concentration represents the sorption isotherm, it is a preferable alternative to express the uranyl concentration [*X*] as a function of the total uranium concentration and proton concentration. In fact, the total uranium concentration is the parameter most conveniently determined during batch experiments. Therefore, it is more feasible to determine the uranyl concentration through measuring total uranium concentration than through measuring all *other* ionic species in the system. For a batch equilibrium system whereby solution pH is maintained at a known level, the mass balance equation (4.1-22) can be easily solved to achieve this purpose. The resulting expression of uranyl concentration [*X*] is as follows:

$$[X] = \frac{[H]\left(\sqrt{([H]+K_{cz})^2 + 8K_{cy}U_t} - ([H]+K_{cz}) \right)}{4K_{cy}} \qquad (4.1\text{-}28)$$

As a result, the equilibrium uranium uptake can be calculated from the total uranium concentration and proton concentration in solution.

Thus, for a equilibrium batch system under a fixed solution pH, the concentrations of the hydrolyzed uranium species can be calculated by two methods, either using the charge balance equation (4.1-27) or the mass balance equation (4.1-28). The results calculated from both methods are listed and compared in Tables 4.1- 4 and 4.1-5 at pH 4.0 and pH 3.8, respectively. For each section in the tables, the upper row represents the results of equation (4.1-27) and the middle row represents results from equation (4.1-28). The lithium concentration and solution pH are measured experimentally. The nitrate concentration is inferred from the known molecular formula stoichiometry. Since no other anions except [NO_3^-] and [OH^-] are present in the system, [A^-] = 0.

Table 4.1.4. Calculation results from equation (4.1-27) and equation (4.1-28), pH 4.0

	[X] (mM)	[Y] (mM)	[Z] (mM)	U_t = [X]+2[Y]+[Z] (mM)
$[NO_3^-]$ =1.0 mM $[Li^+]$= 0 pH = 4.02	0.41	4.4×10^{-2}	6.8×10^{-3}	0.50
U_t = 0.5 mM pH = 4.0	0.41	4.4×10^{-2}	6.8×10^{-3}	0.50
Difference	0	0	0	0
$[NO_3^-]$ =2.0 mM $[Li^+]$= 0.15 mM pH = 4.0	0.74	0.13	1.2×10^{-2}	1.01
U_t = 1 mM pH = 4.0	0.73	0.13	1.2×10^{-2}	1.00
Difference	-1.4%	0	0	-1.0%
$[NO_3^-]$ =4 .0 mM $[Li^+]$= 0.64 mM pH = 4.0	1.25	0.37	2.0×10^{-2}	2.01
U_t = 2.0 mM pH = 4.0	1.24	0.37	2.0×10^{-2}	2.00
Difference	-0.8%	0	0	-0.5%
$[NO_3^-]$ =10.0 mM $[Li^+]$= 2.62 mM pH = 4.0	2.32	1.29	3.7×10^{-2}	4.95
U_t = 5.0 mM pH = 4.0	2.34	1.31	3.7×10^{-2}	5.00
Difference	+0.9%	+1.6%	0	+1.0%

Table 4.1.5. Calculation results from equation (4.1-27) and equation (4.1-28), pH 3.8

	[X] (mM)	[Y] (mM)	[Z] (mM)	U_t = [X]+2[Y]+[Z] (mM)
$[NO_3^-]$ =2.0 mM $[Li^+]$= 0 pH = 3.80	0.85	6.9×10^{-2}	8.5×10^{-3}	0.99
U_t = 1.0 mM pH = 3.80	0.85	6.9×10^{-2}	8.5×10^{-3}	1.00
Difference	0	0	0	+1.0%
$[NO_3^-]$ =4.0 mM $[Li^+]$= 0.25 mM pH = 3.79	1.56	0.22	1.5×10^{-2}	2.02
U_t = 2.0 mM pH = 3.79	1.55	0.22	1.5×10^{-2}	2.00
Difference	-0.6%	0	0	0
$[NO_3^-]$ =10.0 mM $[Li^+]$= 1.574 mM pH = 3.81	3.14	0.98	3.2×10^{-2}	5.14
U_t = 5.0 mM pH = 3.81	3.08	0.95	3.2×10^{-2}	5.00
Difference	-1.9%	-3.1%	0	-2.7%

It can be seen that concentrations of hydrolyzed uranium species calculated with using equation (4.1-27) and equation (4.1-28) agree well within a maximum difference of 3.1%. The charge balance equation (4.1-24) is obeyed if the values of [X], [Y] and [Z] calculated by mass balance equation (4.1-28) in the above tables are substituted. For

example, at pH 4.0 and total uranium concentration 2.0 mM, the lithium concentration calculated by equation (4.1-24) is 0.66 mM which is very close to the experimentally measured value, 0.64 mM. Since determination of equilibrium uranium concentration in the solution is easier than measuring concentrations of all ionic species except uranium, the mass balance based equation (4.1-28) will be adopted because of its simplicity for further model calculations instead of the charge balance equation. It should, however, be noted that this method is valid only for batch equilibrium systems when pH is controlled. Without specifying the equilibrium solution pH, incorporation of only the mass balance equation is not sufficient for solving the equilibrium system compositions from the initial concentrations. Since biosorption applications are performed under a controlled solution pH in many cases, this method is still useful for those situations.

Equations (4.1-16), (4.1-21) and (4.1-28) express the proton uptake and the uranium biosorption uptake as an explicit function of the total uranium concentration and the solution pH which fulfils the main modelling objective of sorption isotherm study.

If hydrolysis is neglected, the hydrolysis constants in equations (4.1-6) and (4.1-7) become zero, i.e. $K_{cy} = K_{cz} = 0$ and the UO_2^{2+} concentration $[X]$ would be the same as the total uranium concentration U_t in Equation (4.1-23). Therefore the HIEM model equation (4.1-21) may be reduced to the form of Scheiwer's model (equation 4.1-29) which was proposed for non-hydrolyzable metal ions such as cadmium, copper and zinc.

$$q_U = \frac{0.5\, C_t \sqrt{K_x [X]}}{1 + K_h [H] + \sqrt{K_x [X]}} \qquad (4.1\text{-}29)$$

4.1.6 Determination of HIEM model parameters and modelling of experimental data

The apparent hydrolysis equilibrium constants K_{cy} and K_{cz} can be calculated from equations (4.1-6) and (4.1-7). The overall activity coefficients γ_α and γ_β can be evaluated from equations (4.1-8), (4.1-9) and Davies equation (Stumn and Morgan, 1996):

$$\lg \gamma_i = -0.5 Z_i^2 \left(\frac{\sqrt{I}}{1+\sqrt{I}} - 0.2I \right) \qquad (I < 0.5\ M) \qquad (4.1\text{-}30)$$

where γ_i and Z_i are the activity coefficient and the charge of the ion, respectively. I is ionic strength in aqueous solution. The ionic strength can be calculated from the concentration of the ions, C_{Zi}, and the charge of ions, Z_i, as follows:

$$I = \frac{1}{2} \sum Z_i^2 C_{Zi} \qquad (4.1\text{-}31)$$

Since the uranium hydrolysis results in the reduction of the total charge of hydrolyzed ions for a given overall uranium concentration in the aqueous solution (stoichiometry equations 4.1-1 and 4.1-2), the accurate calculation of ionic strength and activity coefficients of ions only can be carried out by iteration. In order to obtain an explicit calculation formula, an proper approximation of the overall activity coefficients γ_α and γ_β is necessary. Since γ_α and γ_β are of the same value if they are calculated using Davies equation (4.1-30), both parameters are represented by a new parameter, γ_t. In this study, the typical total uranium concentration ranges from 0 - 6.0 mM. Under pH 4.0 and total uranium concentration of 3.0 mM, the value of γ_t calculated from equations (4.1-8) or (4.1-9) and (4.1-30) is 1.18. This value is used as an approximation of γ_α and γ_β in equations (4.1-6) and (4.1-7). The following tables 4.1.6 and 4.1.7 demonstrate the comparison of the calculated uranyl concentration [X] using equation (4.1-28) with real γ_t values evaluated from equations (4.1-30) and (4.1-31) and with the constant approximation value of $\gamma_t = 1.18$.

Table 4.1. 6 Comparison of [X] calculated with real and approximate γ_t (pH 2.5)

U_t (mM)	I^* (mM)	γ_t	$[X]_{Real}\gamma_t$ (mM)	$[X]\ \gamma_{t=1.18}$ (mM)	Errors (%)
0.1	3.36	1.14	0.10	0.10	0
0.5	4.16	1.15	0.50	0.50	0
1.0	5.16	1.17	1.00	1.00	0
2.0	7.16	1.20	2.00	2.00	0
3.0	9.16	1.23	3.00	3.00	0
4.0	11.16	1.25	3.99	3.99	0
5.0	13.16	1.28	4.99	4.99	0
6.0	15.16	1.30	5.98	5.98	0

* All uranium species are assumed divalent.

Table 4.1.7 Comparison of [X] calculated with real and approximate γ_t (pH 4.0)

U_t (mM)	I^* (mM)	γ_t	$[X]_{Real}\gamma_t$ (mM)	$[X]\ \gamma_{t=1.18}$ (mM)	Error (%)
0.1	0.3	1.04	0.094	0.095	+1.1%
0.5	1.1	1.08	0.42	0.42	0
1.0	2.1	1.11	0.75	0.76	+1.3%
2.0	4.1	1.15	1.29	1.30	+0.8%
3.0	6.1	1.18	1.74	1.74	0
4.0	8.1	1.21	2.15	2.13	-0.9%
5.0	10.1	1.24	2.52	2.48	-1.6%
6.0	12.1	1.26	2.86	2.80	-2.1%

* All uranium species are assumed divalent.

From the above comparison, it can be seen that the approximation with γ_t =1.18 only produce a relative error within 2.1% over a wide uranium concentration range.

Particulary, under low pH 2.5, the calculated uranyl concentrations are close to the total uranium concentrations as they shall be. Therefore, the apparent hydrolysis equilibrium constant can be calculated from equations (4.1-6) and (4.1-7) with $\gamma_\alpha = \gamma_\beta = 1.18$.

The four biosorption equilibrium constants, K_h, K_x, K_y and K_z, for protons and the hydrolyzed uranium complex ions UO_2^{2+}, $(UO_2)_2(OH)_2^{2+}$and UO_2OH^+ are regressed from the uranium isotherm experimental data at various pH values. The total binding capacity of the biomass, C_t, can be determined by acid-base titration of the protonated biomass.

A non-linear least square method was used to find the optimal combination of the parameter sets. The objective function for the optimal regression is as follows:

$$\varphi = \sum_{i=1}^{N} \left(q_{model} - q_{exp}\right)_i^2 \qquad (4.1\text{-}32)$$

where φ is the least-square error, i is the experimental sample number and N is the number of samples. While q_{exp} represents the experimental uranium biosorption uptake, q_{model} stands for that calculated from model equations (4.1-21) and (4.1-28). As part of this thesis a computer program in MATLAB™ (Mathworks, 1993) was developed for regression of these parameters.

The first model parameter C_t, the amount of the biomass binding sites, was determined to be 2.25 mmol/g by acid-base titration of the *Sargassum* biomass (Schiewer et al., 1995; Fourest et al., 1996). At pH 2.5, the free ion UO_2^{2+} is predominant in the uranium solution according to the calculation results from the computer program MINEQL$^+$ (Westall, et al., 1986). The hydrolyzed ions $(UO_2)_2(OH)_2^{2+}$ and UO_2OH^+ are not present in significant quantities at such a low pH. Therefore, setting the values of K_y and K_z to zero is appropriate as an initial guess. K_h and K_x were then regressed by fitting the experimental data to the model at pH 2.5. Next, K_y and K_z were regressed by using experimental data at pH 4.0. An iterative process was used to find the values of K_y and K_z for curves at pH 2.5 and pH 4.0. The regressed parameters are listed in Table 4.1.8. The source code for the MATLAB™ (Mathworks, 1993) regression program used in the above procedure is listed in Appendix A.

Table 4.1.8 HIEM model parameters (for uranium)

C_t (mmol/g)	K_h (L/mol)	K_x (L/mol)	K_y (L/mol)	K_z (L/mol)	E*
2.25	2.32×10^2	1.09×10^3	1.93×10^4	1.25×10^4	5%

* Average relative regression error.

Using the obtained model parameters, the model equations could be applied to predict the uranium isotherms at pH 3.0 and pH 3.5. The experimental isotherm data used in section 4.1.1 for uranium at different pH were used to test the model prediction under given pH values. The results are illustrated in Figure 4.1.9. The scattered points represent the experimental data. The curves at pH 2.5, pH 4.0 are model-fitted whereas those at pH 3.0 and 3.5 are model predictions.

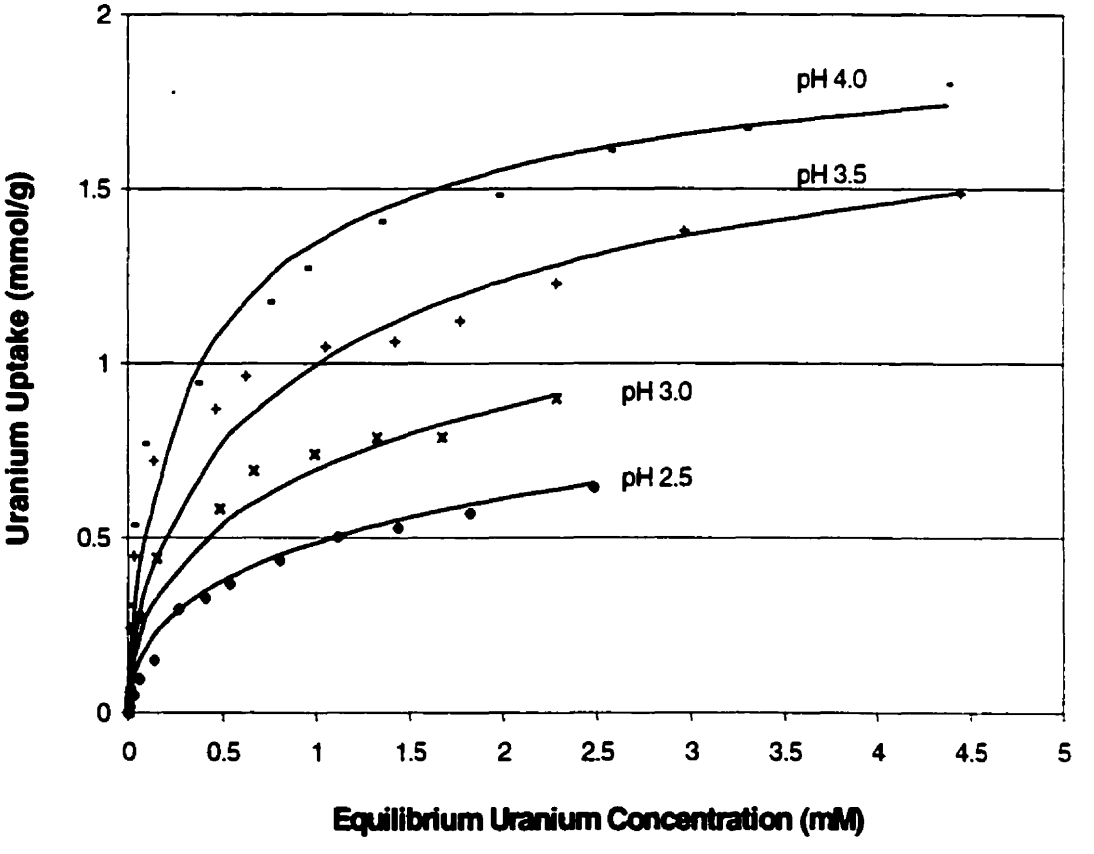

Figure 4.1.9: Comparison of experimental uranium isotherms and HIEM calculations at different solution pH values.

In the above figure, scattered experimental points are the same as those in Figure 4.1.1. Although the solid model curves are similar in appearance in both figures, they are quite different in nature. The HIEM model curves are calculated from the same set of model parameters. However four separate sets of Langmuir parameters were required in order to calculate the curves at various solution pH values in Figure 4.1.1. Experimental observations that uranium uptake at a higher pH and equilibrium concentrations exceed the amount of biomass binding sites (in meq/g units) can not explained by the Langmuir model, however it is predicted by the HIEM model with a regression correlation coefficient of 0.99. The model-predicted values match the isotherm experimental points at pH 3.5 and pH 4.0 within an average deviation of 5 %, which represents a major improvement over the Langmuir model.

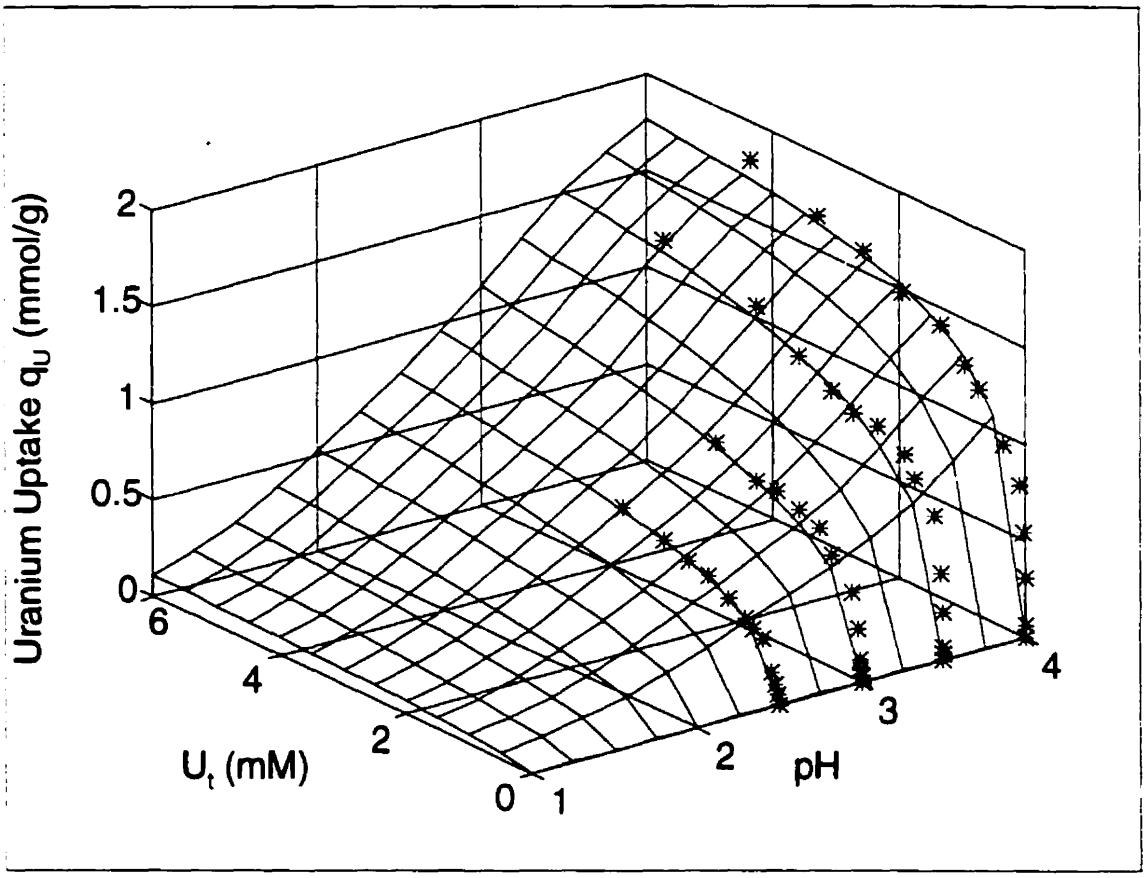

Figure 4.1.10: Uranium sorption isotherm surface. Solutions pH 2.5 – 4.0, uranium concentration 0.0 – 6.0 mmol/L.

Furthermore, since the proton concentration was included in the HIEM model, the model-calculated uranium uptake becomes a function of both independent variables, pH and the equilibrium uranium concentration. In this situation, an isotherm surface is more appropriate to describe the biosorption performance, as demonstrated in Figure 4.1.10. The scattered points represent the experimental uranium uptakes and the 3-dimensional surface was plotted from model-calculated uptake values. With increasing solution pH and in particular the uranium concentration, the uptake surface becomes higher. In order to demonstrate the influence of pH on the uptake at different equilibrium uranium concentrations, a series of curves were obtained by cutting the sorption isotherm surface at given uranium equilibrium concentrations. These relationships are plotted in Figure 4.1.11. For different uranium concentrations, the uranium uptake increases with increasing solution pH. The influence of solution pH on the uptake appears to be less significant at lower uranium concentrations compared with that occurring at higher uranium concentration.

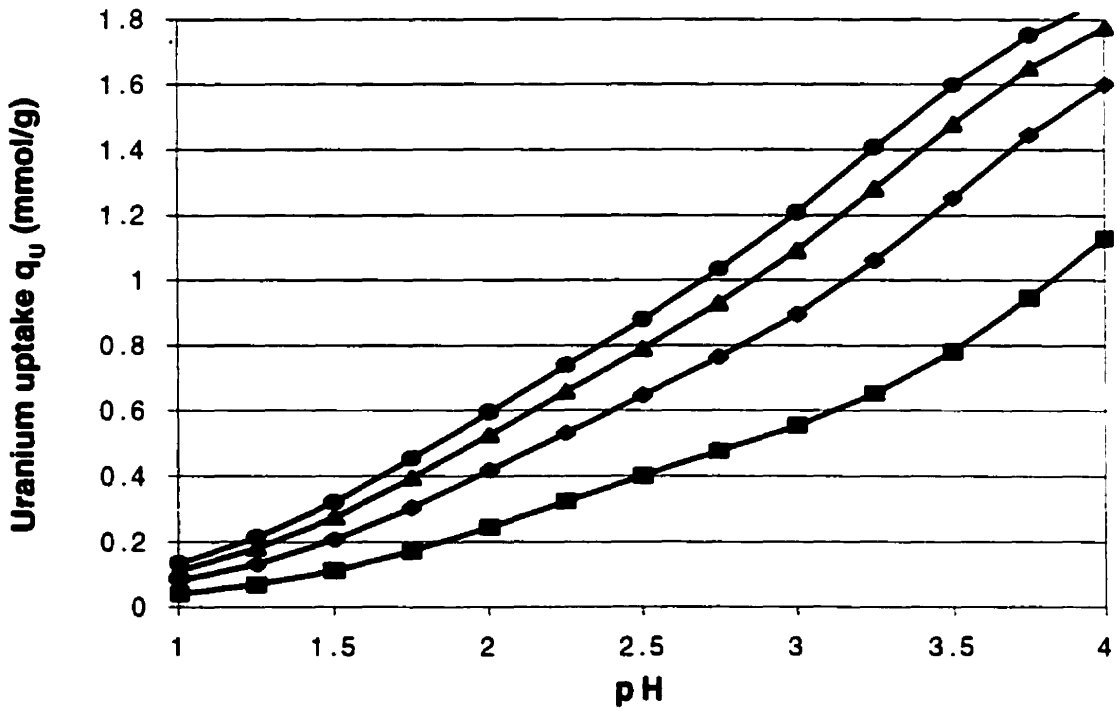

Figure 4.1.11: Influence of pH on uranium sorption at fixed uranium equilibrium concentrations. (●) U_f = 6.0 (mmol/g); (▲) U_f = 4.0 (mmol/g); (◆) U_f = 2.0 (mmol/g); (■) U_f = 0.5 (mmol/g);

4.1.7 Uranium speciation and distribution in the biomass

The distribution of hydrolyzed uranium ions in aqueous solution is dependent on both the solution pH and the total uranium concentration. It is calculable from the hydrolysis equilibrium constants. Combining model equation (4.1-24) with equations (4.1-4), (4.1-5), the concentrations of the complex ion species UO_2^{2+}, $(UO_2^{2+})_2(OH)_2^{2+}$ and $(UO_2^{2+})(OH)^+$ may be calculated from the solution pH and the total uranium concentration. The results of the calculations are presented in Figure 4.1.12, where the x-axis represents solution pH, the y-axis uranium normality and the 3-D surfaces the percentage of various uranium ionic species in aqueous solution as a function of solution pH and uranium normality.

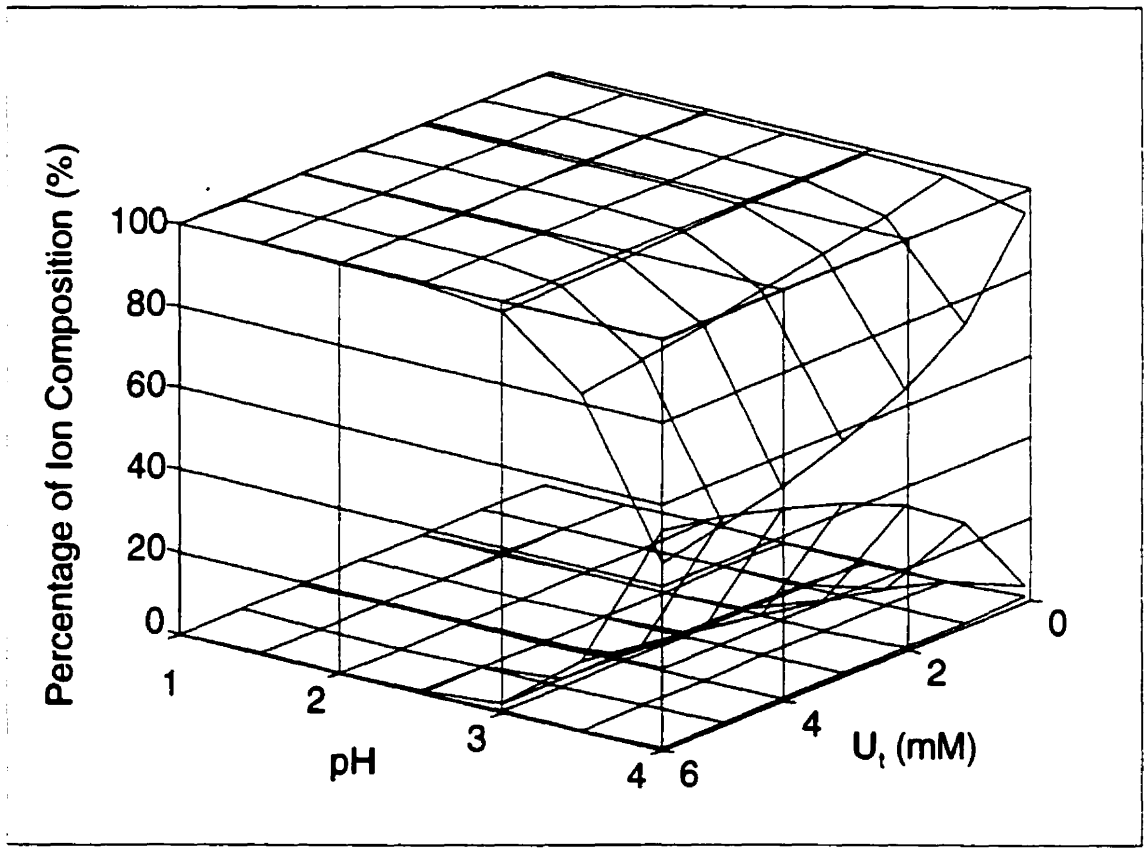

Figure 4.1.12: Speciation of hydrolyzed ionic uranium.

Top mesh: UO_2^{2+}; Middle mesh: $(UO_2^{2+})_2(OH)_2^{2+}$;

Bottom mesh: $(UO_2^{2+})(OH)^+$;

For solution pH values below pH 2.7, UO_2^{2+} is the predominant cation. Above pH 2.7, the percentage of UO_2^{2+} starts to decrease with solution pH while that of the $(UO_2)_2(OH)_2^{2+}$ concentration increases with pH and the total uranium concentration. At pH 4.0 and high uranium normality, more than 50% of uranium species exist as the complex $(UO_2)_2(OH)_2^{2+}$. The monovalent UO_2OH^+ represents less than 1% of U_t even at a higher pH and total uranium concentrations. According to Collins and Stotzky (1992), hydrolyzed species are better sorbed than the free hydrated ions. Thus the binding of hydrolyzed ionic species to biomass should drive the hydrolysis reaction towards the formation of more hydrolyzed species at a fixed pH which is maintained by adding a LiOH solution to neutralize the released protons. This in turn results in more binding of hydrolyzed ions. The "hydrolysis equilibrium" which is to say the equilibrium that exists between the hydrolyzed uranium ions and the biomass displays a different stoichiometry than is typically displayed during the ion exchange of non-hydrolyzable species. This is due the fact that the hydrolyzed species contain more uranium per equivalent charge. This is in contrast to a 1:2 stoichiometric relationship for the uranyl complex ion (UO_2^{2+}). In the case of uranium hydrolyzed species the ratio of uranium/proton would be 1 : 1 for $[(UO_2)_2(OH)_2^{2+}]_{0.5}$-Biomass and $[(UO_2)(OH)^+]$-Biomass. The maximum molar uranium uptake therefore becomes higher than would be expected on the basis of previous ion exchange models and assumptions whereby the value for the total binding capacity of the biomass is 2.25 meq/g.

According to equations (4.1-1) and (4.1-2), the formation of one mole of each of the species $[(UO_2)_2(OH)_2^{2+}]_{0.5}$ and $[UO_2OH^+]$ results in the corresponding production of one mole of proton per specie. In addition, the binding of either of the two species will result in the exchange and release of one mole of proton to the aqueous phase. Therefore the final result is that the binding of one hydrolyzed uranium specie results in an observable increase in proton concentration by two moles of protons: one proton produced by the hydrolysis of uranyl and a second due to ion exchange. The resultant decrease in pH appears to be the same as that for the direct ion exchange of UO_2^{2+} for a proton, despite the fact the mechanisms are different. In order to maintain a constant solution pH of 4.0, two moles of LiOH are required to neutralize the released protons for every mole of uranium sequestered. This was supported by the results obtained from the

stoichiometric study which is demonstrated in Figure 4.1.8. The slope was regressed and found to be 2.05.

Whereas in the previous paragraphs we have dealt with uranium *aqueous* phase distribution this section will now deal with uranium complexes as they occurs bound to the biomass phase. The species distribution in the biomass phase, calculated by using model equations (4.1-17), (4.1-18), (4.1-19) together with equation (4.1-24), is presented in Figure 4.1.13.

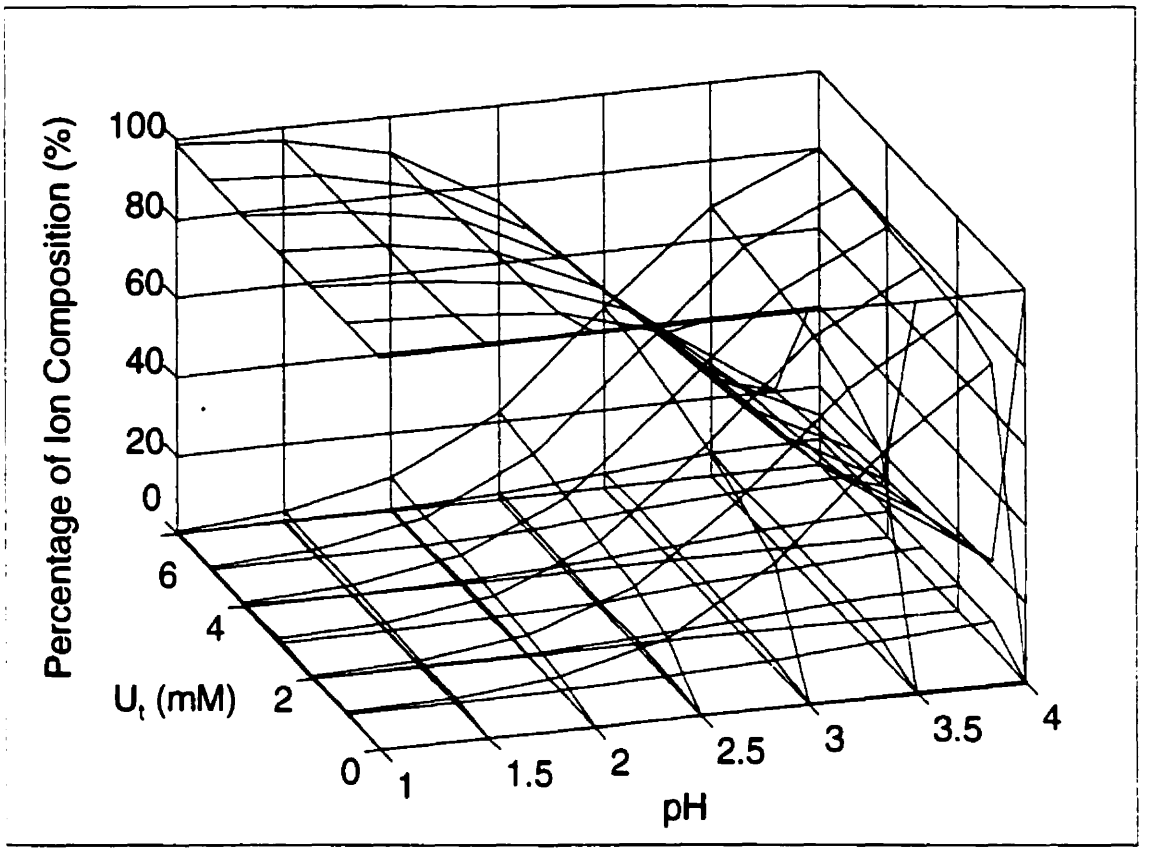

Figure 4.1.13: Distribution of the hydrolyzed ionic uranium species in the biomass. Top mesh: UO_2^{2+}; Middle mesh: $(UO_2^{2+})_2(OH)_2^{2+}$; Bottom mesh: $(UO_2^{2+})(OH)^+$.

It can be seen that $(UO_2)_2(OH)_2^{2+}$ becomes significant even at very low pH values. For instance, more than 20% of bound uranium exists in the form of $(UO_2)_2(OH)_2^{2+}$ at pH 2.5 when the total uranium concentration is high enough. Whereas the corresponding total equilibrium uranium concentration has a minor effect on the ionic

distribution in the biomass, the percentage of $(UO_2)_2(OH)_2^{2+}$ in the biomass phase increases significantly when the corresponding solution pH level rises. At pH 4.0, approximately 70 – 80% of total uranium exists in as the $(UO_2)_2(OH)_2^{2+}$ complex. In addition, despite the relatively lower quantity of UO_2OH^+, this ion exists over a wide range of pH values. Furthermore, both complex ions contain twice the number of uranium atoms as UO_2^{2+} per equivalent charge and results in a higher overall uranium uptake. This conclusion was well supported by the experimental data as described in the previous sections.

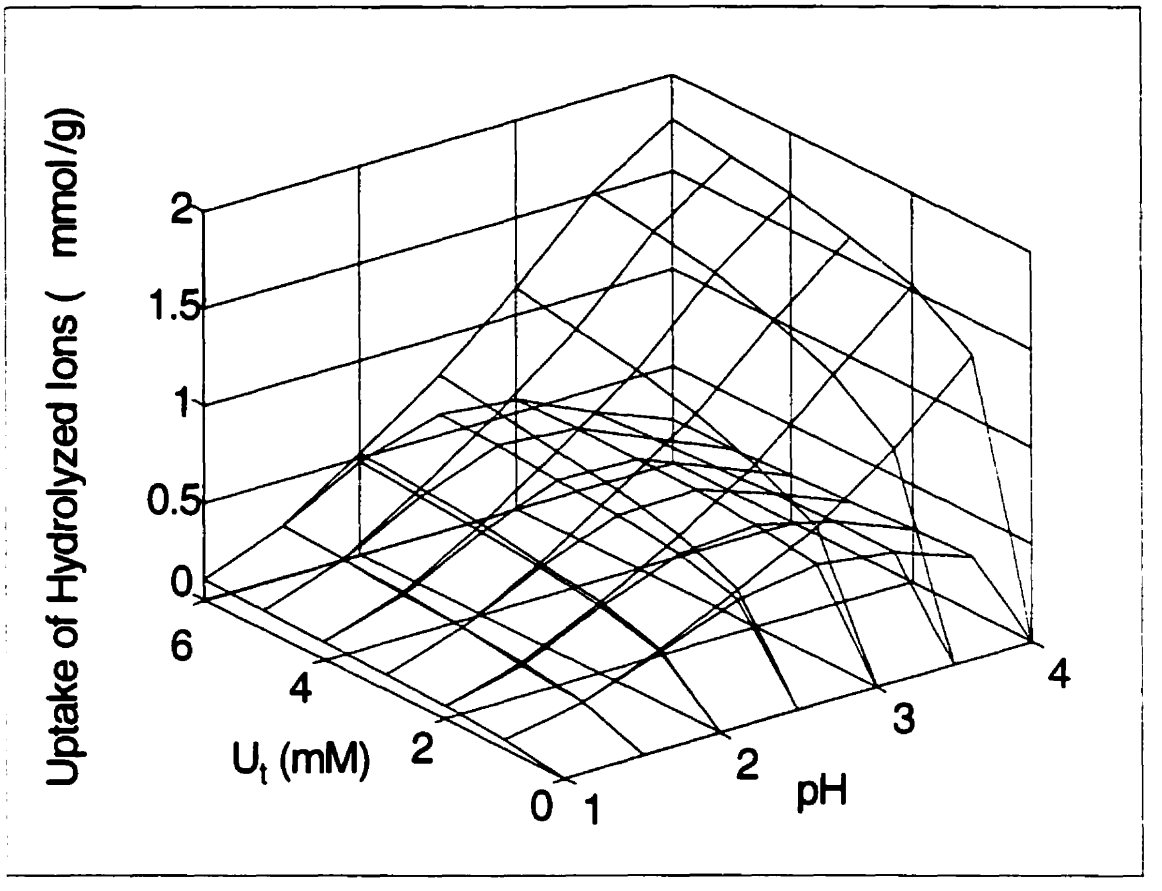

Figure 4.1.14: Influence of solution pH and equilibrium uranium concentration on the contribution of ionic specie UO_2^{2+} to the total uranium uptake.
Top mesh: total uranium uptake (mmol/g);
lower mesh: uptake of UO_2^{2} (mmol/g).

Figures 4.1.14 and 4.1.15 illustrate the contribution of the uranyl ion (UO_2^{2+}) and the hydrolyzed ion {$(UO_2)_2(OH)_2^{2+}$} to the total uranium uptake of the biomass, respectively. At pH 2.5, the bound uranium consists primarily of the free uranyl ion, while the uranium uptake at pH 4.0 is mainly attributed to the binding of the $(UO_2)_2(OH)_2^{2+}$ specie.

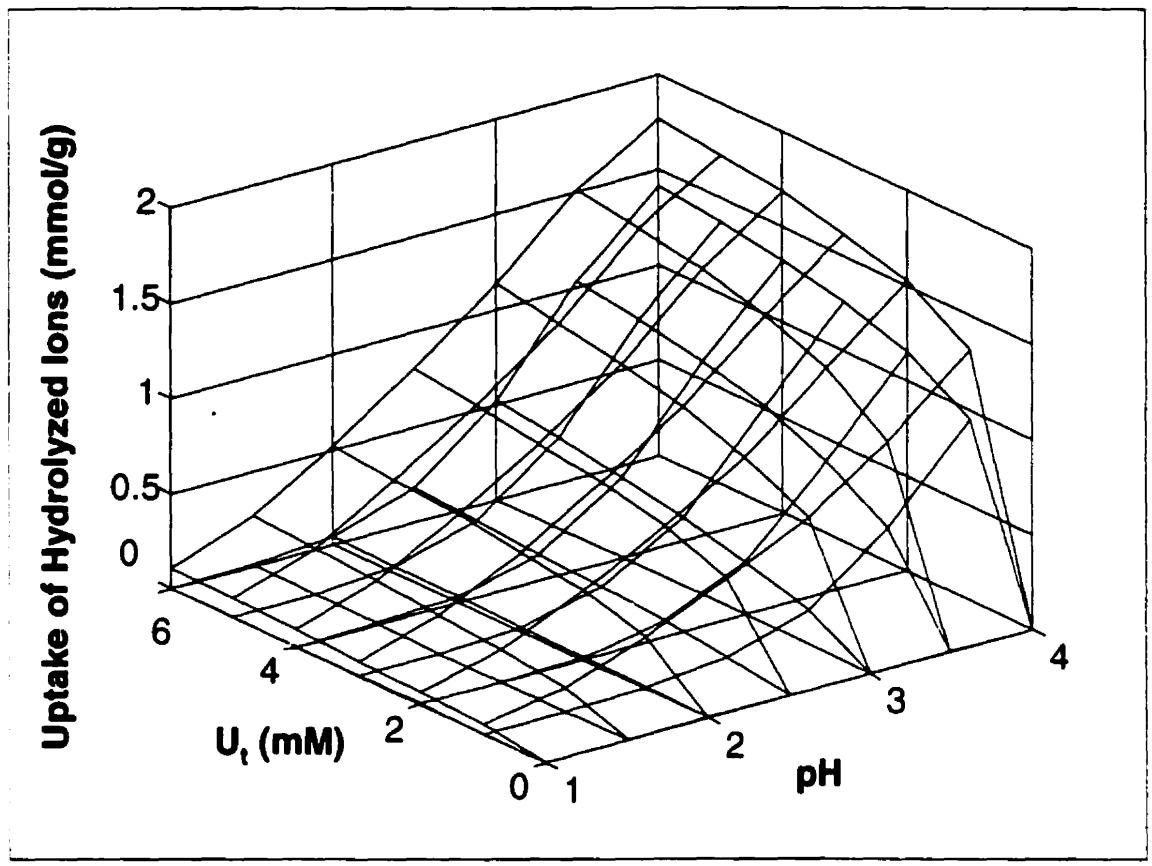

Figure 4.1.15: Influence of solution pH and equilibrium uranium concentration on the contribution of the ionic specie $(UO_2^{2+})_2(OH)_2^{2+}$ to the total uranium uptake.

Top mesh: total uranium uptake (mmol/g);

Lower mesh: uptake of $(UO_2^{2+})_2(OH)_2^{2+}$ (mmol/g).

4.1.8 Prediction of equilibrium uranium concentration at low pH (desorption conditions)

If the initial uranium concentration and solution pH are specified, the final equilibrium uranium concentration and biosorption uptake may be obtained by iterating equations (4.1-21), (4.1-28) with the sorption mass balance equation (3.1). In Figure 4.1.10, the uranium uptake surface falls rapidly with decreasing pH. This also indicates that the metal-laden biomass may be eluted efficiently under acidic conditions. This also agrees with the experimental observations described in section 4.1.2, whereby 0.1 N HCl was capable of effectively removing various types of heavy metals such as uranium and cadmium from *Sargassum* seaweed biomass without incurring structural damage. The following mass balance equation holds for desorption of uranium:

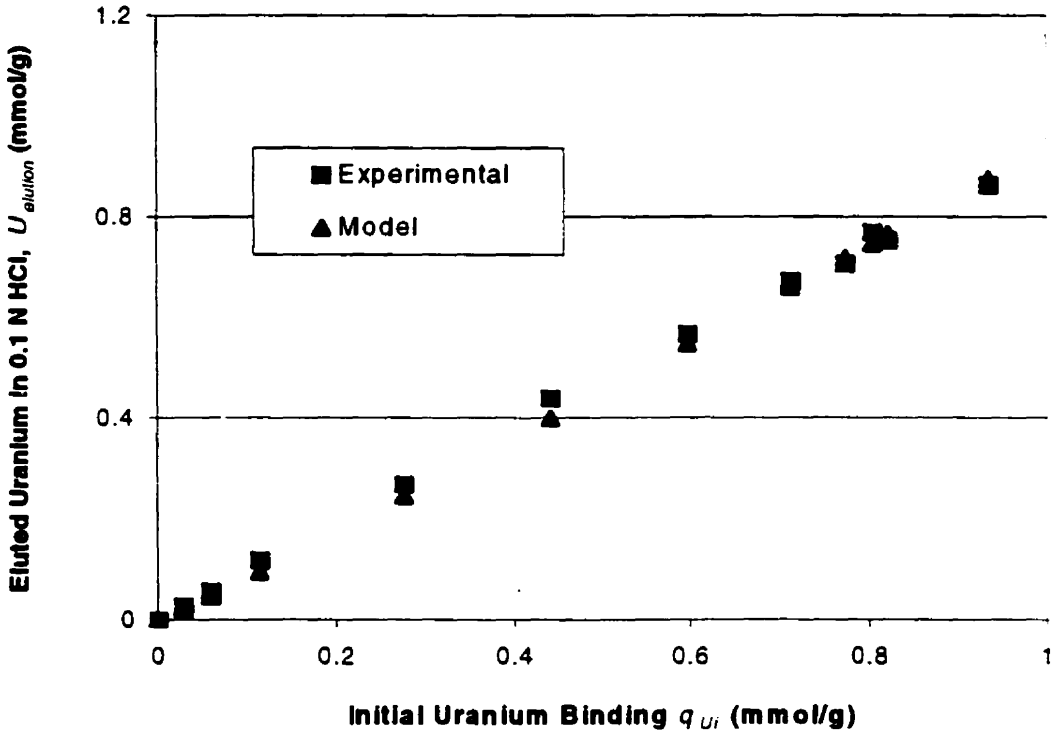

Figure 4.1.16: Total number of moles of uranium eluted in 0.1 N HCl.

$$q_u + U_{des}.V / W = q_u^0 \qquad (4.1\text{-}33)$$

In equation (4.1-33), q_u^0 is the initial uranium uptake. The uranium metal concentration of the acid rinse solution for a given initial biomass loading may be calculated by solving equations (4.1-33), (4.1-21) and (4.1-28) at the specified elution pH. The results calculated for elution of uranium-laden biomass in 0.1 N HCl, with a biomass / acid ratio of 2 g/L, are plotted in Figure 4.1.16. The scattered points represent the experimentally determined total number of moles of uranium eluted per gram of biomass for the initial uranium uptake. These model-calculated values deviate by less than 5% from the experimental data.

4.1.9 Section summary

In this section it was established that the biosorption of uranium was enhanced at higher solution pH. This experimental phenomenon can not be described well by the extensively used Langmuir model. Langmuir model also can not predict the influence pH has on biosorption behavior. Schiewer and Volesky (1995; 1996) proposed a model which was based on the ion exchange process between the heavy metal cations (Cd^{2+}, Cu^{2+}, Zn^{2+}) and protons. Their model could adequately predict the biosorption isotherms at various pH values, however, the model failed during application to the uranium biosorption system due to the more complex nature of uranium solution chemistry.

Hydrolyzed uranium ions may also be exchanged for protons of the seaweed biomass binding sites. The presence of the divalent $(UO_2)_2(OH)_2^{2+}$ specie results in a significant contribution to the increase in total uranium uptake due to the doubling of uranium content in this complex specie. The fixed number of available binding sites may therefore accept at least twice as much uranium as would be otherwise bound by the divalent uranyl ion UO_2^{2+}. As a consequence the maximum uranium uptake at pH 4.0 was as high as 480 mg/g or 2.08 mmol/g. This approximates the total number of biomass binding sites.

A new mathematical model (HIEM) which is based on the ion exchange between hydrolyzed uranium complex ions and protons incorporates proton concentration and hydrolysis equilibrium constants into the model equation. This model is capable of calculating the equilibrium uranium uptake from the equilibrium uranium concentration and solution pH. When the solution pH is controlled at a constant level, the equilibrium uranium concentration and uptake can be calculated from initial state for uranium biosorption. For metals such as cadmium, which does not hydrolyze, the HIEM model equation reduces to the Schiewer-Volesky equation for one-site biosorption.

It must be noted that this method is valid only for a batch equilibrium system under a controlled pH. Without giving the equilibrium solution pH, the HIEM model can not predict the equilibrium compositions from the initial concentrations. On the other side, biosorption applications are performed under a controlled solution pH in many cases, the model still can be used in those situations.

4.2 Biosorption batch dynamics

The equilibrium biosorption of uranium and cadmium by *Sargassum* biomass was studied. The equilibrium metal uptake could be predicted for given initial experimental conditions by using various equilibrium models. As mentioned in the introduction of section 2.4, sorption rate and the dynamic behavior of the metal-biomass system is of particular importance to process design and operation. This may be appropriately studied as a batch system. Experimentally obtained linear and Langmuir equilibrium relationships were incorporated into rate equations which were based on the intraparticle diffusion of uranium or cadmium species inside the biomass.

4.2.1 Titration curves obtained from end-point titration

A typical titration curve is depicted in Figures 4.2.1 and 4.2.2 for uranium and cadmium, respectively, where the change in pH, metal concentration and proton release were plotted as a function of sorption contact time.

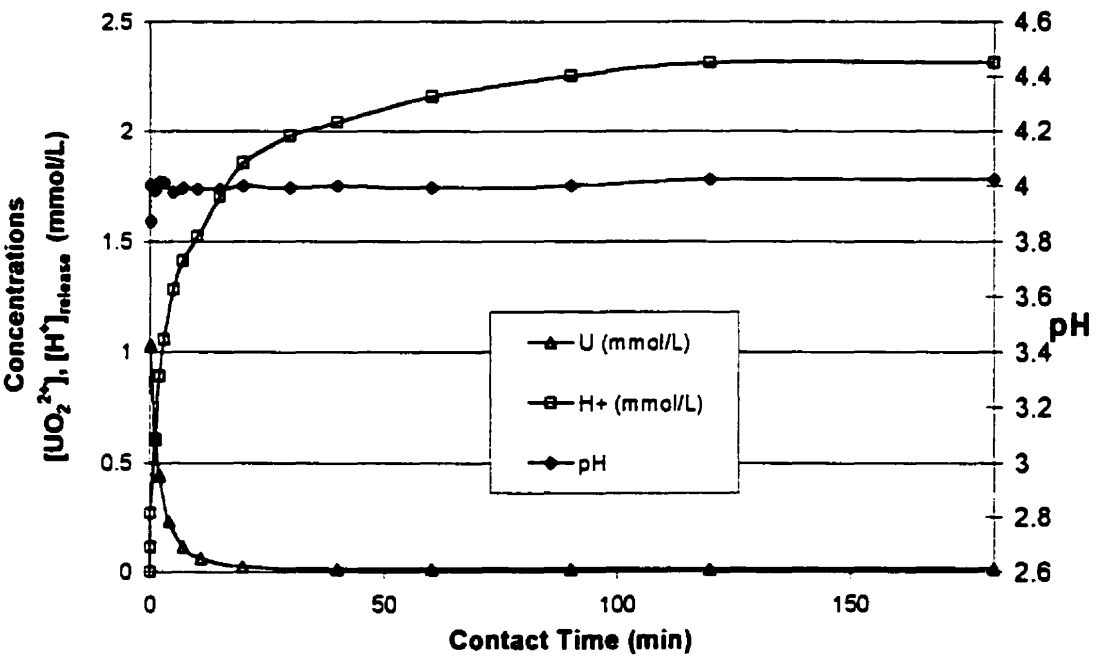

Figure 4.2.1: End-point titration of the uranium batch sorption system (pH 4.0).

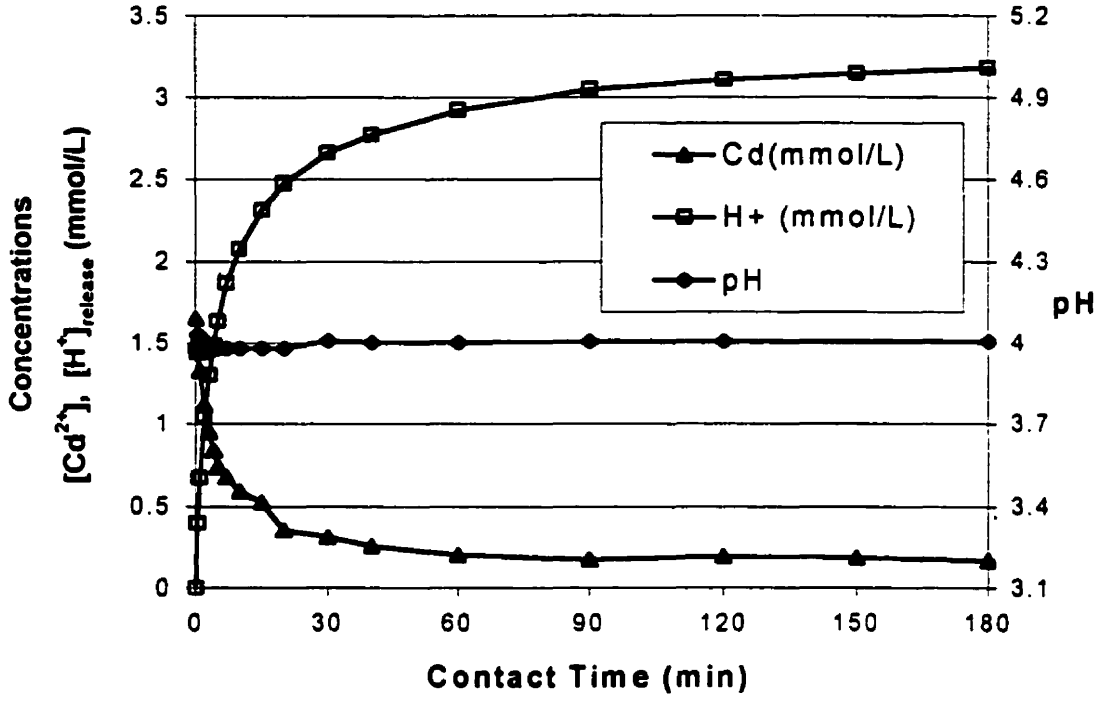

Figure 4.2.2: End-point titration of the cadmium batch sorption system (pH 4.0).

The solution pH was maintained at constant pH 4.0 with only slight deviation. The metal concentration decreases with the time rapidly. Within approximately 15 minutes of the start point, approximately 75% of the metal is sequestered. Equilibrium is reached after 2 – 3 hours. The amount of proton released, which was monitored by LiOH addition increased with elapse time for the duration of the experiment. The titration curve is characteristic of the biosorption dynamic system and can be used to determine the biosorption rate.

Almost all the cadmium was present as the free form, i.e. Cd^{2+} at the experimental pH of 4.0 according to computer program MINEQL$^+$ (Schecher, 1991). As a result, the consumption or release of protons due to water hydrolysis in the aqueous solution phase was negligible. No precipitation was observed in the experimental process as predicted by the MINEQL$^+$. Consequently, the base concentration profile *versus* time of Figure 4.2.2 reflects the rate of cadmium biosorption. On the other hand, the hydrolysis of uranium is significant. At pH 2.5, the free uranyl ion UO_2^{2+} is the predominant form. At higher solution pH values, several types of uranium complexes are formed due to hydrolysis. Therefore the base and uranium concentration *versus* time profile illustrated

in Figure 4.2.1 represents not only the biosorption rate of the free uranyl ion UO_2^{2+}, but it represents the overall biosorption rate for the various hydrolyzed uranium complexes at solution pH 4.0 as well.

4.2.2 Elimination of external mass transfer

External and internal mass transfer resistance of the biomass particle are a major concern for sorption dynamics. Intraparticle mass transfer has been established to be the rate controlling step by many researchers, as discussed in the literature review (section 2.4). The effect of external mass transfer must be eliminated before the intraparticle mass transfer rate can be determined experimentally. External mass transfer resistance is proportional to the thickness of the stationary fluid layer or film which surrounds the biomass particles and this in turn is controlled by agitation in the bulk solution. Strong stirring decreases the film thickness and should eventually eliminate film resistance. A series of sorption experiments were carried out at different agitation rates. The resulting metal concentration profiles as a function of time are presented in Figures 4.2.3 and 4.2.4 for uranium and cadmium, respectively.

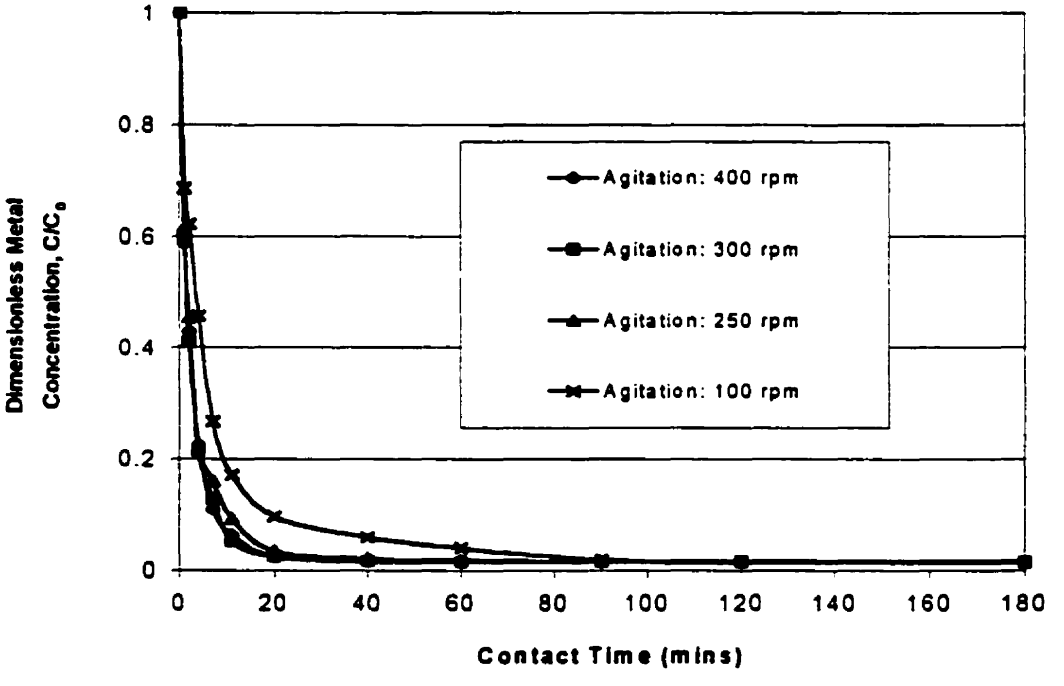

Figure 4.2.3 Influence of agitation speed on uranium biosorption dynamics.

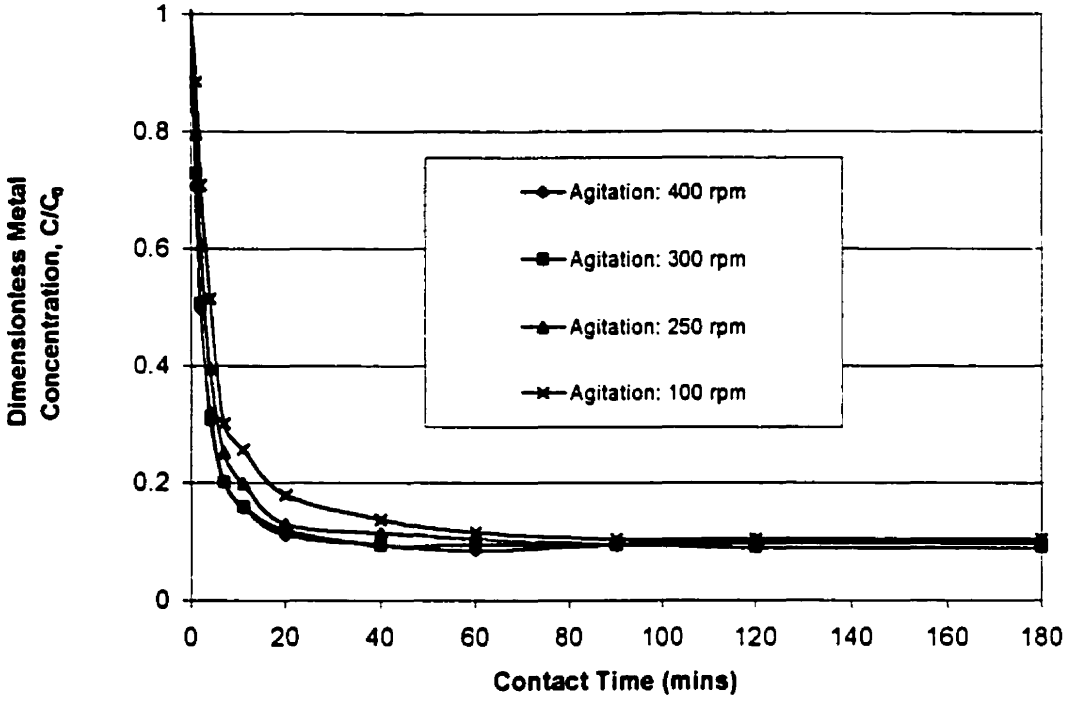

Figure 4.2.4: Influence of agitation speed on cadmium biosorption dynamics.

The biomass/liquid ratio is 2.0 g / L for the dynamic experiments. The agitation rate increased beyond a critical point (for example, 3 Hz), at which time the resulting metal concentration profiles stabilized and did not deviate by more than 5%. This indicated that the fluid-to-particle mass transfer resistance was minimized and could therefore be neglected.

4.2.3 Influence of the biosorbent particle size on metal sorption rate

A separate set of experiments were performed in order to determine the extent to which the size of the biosorbent particles influenced the metal sorption rate. This was achieved by carrying out several end-point titrations each with different biomass particle sizes. Profiles which display dimensionless metal concentration as a function of contact time are shown in Figure 4.2.5 for uranium, and in Figure 4.2.6 for cadmium.

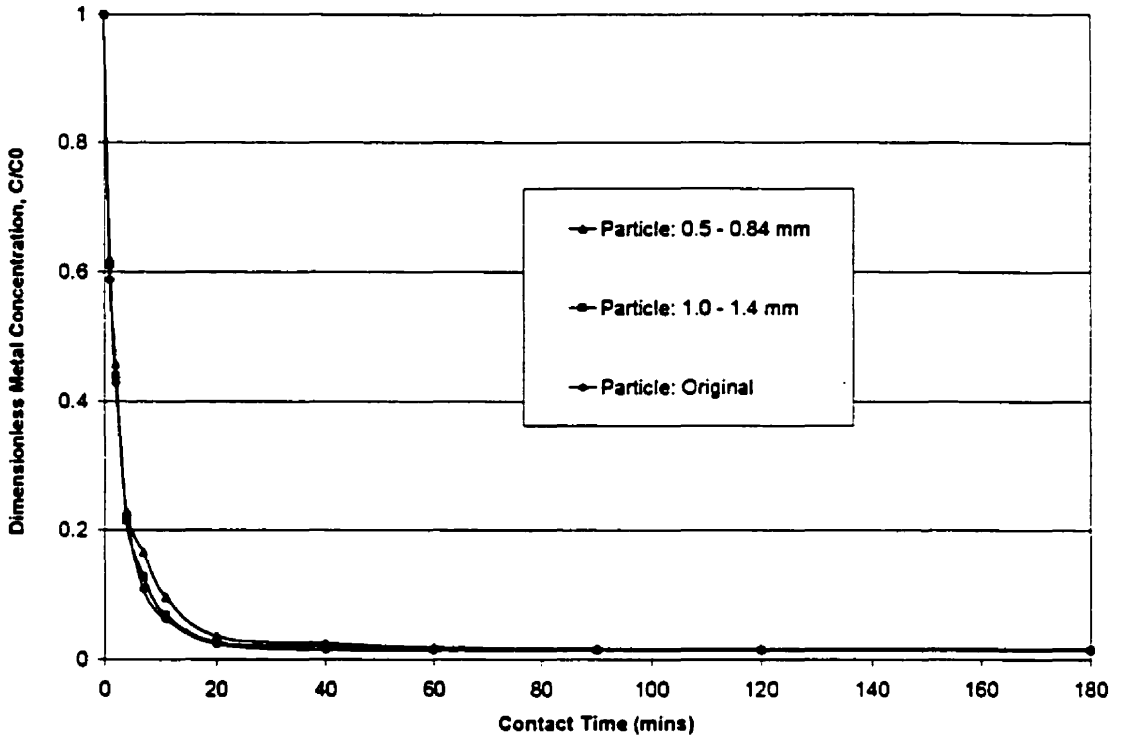

Figure 4.2.5: Influence of biomass particle size on uranium biosorption rate.

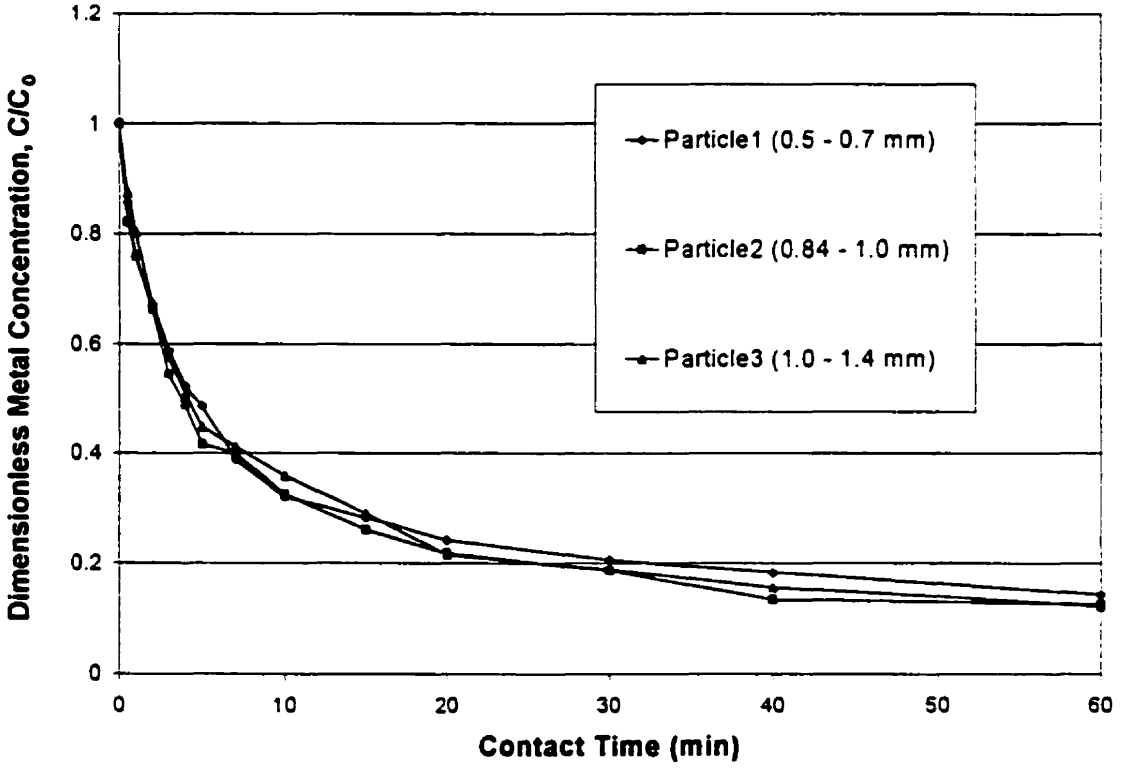

Figure 4.2.6: Influence of biomass particle size on cadmium biosorption rate.

The concentration profiles for the three different particle sizes of (0.5 - 0.7) mm, (1.0-1.4) mm and a "native" whole (not cut) seaweed for uranium, (0.5 - 0.7) mm, (0.84-1.00) mm and (1.0-1.4) mm for cadmium, agreed with each other within a 5% deviation. This indicates that the overall biosorption rate for uranium and cadmium was independent of biosorbent particle size. This seems to be contradictory to the general notion that intraparticle diffusion controls the overall sorption process. Usually, the particle size is related to the diffusion distance that the metal ion must travel through for the case of a spherical biosorbent particle. Thus decrease in particle diameter normally reduces the diffusion distance and therefore accelerates the overall sorption rate. However, grinding the seaweed biomass results in particles with a non-spherical shape. The resulting chip-like particles are actually of the same thickness for all size fractions. Furthermore, the thin chips generally display a width and length that greatly exceeds the thickness. Therefore diffusion parallel to the normal of the surface represents the shortest diffusion distance and determines the overall diffusion rate. As a result, a mathematical model which treats the intraparticle diffusion field as a uni-dimensional thin plate was found to be more suitable for describing the biosorption rate than a conventional spherical particle assumption.

The matrix structure of the biomass material is another important factor that may have an impact on the biosorption rate. By processing the *Sargassum* biomass with a mixed solution of HCl and formaldehyde in order to cross-link the alginate polysaccharide an internal reinforcement could be achieved. While increasing the mechanical strength, cross-linking may also increase mass transfer resistance to the metal ion diffusion. Therefore biosorption rates for heavy metals of cross-linked biomass may decrease relative to that for native uncross-linked biomass. The experimentally determined biosorption rates for both cross-linked and uncross-linked biomass types are depicted in Figure 4.2.7. The dimensionless cadmium solution concentration is plotted as a function of time. The formaldehyde cross-linked biomass's biosorption rate was significantly lower than that for the uncross-linked biomass.

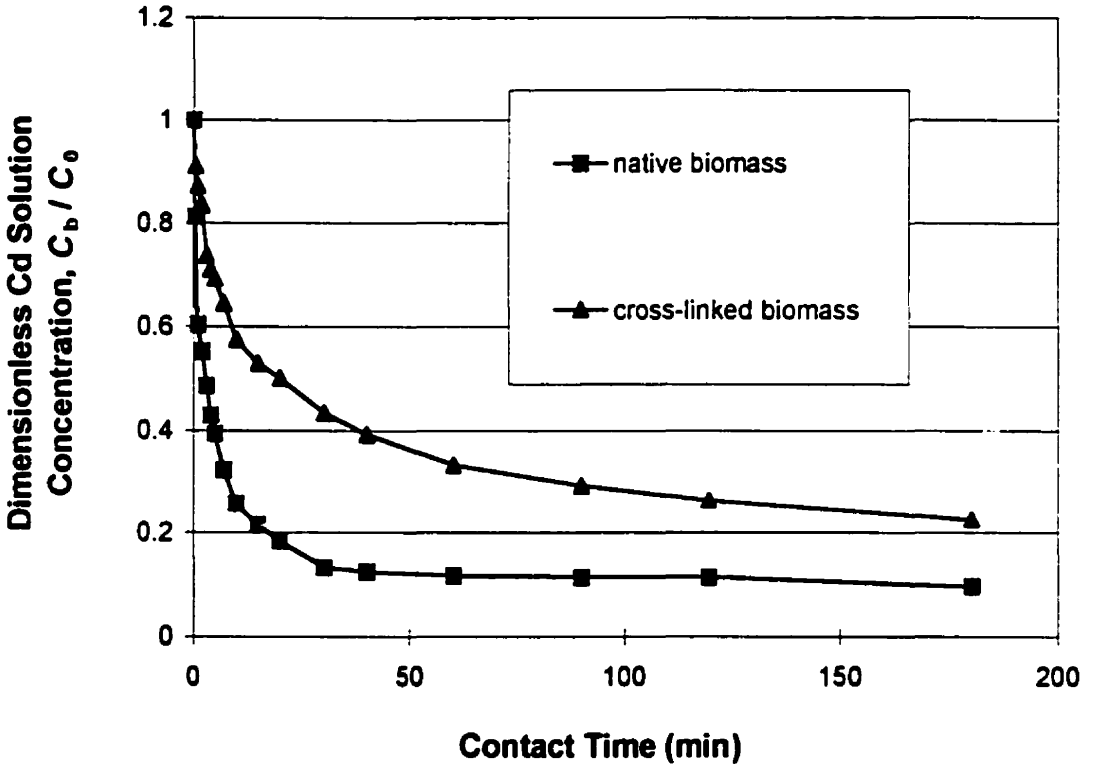

Figure 4.2.7: Influence of formaldehyde cross-linking on cadmium biosorption rate.

4.2.4 Rate of metal uptake and proton release

Metal sorption was rapid during the initial stage of contact. The concentration profile curve for cadmium is displayed in Figures 4.2.8.

The rate curves can be divided into two stages. The first stage was fast whereby approximately 75% of the total cadmium sorption took place within 15 min. The second stage was slower taking approximately 3 hours for sorption equilibrium to be reached. Applying the first-order rate method of Crist et al. (1996) for the exchange of calcium ions with protons by peat moss, the sorption rate was assumed to be proportional to binding capacity, i.e.:

$$d[H]/d\tau = k([H]_\infty - [H]) \qquad (4.2\text{-}1)$$

where τ is the contact time, k is the rate constant and $[H]$ and $[H]_\infty$ represent the instantaneous and maximal proton releases, respectively. The integrated form of the first-order rate equation is as follows:

$$\ln([H]_\infty - [H]) = k\,\tau \qquad (4.2\text{-}2)$$

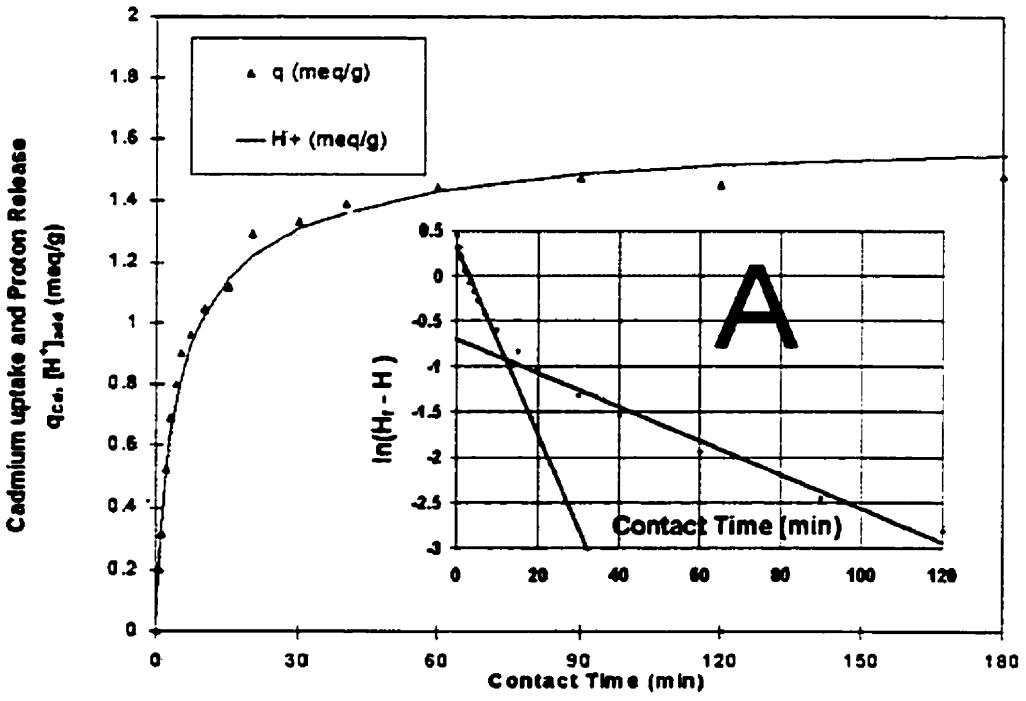

Figure 4.2.8: Cadmium biosorption rate and proton release rate at pH 4.0.
4.2.8A: Two stages of cadmium biosorption rate

Plots of simulations which use equation (4.2-2) with an experimental data set (for cadmium) are shown in Figure 4.2.8A. The slope of the lines represent the sorption rate constant. In Figure 4.2.8A, the slope during the initial 10 minutes was calculated to be k_1 = -0.123 and that for the remaining contact time was k_2 = -0.0214. The difference between the slopes was significant, whereby k_1 was approximately 5.7 times that of k_2. This reflects the two different rate processes for the initial and final stages. Similar results were obtained for other biomass particle sizes.

The same type of rate curves have been reported by other researchers. According to the explanations of Crist et al. (1996) and Brassard et al. (1996), the initial metal sorption rate was attributed to surface binding and a slower sorption to interior penetration. For the case of *Sargassum* seaweed particles, the initial sorption rate is accelerated due to the active binding groups which reside in the cell wall and the surface area. The actual mechanism of heavy metal sequestration has been studied to a limited extent (Crist, et al., 1988) and should be further investigated.

The initial stage of the sorption process is more significant in the overall sorption process. However, it is physically difficult to acquire samples from the reaction solution at this stage. As a result fewer data points are available to regress thus limiting the accuracy in the determination of the diffusion coefficient. The agreement in stoichiometry of metal uptake and proton release data during the sorption process indicates that ion exchange occurs between uranium or cadmium ions and protons. Therefore, the computer-recorded LiOH (up to 8 points per second) titration curves may be used to represent the metal concentration profile for the regression of the effective diffusion coefficient. This provided a rapid and easy method for the evaluation of sorption rate thus avoiding the more tedious procedure of sampling the reactor for metal concentration.

4.2.5 Mass transfer model for biosorption rate

A mathematical model for a quantitative analysis of biosorption dynamics is useful if it is capable of representing metal concentration change as a function of contact time. Metal biosorption is the result of three consecutive processes. First, metal ions must diffuse across the particle-to-fluid film from the bulk solution. Second, they must diffuse through the gel phase of the *Sargassum* algal biomass to the binding sites. Finally, the ions must react with the acid functional groups of the biomass. In the experimental set-up, particle-to-liquid mass transfer resistance has been eliminated by generating adequate turbulence with agitation by baffles. In this situation the intraparticle diffusion of the metal ions is again assumed to be the rate controlling step. The model assumption details are as follows:

1. The reaction time for sorption (i.e. binding to the functional group) is much shorter than that for diffusion of the ions through the biomass.
2. Chip-like *Sargassum* biomass particles are considered to be uni-dimensional thin plates. Therefore, the overall sorption rate is controlled by intraparticle diffusion in the direction normal to the surface of the particles.
3. The quantity of bound metal is in equilibrium with the metal concentration of the aqueous phase as formulated in the Langmuir sorption isotherm relationship.

During the biosorption process the diffusion of metal ions into the biomass must be accompanied by the release of protons by diffusion to the bulk liquid. The diffusion coefficient for H^+ is several times higher than that for heavy metal ions present in infinitely diluted aqueous solutions (Dobos, 1994; Horvath, 1985). Therefore, the assumption that the overall sorption rate is controlled solely by heavy metal diffusion is reasonable. Furthermore, Crist et al. (1994) showed that the Langmuir isotherm model could be used for ion exchange rate calculations for algal biomass over a wide concentration range.

Based on these assumptions, the mass conservation equations are as follows:

$$\varepsilon \frac{\partial C_r}{\partial \tau} + \rho \frac{\partial q}{\partial \tau} = D_e \frac{\partial^2 C_r}{\partial r^2} \qquad (4.2\text{-}3)$$

$$\frac{d(V C_b)}{d\tau} = -D_e S_t \frac{\partial C_r}{\partial r}\Big|_{r=R} \qquad (4.2\text{-}4)$$

whereby r is the arbitrary position coordinate from the central line of the biomass particle in the direction that is normal to the surface. τ is the time elapsed for sorption. C_b and C_r represent the metal concentrations of the bulk solution and for the pore liquid phase at layer r inside the biomass, respectively. R is the half-thickness, ε is the porosity and ρ is the density. V is the volume of bulk solution and S_t is the total surface area of particles that is calculable from the assumed geometry of the particle. D_e represents the effective intraparticle diffusion coefficient.

The boundary and initial conditions for the sorption process are as follows:

$$C_{r|_{r=R}} = C_b \qquad (r = R, \quad \tau > 0) \qquad (4.2\text{-}5)$$

$$\frac{\partial C_r}{\partial r}\Big|_{r=0} = 0 \qquad (r = 0, \quad \tau > 0) \qquad (4.2\text{-}6)$$

$$C_b = C_0 \qquad (\tau = 0) \qquad (4.2\text{-}7)$$

$$C_r = 0 \qquad (\tau = 0, \quad 0 \le r < R) \qquad (4.2\text{-}8)$$

where C_0 is the initial metal concentration in the solution.

Since the volume change due to LiOH additions and sampling is less than 3% of the total volume, equation (4.2–4) may be approximated as:

$$V\frac{dC_b}{d\tau} = -D_e S_t \frac{\partial C_r}{\partial r}\Big|_{r=R} \qquad (4.2\text{-}4A)$$

By differentiating the isotherm equation (2.1), we obtain:

$$\frac{\partial q}{\partial C_r} = \frac{K q_m}{(K + C_r)^2} \qquad (4.2\text{-}9)$$

Introducing dimensionless variables $x = \frac{r}{R}$, $C(x,t) = \frac{C_r}{C_0}$, $\overline{C}(t) = \frac{C_b}{C_0}$, and substituting equation (4.2-9) into the rate equation (4.2-3), then rewriting equation (4.2-4A), results in the following coupled equations:

$$f(C)\frac{\partial C}{\partial \tau} = \alpha \frac{\partial^2 C}{\partial x^2} \qquad (4.2\text{-}10)$$

$$\omega \frac{d\overline{C}}{d\tau} = -\alpha \frac{\partial C}{\partial x}\Big|_{x=1} \qquad (4.2\text{-}11)$$

where $f(C)$ is defined as a non-linear function of the dimensionless concentration C as follows:

$$f(C) = \left(\varepsilon + \frac{\gamma_1 \gamma_2}{(C+\gamma_1)^2} \right) \qquad (4.2\text{-}12)$$

$\omega = \frac{V}{S_t R}$, $\gamma_1 = \frac{K}{C_0}$ and $\gamma_2 = \frac{\rho q_m}{C_0}$ are auxiliary dimensionless parameters, while $\alpha = \frac{D_e}{R^2}$ has the units of sec^{-1}.

The corresponding boundary and initial conditions are as follows:

$$C(1,\tau) = \overline{C}(\tau) \qquad (x = 1,\ \tau > 0) \qquad (4.2\text{-}13)$$

$$\frac{\partial C}{\partial x}\Big|_{x=0} = 0 \qquad (x = 0,\ \tau > 0) \qquad (4.2\text{-}14)$$

$$\overline{C}(0) = 1 \qquad (\tau = 0) \qquad (4.2\text{-}15)$$

$$C(x,0) = 0 \qquad (\tau = 0, 0 \le x < 1) \qquad (4.2\text{-}16)$$

Equations (4.2-10) and (4.2-11) are simultaneous non-linear partial differential equations (PDEs) with respect to C and $\overline{C}$, respectively. They are similar to the ones used for diffusion of a gas in polymer microvoids. For a linear isotherm, an analytical solution was developed by Crank (1975). For the case of a non-linear isotherm, such as

the Langmuir isotherm, an analytical solution is not available and a numerical method must be used.

4.2.6 Numerical solution of the batch dynamics model equations

In this work, the Galerkin Finite Element Method (GFEM) (Lapidus and Pinder, 1982) was applied to discretize the model PDEs, leading to a series of ordinary differential equations (ODEs). The Euler backward integration in time was applied to obtain the numerical solution for dimensionless intraparticle concentration $C(x, \tau)$ and dimensionless bulk concentration $\overline{C}(\tau)$.

Assuming an approximate solution for the concentration at finite element nodes:

$$C = \sum_{i=1}^{N} C_i(\tau)\phi_i(x) \tag{4.2-17}$$

where C_i $(i = 1.2...N)$ are the N unknown coefficients and ϕ_i is the linear base function in GFEM (Lapidus and Pinder, 1982), the derivative is:

$$\frac{\partial C}{\partial x} = \sum_{i=1}^{N} C_i(\tau)\frac{\partial \phi_i}{\partial x} \tag{4.2-18}$$

The integral of the weighted residual for governing equation (4.2-10) is:

$$\begin{aligned} F_i &= \int_0^1 \left\{ -f(C)\frac{\partial C}{\partial \tau} + \alpha \frac{\partial^2 C}{\partial x^2} \right\} \phi_i dx \\ &= -\int_0^1 f(C)\frac{\partial C}{\partial \tau}\phi_i dx + \int_0^1 \alpha \frac{\partial^2 C}{\partial x^2}\phi_i dx \\ &= 0 \end{aligned} \tag{4.2-19}$$

Separately integrating the second term:

$$F_i = -\int_0^1 f(C)\frac{\partial C}{\partial \tau}\phi_i dx + \left[\alpha\phi_i \frac{\partial C}{\partial x}\right]_{x=0}^{x=1} - \int_0^1 \alpha \frac{\partial C}{\partial x}\frac{\partial \phi_i}{\partial x} dx$$
$$= -\int_0^1 f(C)\frac{\partial C}{\partial \tau}\phi_i dx - \int_0^1 \alpha \frac{\partial C}{\partial x}\frac{\partial \phi_i}{\partial x} dx + \delta_{i,N}\alpha\phi_i \frac{\partial C}{\partial x}|_{x=1} - \delta_{i,N}\alpha\phi_i \frac{\partial C}{\partial x}|_{x=0} \quad (4.2\text{-}20)$$

where the following applies:

$$\delta_{i,N} = 1 \quad (i = N)$$

$$\delta_{i,N} = 0 \quad (i \neq N)$$

Substituting the boundary conditions (4.2-6) and (4.2-11) in to the last two terms yields:

$$F_i = -\int_0^1 \left(f(C)\frac{\partial C}{\partial t}\phi_i dx + \alpha \frac{\partial C}{\partial x}\frac{\partial \phi_i}{\partial x} \right) dx - \delta_{i,N}\beta \frac{d\bar{C}}{dt} \quad (4.2\text{-}21)$$

Substituting the approximate solution equation (4.2-17), and its derivative (4.2-18) into equation (4.2-21) yields:

$$F_i = -\int_0^1 \left[\sum_{j=1}^{N} \frac{\partial C_j}{\partial \tau}\phi_i\phi_j f(C) + \alpha \sum_{j=1}^{N} C_j \frac{\partial \phi_i}{\partial x}\frac{\partial \phi_j}{\partial x} dx \right] dx - \delta_{i,N}\omega \frac{d\bar{C}}{dt}$$
$$= \sum_{j=1}^{N} \frac{\partial C_j}{\partial \tau} \int_0^1 \phi_i\phi_j f(C) + \sum_{j=1}^{N} C_j \int_0^1 \alpha \frac{\partial \phi_i}{\partial x}\frac{\partial \phi_j}{\partial x} dx - \delta_{i,N}\omega \frac{d\bar{C}}{dt} = 0 \quad (4.2\text{-}22)$$

We may rewrite the above equation in matrix form as:

$$F_i = \bar{\bar{M}}\frac{d\vec{C}}{d\tau} + \bar{\bar{K}}\vec{C} - \delta_{i,N}\beta\delta_{i,N}\omega\frac{d\vec{C}_N}{d\tau} = 0 \quad (4.2\text{-}23)$$

where the matrices are:

$$M_{ij} = \int_0^1 \phi_i \phi_j f(C) dx$$

$$K_{ij} = \int_0^1 \alpha \frac{\partial \phi_i}{\partial x} \frac{\partial \phi_j}{\partial x} dx \qquad (i, j = 1,2...N) \qquad (4.2\text{-}24)$$

Substituting these derivatives in equation (4.2-23) with their corresponding differences as follows:

$$\frac{d\vec{C}}{d\tau} = \frac{\vec{C} - \vec{C}^{old}}{\Delta t}$$

$$\frac{d\vec{C}_N}{d\tau} = \frac{\vec{C}_N - \vec{C}_N^{old}}{\Delta t} \qquad (4.2\text{-}25)$$

Then the final matrix equation is:

$$\left(\overline{\overline{M}} + \Delta t \overline{\overline{K}}\right)\vec{C} = \overline{\overline{M}}\vec{C}^{old} + \delta_{i,N}\omega\left(C_N - C_N^{old}\right) \qquad (4.2\text{-}26)$$

Equation (4.2-26) is a linear equation with a tri-diagonal coefficient matrix and can be solved by a standard TDMA method (Lapidus and Pinder, 1982). The source code in FORTRAN is listed in the Appendix B. The Microsoft FORTRAN 77 compiler was employed.

4.2.7 Regression of model parameters

Of the model parameters, K and q_m may be obtained from batch equilibrium experiments. R (0.2 mm in average), ε (0.67) and ρ (1.05) were measured directly and S_t (in cm^2) was decided by the weight of the biomass used W (0.1 g) for the thin plate geometry of the biomass particle, $S_t = W / (\rho R)$. All other parameters, except D_e , may be calculated once the volume V (50 ml) and the concentration of the metal solution in the reactor are specified. This means that the numerical solution for the model equations

is uniquely determined by the value of D_e. In other words, a specific value of D_e corresponds to a specific simulated concentration profile of $\overline{C}(t)$ as a function of time. The intraparticle diffusion coefficient D_e may therefore be regressed from the comparison of the simulated profile curves and the experimental results by minimizing the following objective function:

$$\varphi = \sum_{i=1}^{n} \left| \left(\overline{C}^{Model} - \overline{C}^{Experimental} \right) \right|_i \qquad (4.2\text{-}27)$$

where i is the i^{th} experimental data point and n is the total number of experimental data points.

Biosorption equilibrium was discussed in Chapter 4.1 and the Langmuir biosorption isotherm model parameters q_m and K can be obtained from Table 4.1.1 for various pH values. Simulations of biosorption rate were conducted for uranium and cadmium at those pH values. The corresponding values for D_e were regressed by comparing the model simulation curves and the corresponding experimental data. The results are listed in Table 4.2.1.

Table 4.2.1 The regressed diffusion coefficients D_e (cm^2/sec)

	pH 2.5	pH 3.0	pH 3.5	pH 4.0	Average
Uranium	4.0	6.0	6.0	6.0	5.5
Cadmium	6.0	5.0	6.0	6.0	5.75

The average diffusion coefficients for uranium and cadmium were 5.5×10^{-6} cm^2/sec and 5.75×10^{-6} cm^2/sec, respectively. These diffusion coefficient values are of the same order of magnitude as their respective molecular diffusivities, which are 7.21×10^{-6} cm^2/sec and 7.19×10^{-6} cm^2/sec respectively (Dobos, 1994; Horvath, 1985). Values for the effective diffusion coefficient may vary and can differ by several orders of magnitude even under similar experimental conditions. The cadmium diffusion coefficient for formaldehyde cross-linked biomass was regressed by the model with the experimental data presented in Figure 4.2.7. The value was approximately 1.5 - 2.5 cm^2/sec, which is much smaller than for those of the uncross-linked biomass and correctly reflects the

retarding effect of cross-linking on the biosorption rate. A comparison of model-fit concentration profiles and experimental data points for pH 2.5 - 4.0 is plotted in Figure 4.2.9 for uranium and for cadmium in Figure 4.2.10.

In general, diffusion will occur faster in a fluid phase unless it is impeded by the presence of a porous material. For the case where such a porous material contains the same fluid as the external fluid phase, diffusion through the porous material will obviously be slower than in the external liquid phase (Helfferich, 1962; Westrin and Axelsson, 1991). As previously discussed, alginate is the main polysaccharide responsible for sorption by *Sargassum* (Fourest and Volesky, 1997). The gel nature of this polysaccharide approximates a very porous material which is highly permeable to ionic species (Dodge, 1973; Percival and McDowell, 1967b). The calculated intraparticle diffusion coefficient is an effective diffusion coefficient, D_e, and it is usually smaller than the molecular diffusion coefficient D_m which is considered in the absence of the sorbent material matrix.

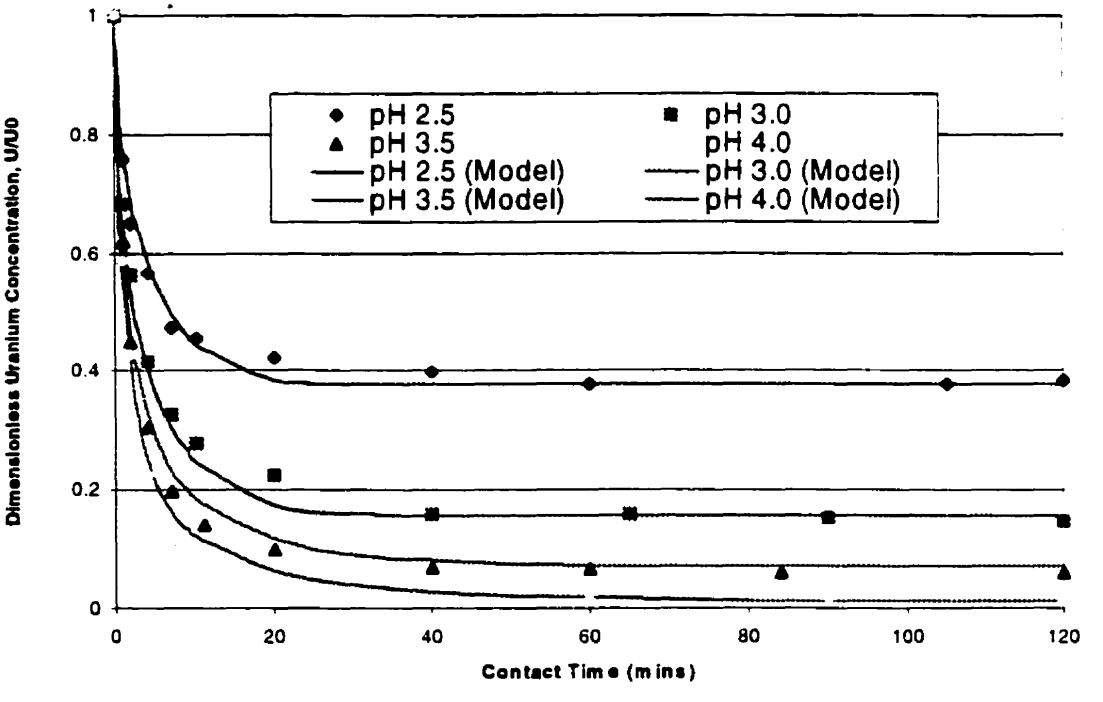

Figure 4.2.9: Modelling uranium concentration-time profiles at different solution pH values.

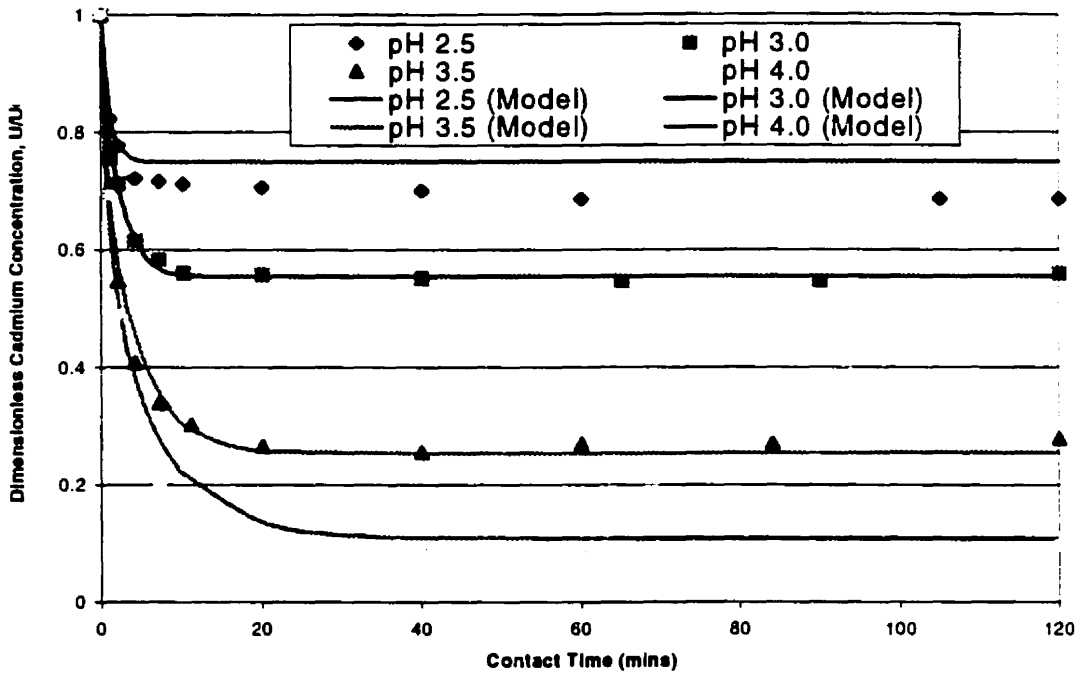

Figure 4.2.10: Modelling cadmium concentration-time profiles at different solution pH values.

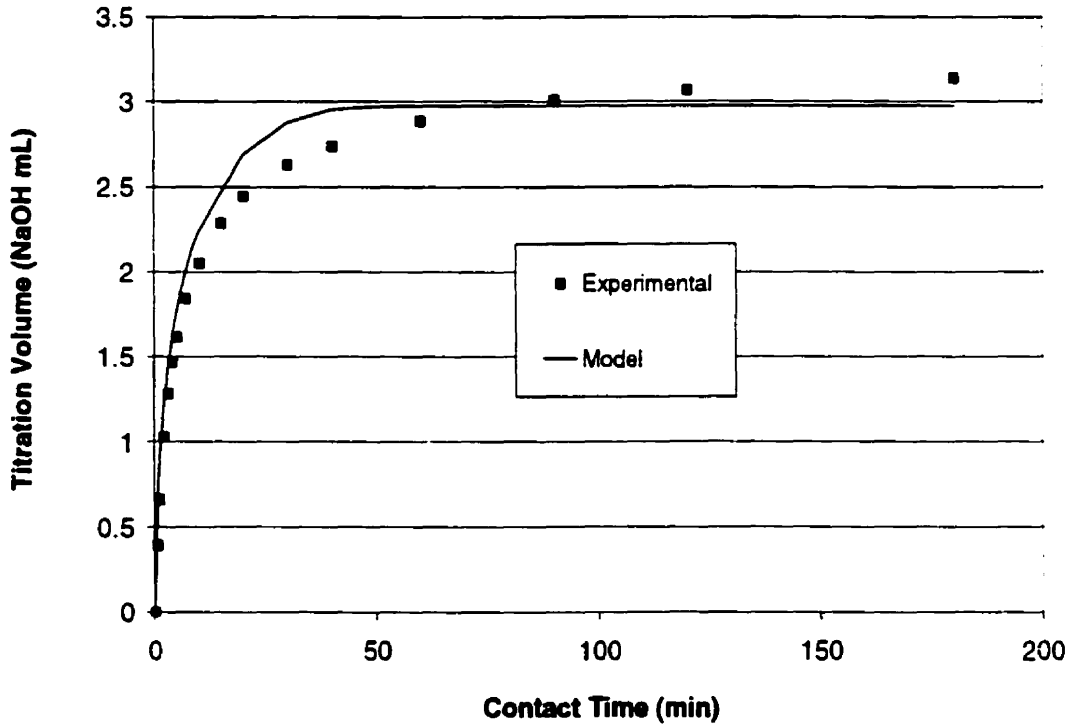

Figure 4.2.11: Numerical simulated end-point titration volume profile.

LiOH volume is plotted as a function of time in Figure 4.2.11 for pH 4.0. The solid curve is calculated with the mass transfer model using an average regressed diffusion coefficient $D_e = 5.75$ cm^2/sec. The trend in the simulated curve agrees with the experimental data but there was an average deviation of approximately 10%. This was calculated by the statistical method "trend in residual analysis" and shows that the model simulation does not represent the experimental data well. The data points of the transient range (i.e. the transition between the two sorption stages) contribute most of the deviation. Schiewer and Volesky (1997) observed that the swelling of *Sargassum* seaweed biomass is not significant at low pH. However, swelling may affect model accuracy at higher pH values, for example at pH 4.0. Swelling is characterized by specific particle volume and has been found to be negatively correlated to the concentration of free binding sites which, in turn, influences heavy metal uptake. Therefore the specific particle volume is not a constant value since the concentration of the free binding sites changes during the sorption process. Despite the limitations of the simulation model the profile may be used to show the trend in the experimental data. The rate of proton release also does not agree with the uranium uptake profile and this may be due to the hydrolysis of uranium at higher pH.

4.2.8 Desorption rate

Desorption of metals may be carried out under acidic conditions. During the desorption process, heavy metals present within the biomass are replaced by protons diffusing in from the bulk eluant solution. As a result, the eluted metal ions diffuse through the permeable biomass toward the particle surface. Finally, the ions diffuse across the stationary liquid layer (film) that surrounds the biomass particles to the bulk solution. Again, the internal diffusion constitutes the main resistance to the overall desorption process and in desorption dynamic experiments, film resistance is reduced significantly by strong agitation. The acid concentration is much higher than the metal concentration in the elution solution and the corresponding increase in pH which results from proton consumption during desorption is negligible due to the relatively low amount of metals in the biomass-liquid system. Therefore, the pH of the eluant does not change during the desorption process and no titration is necessary to maintain pH.

Biosorption and desorption rate mechanisms are the same except for initial and boundary conditions. The mathematical model equations (4.2-3) and (4.2-4A) used for biosorption may also be equally applied to the desorption process. The initial and boundary conditions for the desorption process are as follows:

$$C_r|_{r=R} = C_b \qquad (r = R, \quad \tau > 0) \tag{4.2-28}$$

$$\frac{\partial C_r}{\partial r}|_{r=0} = 0 \qquad (r = 0, \quad \tau > 0) \tag{4.2-29}$$

$$C_b = C_0 \qquad (\tau = 0) \tag{4.2-30}$$

$$C_r = C_0 \qquad (\tau = 0, \quad 0 \le r < R) \tag{4.2-31}$$

$$q_r = q_0 \qquad (\tau = 0, \quad 0 \le r < R) \tag{4.2-32}$$

$$\mu (\varepsilon C_f + q_f) + C_f = \mu q_0 \qquad (\tau = \infty) \tag{4.2-33}$$

where C_0 is the initial metal concentration in the eluant solution, and is usually zero. q_0 is the initial metal loading on the biomass. q_f and C_f are the final metal uptake and concentration in the eluant solution, respectively. $\mu = V_p / V$ is the ratio of the total biomass particle volume to the bulk solution volume.

The same numerical techniques as in the sorption process were used to solve the model PDEs. The equilibrium sorption isotherm under elution conditions must be incorporated into the rate model equations in order to solve for concentration. The isotherm for cadmium desorption is depicted in Figure 4.1.7 of section 4.1 and was regressed with the following linear relationship:

$$q = K_c C_f \tag{4.2-34}$$

where K_c is the equilibrium constant and is the metal partitioning coefficient between the metal-containing solution and the biomass. K_c was found to be 0.33 mg/cm^3 by the regression.

The analytical solution using a linear isotherm relationship for the model PDEs (4.2-3) and (4.2-4), according to Crank (1975), is as follows:

$$\frac{C}{C_f} = 1 - \sum_{1}^{n} \frac{6\phi(\phi+1)\exp\left(-\dfrac{D_e\tau}{(\varepsilon+K_c)R^2\delta_n^2}\right)}{6\phi(\phi+1)+R^2\phi^2} \qquad (4.2\text{-}35)$$

where δ_ns are the non-zero roots of the following equation:

$$\tan\delta_n = \frac{3\delta_n}{3+\phi\delta_n^2} \qquad (4.2\text{-}36)$$

and $$\phi = \frac{1}{\mu(\varepsilon+K_c)} \qquad (4.2\text{-}37)$$

All parameters except the effective diffusion coefficient, D_e, are known for the solution equation (4.2-35). Therefore, D_e, may be regressed by the same method as for the biosorption model. Figure 4.2.12 depicts the model-calculated rate curve in addition to the experimental cadmium desorption data for a 0.1 N HCl elution reaction. The model curve agrees with the experimental data with an error of approximately 5%. The effective diffusion coefficient was regressed and found to be $3.5\text{x}10^{-6}$ cm^2/sec, which is lower than, yet of the same order of magnitude as that obtained in biosorption process.

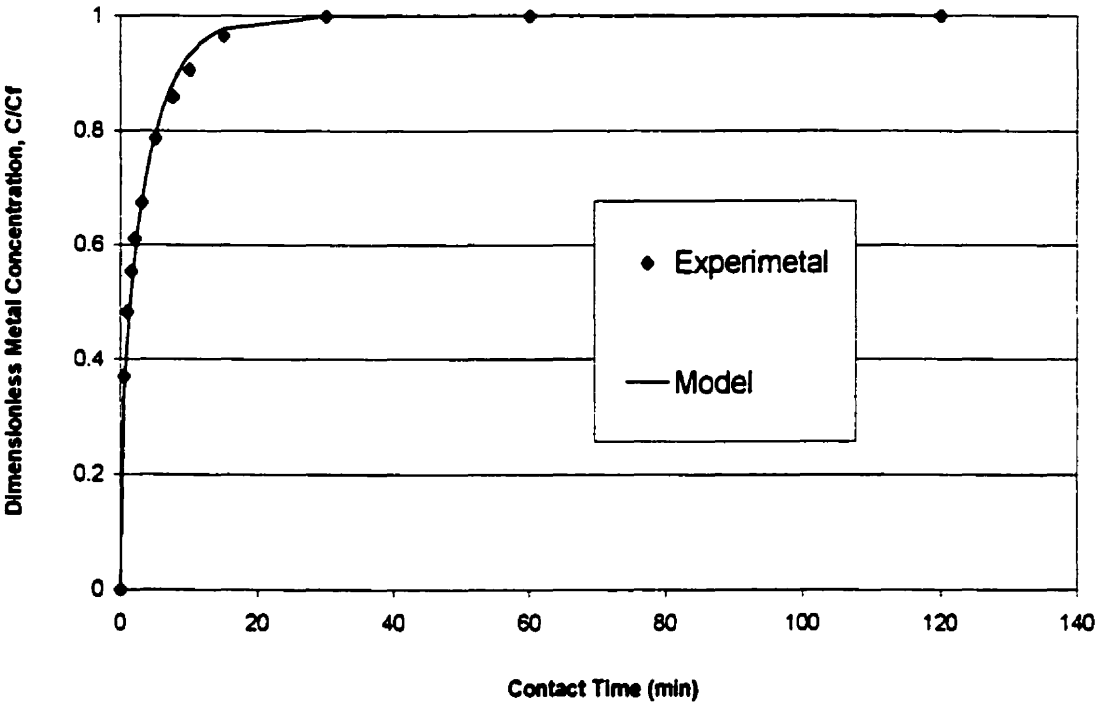

Figure 4.2.12: Desorption rate of cadmium from metal-laden *Sargassum* biomass.

4.2.9 Section summary

The biosorption process can be divided into three steps, external diffusion, internal diffusion and ion exchange reaction. Among these steps, the intraparticle diffusion is the rate controlling one. The dynamics of the desorption process differs only in its initial and boundary conditions from that which occurs in biosorption. The geometry of the algal biomass, *Sargassum*, approximates that of a flat chip, compared to typical spherically shaped sorbent particles. Intraparticle diffusion can therefore be assumed to occur parallel to the normal of the chip surface.

The end-point titration method was applied in the experimental determination of biosorption rate at constant pH for uranium and cadmium by *Sargassum fluitans*. The biosorption and desorption rates can be described by a simple one-dimensional intraparticle diffusion model. The Galerkin Finite Element Method (GFEM) numerical technique was applied to solve the non-linear partial differential model equations. The

effective diffusion coefficients of uranium and cadmium at various solution pH values were regressed by applying the mass transfer model to the end-point titration experimental data. The regressed values for the effective diffusion coefficients are on the same order of magnitude as their respective molecular diffusivities. Under acidic elution conditions, the cadmium isotherm displays a linear relationship between cadmium uptake and equilibrium cadmium concentration. The model equations were solved successfully by analytical methods.

4.3 Biosorption dynamics in a continuous system

Most separation and purification processes that use sorption technology in industry employ continuous flow columns. During this process, the influent is continuously percolated through a sorbent filled column with the undesirable species being retained. The column sorbent gradually becomes saturated whereby this process begins at the feed zone and gradually progresses to the exit. When the sorbate concentration in the effluent stream reaches a pre-defined level, column operation is terminated. At this point the regeneration process may begin before activation of the next cycle of operation.

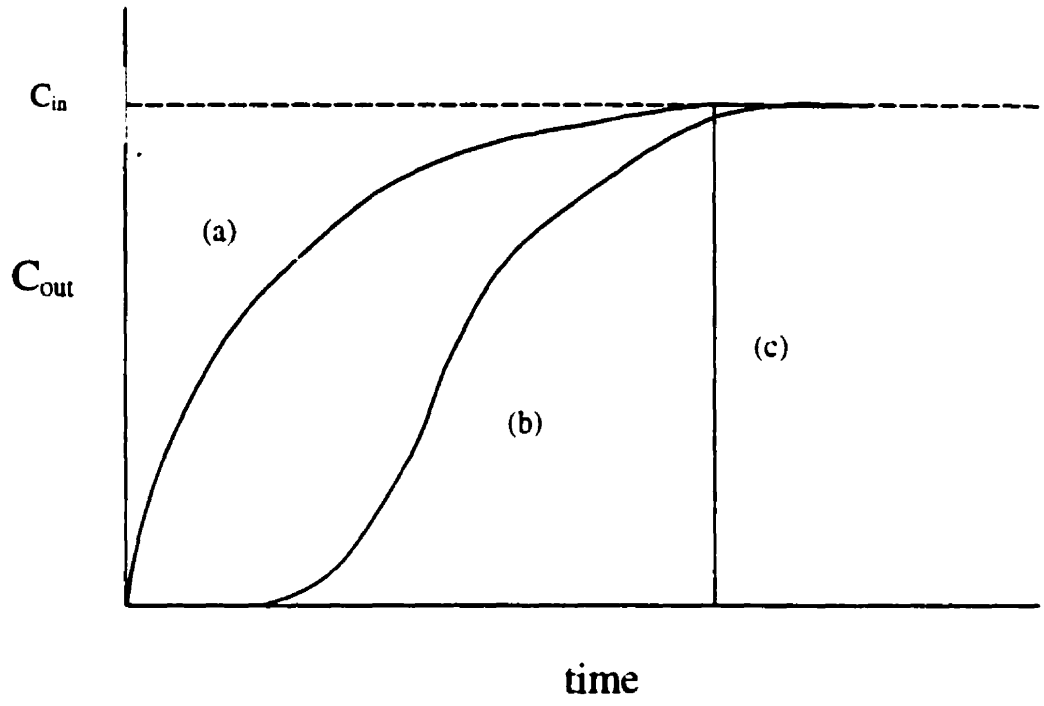

Figure 4.3.1: Schematic representation of breakthrough curves.
(a) Poor sorption (b) normal sorption (c) and strong sorption (with no mass transfer effect)

The breakthrough curve, which represents the history of effluent concentration as a function of time, is characteristic for any given continuous flow column system. The breakthrough time represents the duration of ongoing sorption until a pre-defined exit threshold concentration is reached. Any optimized column system is based on the accurate prediction of the breakthrough time given the specific operating conditions. Three typical types of breakthrough curves may be observed. They either display: (a) poor sorption, (b) normal sorption or (c) strong sorption, whereby no mass transfer occurs in the latter. These breakthrough curves are illustrated schematically in Figure 4.3.1. The factors which may affect the shape of a breakthrough curve include the equilibrium isotherm relationship, the mass transfer coefficients in the column and operation parameters such as flowrate and influent pH.

4.3.1 Uranium biosorption breakthrough curves

For the operation of a uranium biosorption column, an acidic influent, pH 2.5 and a uranium concentration of C_0 = 238 ppm, with an upward flow rate of F = 340 ml/h was used. The empty bed volume was V_{bed} = 280 cm^3 with an average residence time of approximately 49 minutes. The column was loaded with 22.64 g (W; dry weight) of protonated *Sargassum*. Figure 4.3.2. illustrates the resulting breakthrough curves. The uranium concentration and pH values at the column exit are plotted as a function of dimensionless volume (with reference to the bed volume). Comparing Figure 4.3.2 with Figure 4.3.1, the uranium breakthrough curve represents a "normal sorption" curve with a commonly observed S shape. Breakthrough took place after 36.5 bed volumes at which point the exit uranium concentration was 1.0 ppm. Approximately 10 L of 238 ppm uranium influent was processed before breakthrough. The total uranium removed by 22.64 g (dry) of biomass was 2380 mg, yielding an average uranium biosorption capacity of 105 mg U/g (dry biomass). The high initial effluent pH of Figure 4.3.2 is due to the pre-rinsing that was performed prior to the start of column operation. As depicted in Figure 4.3.2, effluent pH decreased until a dimensionless volume of approximately 5 before stabilizing. The pH breakthrough occurred at the same time as for uranium. This is due to ion exchange between uranium complex ions and the protons present in the sorption zone. Therefore, in practice, the pH breakthrough curve may be used as an

indication of metal breakthrough. This would be a much more simple method of terminating a column cycle since pH measurement is obviously simpler than monitoring metal levels. For the above operations, effluent pH was plotted by a computer as the experiment progressed.

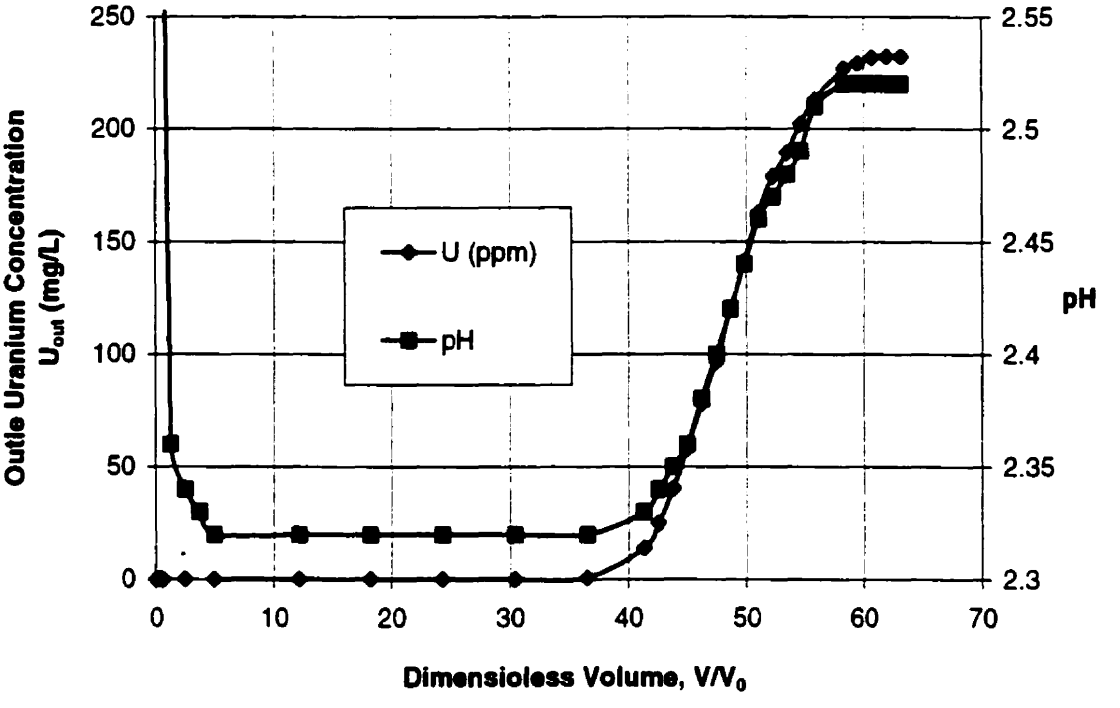

Figure 4.3.2: Uranium biosorption breakthrough curve.

When the biomass was saturated with uranium, 0.1 N HCl acid was pumped through the column with the same flowrate that was used in the sorption process. The bound uranium was therefore removed which regenerated the biomass. The acid elution results are illustrated in Figure 4.3.3 where the uranium concentration and pH of the (0.1N HCl) effluent were plotted as a function of the eluting acid volume.

The uranium concentration of the elution effluent initially displays a high peak that represents the desorption process. The peak concentration was approximately 9000 mg uranium/L and the average concentration was 6000 mg uranium/L for 400 ml of eluting volume. The overall metal concentration factor is defined to be the ratio of the elution concentration to that of the influent concentration for a given sorption run, i.e. $CF = U_E / U_0$. In this experiment, the ratio was determined to be approximately 25. The

elution peak and the low residual uranium concentration (< 1 ppm) indicated a high elution efficiency. Furthermore, for lower elution flowrates, e.g. 175 ml/h, the uranium peak concentration rises e.g. correspondingly 11,000 mg/L. A comparison between the total uranium retained and the total amount of uranium collected by the acid eluant shows that more than 99.5% of the uranium was recovered. The curve (Figure 4.3.3.) for the change in effluent pH as a function of eluant volume corresponded well to the uranium elution curve. This is interpreted to be an indication of the ion exchange mechanism whereby the proton concentration in the eluant is much higher than that of uranium and biomass acid functional groups become protonated upon release of the uranium ions.

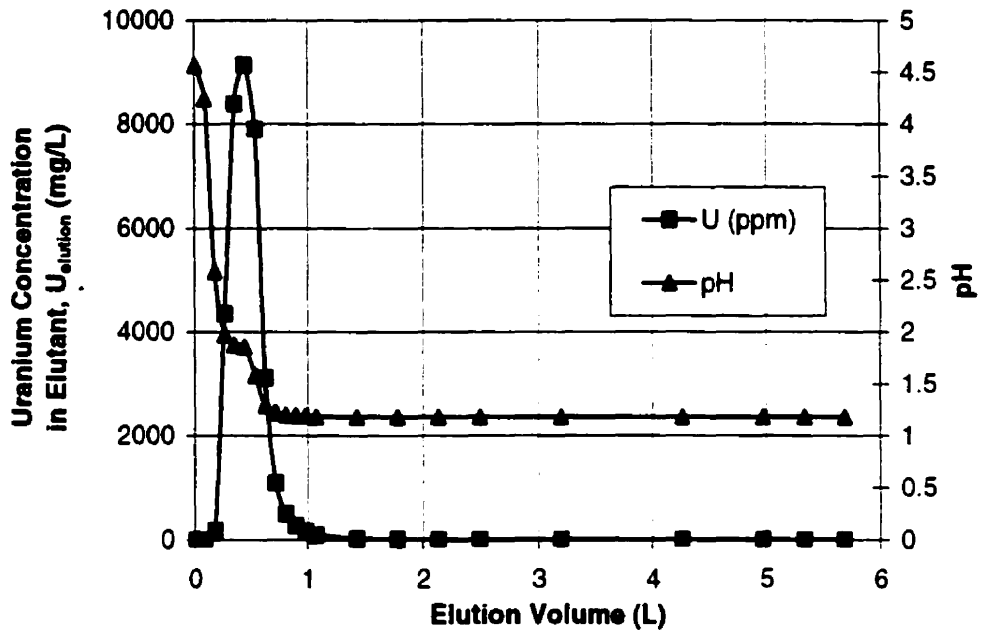

Figure 4.3.3: Elution of uranium by 0.1 N HCl from biosorption column.

The column was rinsed with distilled water after elution and the new cycle subsequently started. Column operation was maintained continuously for one month over which time 5 cycles were completed. The breakthrough curves for the different cycles are illustrated in Figure 4.3.4. Although the shape of breakthrough curves are relatively similar, the breakthrough time decreased with each cycle. This suggests that the biomass binding capacity decreases with increasing usage. The most significant loss in binding capacity occurred immediately after the first cycle of biosorption-desorption operation.

Following the first cycle, the column binding capacity stabilized with only a slight decrease in capacity with each subsequent cycle. The biosorption capacity for the 5th cycle was approximately 20% less than for the fresh biomass; it was approximately 7% lower for the second. The most likely explanation for the drop in biosorption capacity is related to the leaching of the slightly soluble alginate (or alginic acid) which is present in the brown algal cell walls of *Sargassum*. During the changes between cycles, fluctuations in the pH of the solution may result in leaching of the polysaccharide, since alginate becomes increasingly soluble with increasing pH. Figueira et al (1998) also documented the loss in biomass binding capacity and related it to the amount of TOC (total organic content) detected in the effluent during a column operation for cadmium biosorption. However, over the one month period of continuous column operation, no significant visible (structural) damage was incurred by the biomass.

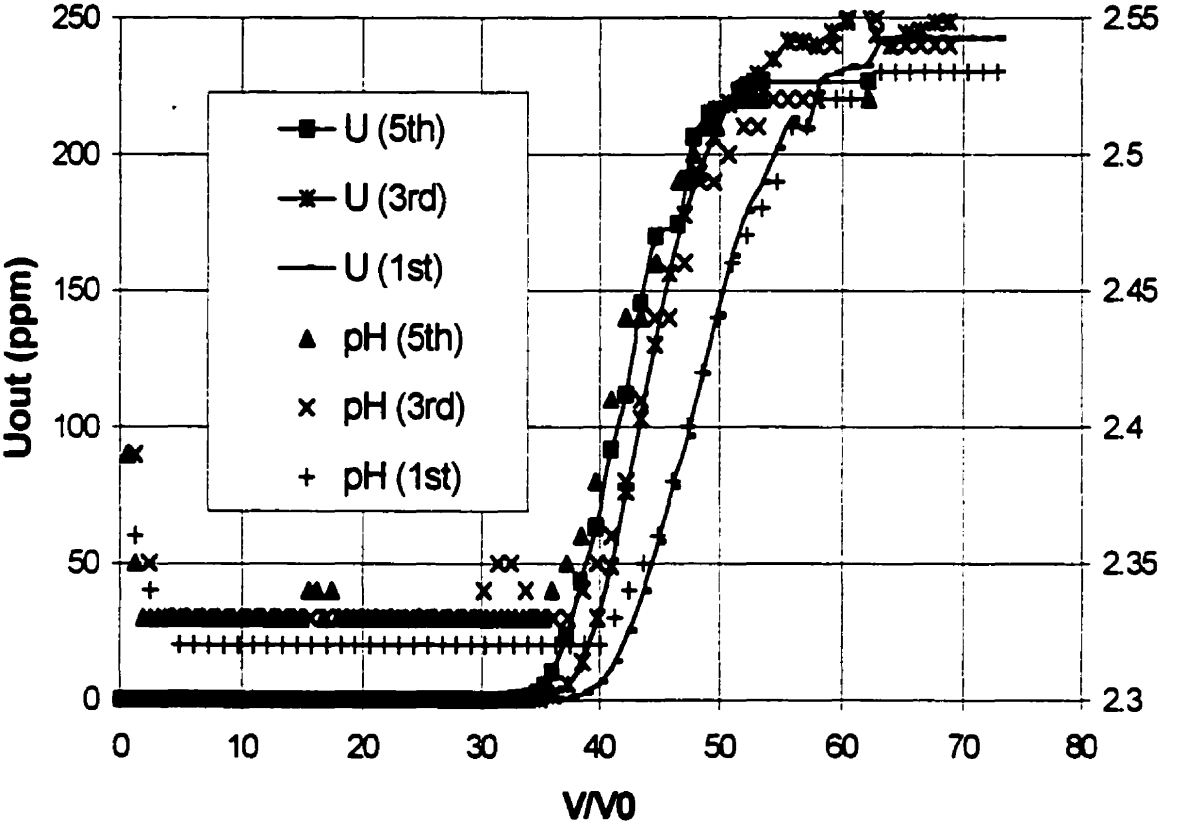

Figure 4.3.4: Breakthrough curves for different sorption-desorption cycles. F=340 ml/h, V_{bed} = 280 cm^3, biomass = 22.642 g

4.3.2 Influence of flowrate on sorption breakthrough curve

Uranium biosorption breakthrough curves are plotted for different flowrates in Figure 4.3.5. The x-axis represents the ratio of the metal solution volume passed through the column to the empty-bed volume and the y-axis represents the ratio of the uranium concentration in column outlet to that of the uranium concentration in the feed. Each curve was obtained by a separate column run each employing fresh biomass.

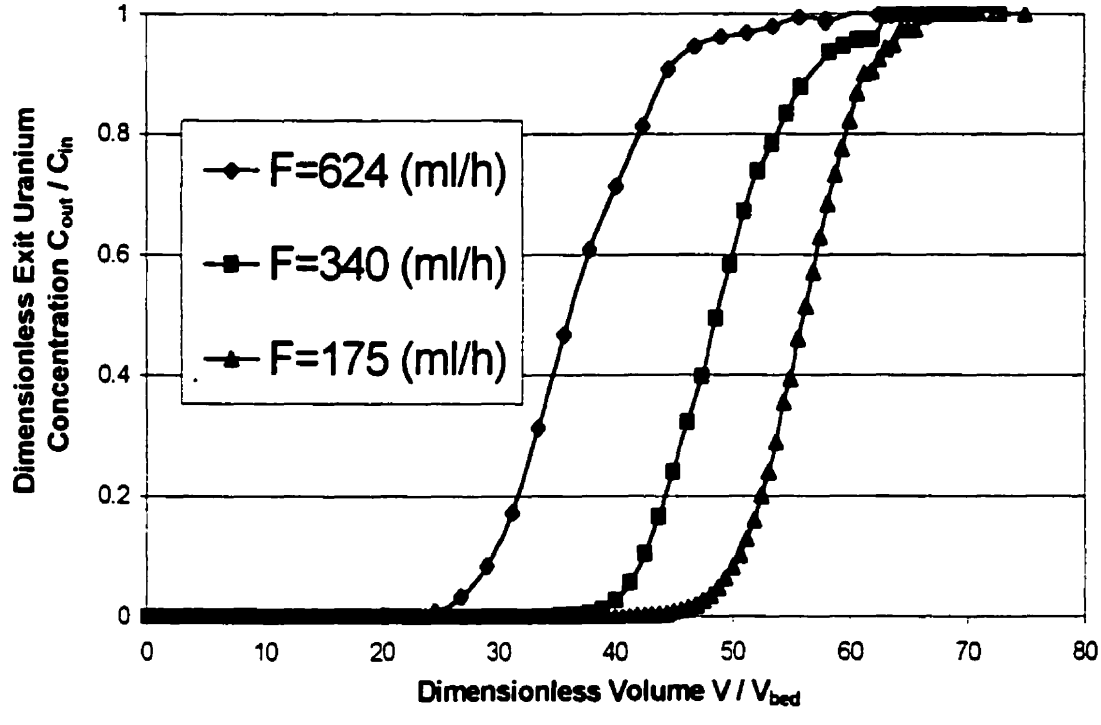

Figure 4.3.5: Influence of flowrate on the break through curve.

The shape of the breakthrough curves for different flowrates are similar. The curve becomes slightly flatter as flowrate is increased although the difference is rather small. This demonstrates that the length of the mass transfer zone for different flowrates must remain nearly constant so that back-mixing is not significant in the column and therefore, axial dispersion (back-mixing) does not play an important role in fluid flow through the column. Breakthrough time is however significantly affected by flowrate. When the flowrate (F) was increased initially from 170 ml/h to 340 ml/h and the

subsequently to 624 ml/h, the breakthrough time decreased (as dimensionless volume) from 42 to 36, and finally to 25 times, correspondingly. Due to the short length (0.45 m) and porous nature of the packed algal biomass, no significant pressure drop was observed across the column. As can be seen in Figure 4.3.5, the highest flow rate has the shortest breakthrough time. Correspondingly, lower flowrates result in longer breakthrough times. The importance of this lies in the realization that a shorter breakthrough time (in practical application) would result in the termination of the cycle (prematurely) since an undesirably high concentration of metal would be flowing out the exit. The problem is that for such a high flowrate, the biomass does not reach its full saturation, i.e. the saturation zone is reduced. When the flowrate is lower, the saturation zone is extended and more metal (or uranium) can be sequestered before the appearance of the breakthrough concentration at the outlet. Despite this, a lower flowrate also implies an undesirable lower productivity. Hence, a feasibility study would need to be conducted before any implementation in order to weight the benefits of reduced service time over that of increased biomass uptake per column packing.

4.3.3 Influence of feed pH on sorption breakthrough curve

For the batch biosorption system, biosorption performance is better at higher pH. However, alginate becomes increasingly soluble with increasing pH. This is also true for continuous flow biosorption column operations, with the addition of some new characteristics. The breakthrough curves for the feed uranium solution at pH 2.5 and pH 4.0 are presented in Figure 4.3.6. The breakthrough time for influent with a pH of 4.0 was approximately twice that of the breakthrough for influent with a pH of 2.5. For both cases the effluent pH decreased quickly after the start of operation. A pH variation across the length of the column can be concluded from the gradual rise in effluent pH depicted in Figure 4.3.6. The differences in pH within the column must therefore influence its binding capacity just as is seen for the case of equilibrium biosorption. For the influent with a pH of 2.5, the pH was relatively invariable and displayed an exit pH of 2.35. The slight decrease in pH did not affect the biomass binding capacity significantly (according to the isotherm model established in section 4.1). For the influent with a pH of 4.0, the pH distribution in the column ranged from 2.7 to 4.0, whereby the pH of 2.7 was constant

before breakthrough. The increasing pH level throughout the column after the breakthrough resulted in a gradually increased uranium binding capacity. This can be seen in the gradually extending column mass transfer zone which is represented by the relatively flat breakthrough curve. Although the higher influent pH resulted in a longer column service time, most uranium waste solutions in industries are acidic (Hu, et al., 1996; Tsezos and Volesky, 1981) making the results obtained under lower feed pH level more valuable for potential application.

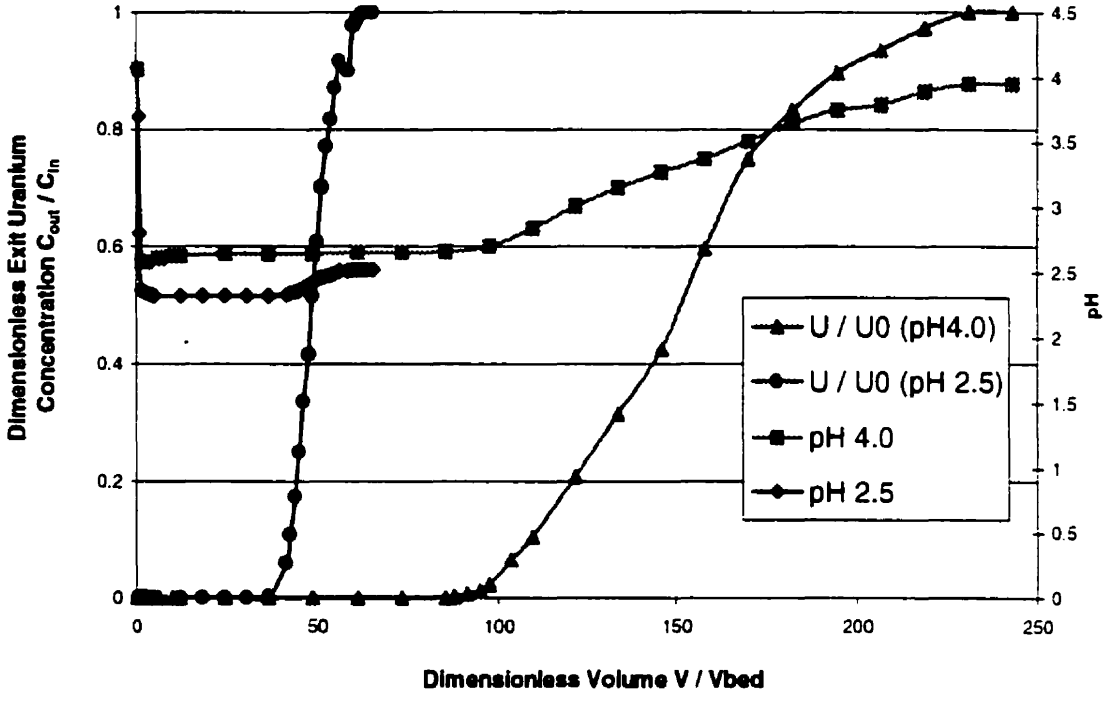

Figure 4.3.6: Uranium and pH breakthrough curves at the feed pH 2.5 and 4.0

4.3.4 Uranium biosorption by calcium pre-treated biomass

As previously discussed in section 4.1, biosorption of uranium by protonated biomass is always accompanied by the release of protons. During continuous flow column operation, this is reflected in the lowering of the solution pH throughout the column. This lower solution pH value in turn reduces the biosorption capacity significantly (section 4.1.1). Since pH control inside the column is difficult, calcium pre-treated biomass was examined as a means to stabilize pH fluctuation. This procedure

could potentially decrease the pH in the column, thereby enhancing biosorption performance. An experimental breakthrough curve obtained under these conditions is shown in Figure 4.3.7. The exit uranium and calcium concentrations and solution pH values are plotted as a function of the effluent volume expressed as empty bed volumes.

While the feed pH was 4.5, the exit solution pH remained constant (pH 4.2 ~ pH 4.3) for most of the experiment before the breakthrough point. The exit pH of 4.2 ~ 4.3 is a lower than that of feed pH yet it is much higher than the exit pH of 2.3 observed with protonated biomass. The calcium release curve indicates that the biosorption of uranium by the calcium pre-treated biomass is an ion exchange process. Compared to the breakthrough time obtained with protonated biomass in Figure 4.3.2, the breakthrough time increased almost two-fold. Biosorption was therefore enhanced through the implementation of calcium pre-treated biomass.

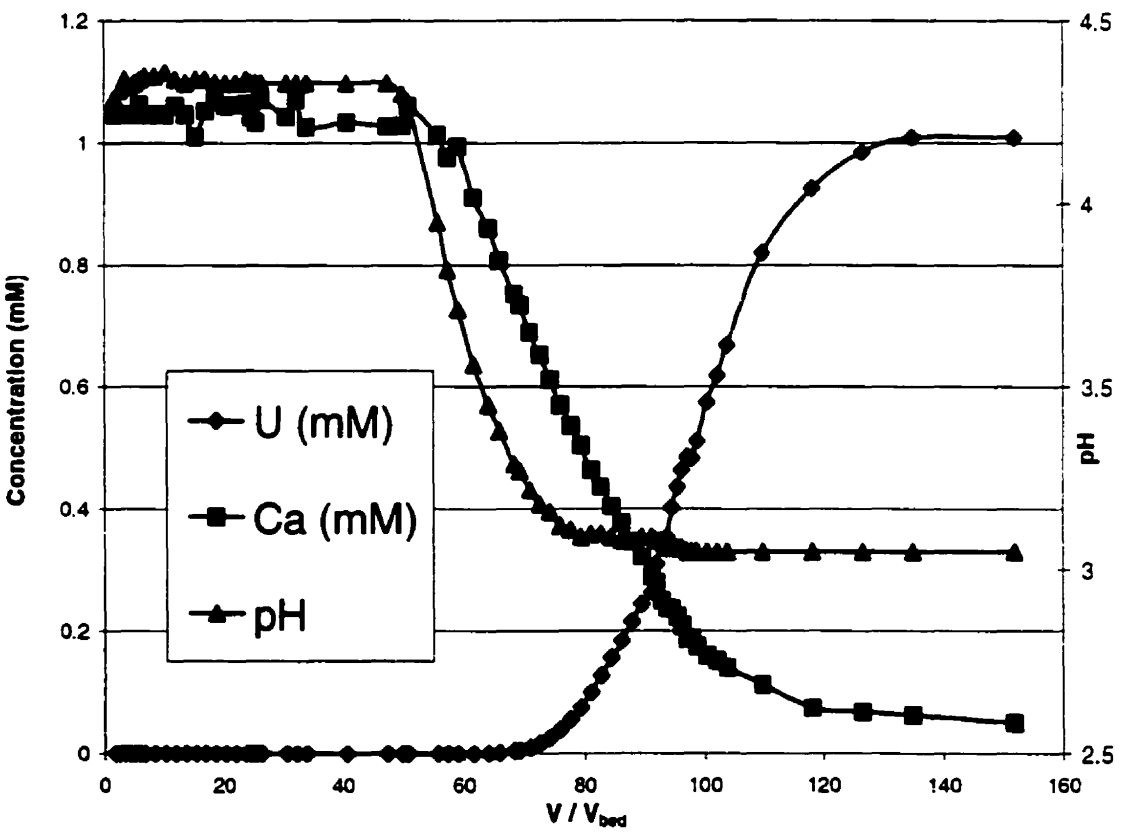

Figure 4.3.7: The breakthrough curve of uranium biosorption on calcium pre-treated biomass.

However, regeneration of calcium biomass is much more difficult to achieve than that for protonated biomass. Protonated biomass was regenerated naturally during the elution process with HCl. However, in order to maintain the calcium biomass, an extra step must be adopted, namely a saturated calcium chloride solution rinse that is pumped through the column for approximately 72 hours. Over this duration the biomass is successfully converted back to the calcium-saturated form. As the consequence, the enhanced biosorption performance may not offset the costs which are likely to be incurred during the extra slow regeneration process. Again, a feasibility and optimization study addressing this issue would need to be carried out.

4.3.5 Evaluation of the possible effect of axial dispersion in the column

During column operation, and when the column was saturated with uranium, the column inlet flow was switched to a distilled water source which resulted in the following uranium effluent concentration profile (Figure 4.3.8).

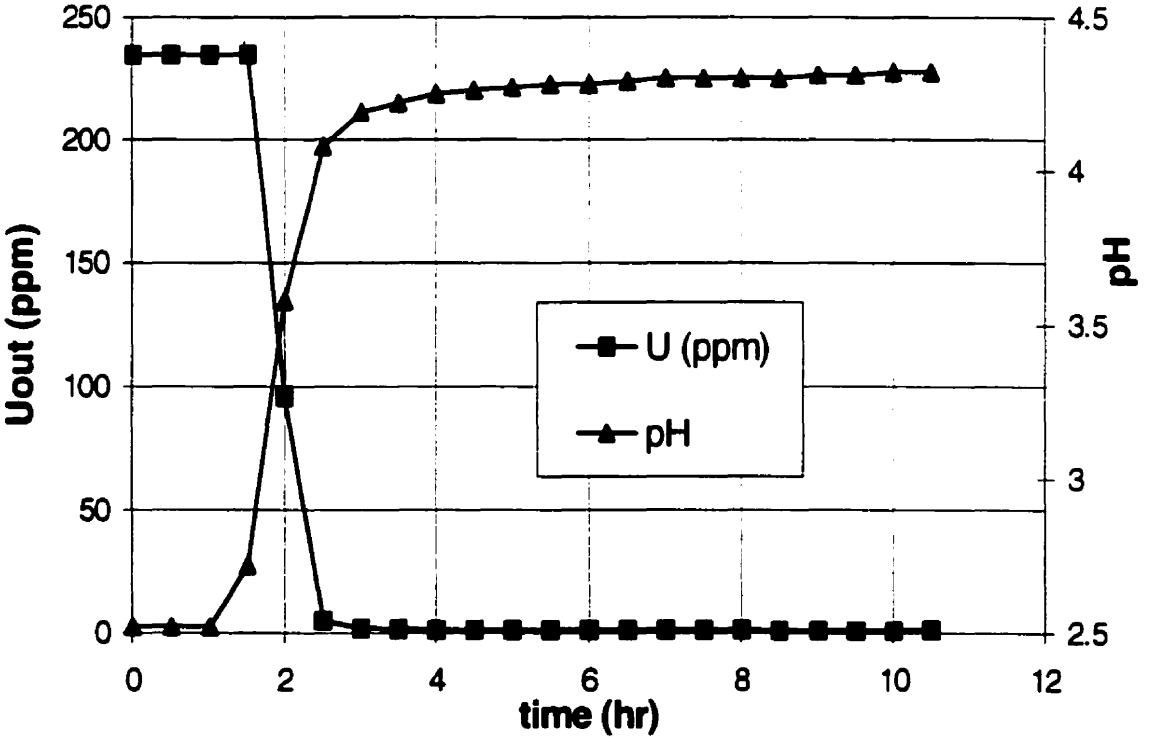

Figure 4.3.8: Response of the column outlet concentration to the step function in the column inlet (switch to distilled water). F=175 ml/h, V_{bed}=280 ml, biomass = 22.64 g

The horizontal axis represents the operation time (switch occurring at $t = 0$ hr) and the vertical axes represents the outlet uranium concentration and pH value, respectively. The initial flat uranium concentration represents the residence time before distilled water exited the column. The sharp decrease in the exit uranium concentration and the corresponding sharp increase in the exit pH value indicate that axial dispersion is not significant in the column and can be neglected without causing large errors in subsequent calculations. This observation agrees with the conclusion of Crittenden and Weber which were made for a fixed-bed carbon adsorber (Crittenden and Weber, 1978a, b, c). They established that column flow dispersion effects could generally be neglected for relatively long columns. Furthermore, Weber and Liu's studies of micro-column systems show that the effect of axial dispersion was negligible as well (Weber and Liu, 1981). The effect of axial dispersion was therefore not included in the present mass transfer model for the biosorption column system.

4.3.6 Mass transfer model for continuous flow columns

The column breakthrough time is a crucial parameter for the design of column system. It is determined by many factors which include the equilibrium isotherm, fluid flow, axial and radial dispersion in the column and the external and internal diffusion resistance of the sorbate material. Although the most important mass transfer resistance for sorption from aqueous solutions has been established to be the internal (intraparticle) diffusion by many researchers (Rosen, 1952, Apel and Torm, 1993), film resistance also plays an important role (Tsezos et. al., 1988). In order to apply the scale-up calculation in a wide range of cases, it is necessary to represent the behavior of the dynamic column by an appropriate mathematical model which can be solved either analytically or numerically. A methodology similar to the previously discussed one for batch system in section 4.2 may be used to develop a model for continuous flow column systems. The model proposed here is based on the same assumptions as described for batch dynamics. The mass conservation equation in the macroscopic fluid is represented by:

$$\varepsilon \frac{\partial C_b}{\partial \tau} + U_s \frac{\partial C_b}{\partial z} + \rho(1-\varepsilon)\frac{\partial \bar{q}}{\partial \tau} = 0 \qquad (4.3\text{-}1)$$

Film mass transfer by:

$$\frac{\partial \bar{q}}{\partial \tau} = K_f a(c_b - c_r|_{r=R}) \tag{4.3-2}$$

Intraparticle diffusion by:

$$\varepsilon_p \frac{\partial C_r}{\partial \tilde{\tau}} + \rho \frac{\partial q}{\partial \tilde{\tau}} = D_e \frac{\partial C_r}{\partial r^2} \tag{4.3-3}$$

Isotherm by:

$$q = f(C_r) \tag{4.3-4}$$

C_b, C_r represent the metal concentrations in the bulk fluid stream and of the fluid in the biosorbent pores, respectively, and q is the metal uptake. τ and $\tilde{\tau}$ represent the bulk fluid and the intraparticle diffusion time , respectively. ε, ε_p are, respectively, the bed porosity and intraparticle porosities. ρ is pellet density and U_s is the fluid superficial velocity, $U_s = F/S$, where F is the feed flowrate and S is the section area of the column. K_f is the mass transfer coefficient across the fluid-particle interface and a is the specific external particle area, i.e. total external surface area per unit volume of the particle. D_e is the effective diffusion coefficient inside the particle. $f(C)$ is the sorption isotherm relationship.

The initial and boundary conditions for equations (1) and (3) are as follows:

$$\tau \leq 0, \quad C_b = 0 \qquad (0 \leq z \leq L) \tag{4.3-5}$$

$$z = 0, \quad C_b = C_{in} \qquad (\tau > 0) \tag{4.3-6}$$

$$\tilde{\tau} \leq 0, \quad C_r = 0 \qquad (0 \leq r \leq R) \tag{4.3-7}$$

$$r = 0, \quad \frac{\partial c_r}{\partial r}|_{r=0} = 0 \qquad (\tilde{\tau} > 0) \tag{4.3-8}$$

$$r = R, \quad D_e \frac{\partial c_r}{\partial r}|_{r=R} = K_f (C_b - C_r|_{r=R}) \qquad (\tilde{\tau} > 0) \tag{4.3-9}$$

Since axial dispersion was neglected, the biosorbent at different axial positions within the column is exposed to the fluid at different times. Accordingly, the following relationship holds:

$$\tilde{\tau} = \tau - \frac{\varepsilon z}{Us} \tag{4.3-10}$$

Defining a new corrected time $\theta = \tilde{\tau} = \tau - \frac{\varepsilon z}{Us}$ and substituting it into the above model equations, the following dimensionless relationships are obtained:

$$\frac{\partial u}{\partial x} + \beta \, Bo \, (u - v|_{y=1}) = 0 \tag{4.3-11}$$

$$\lambda(v) \frac{\partial v}{\partial t} = \frac{\partial^2 v}{\partial y^2} \tag{4.3-12}$$

$$t \le 0, \quad u = 0 \qquad (0 \le x \le 1) \tag{4.3-13}$$

$$x = 0, \quad u = 1 \qquad (t > 0) \tag{4.3-14}$$

$$x = 1 \quad \frac{\partial u}{\partial x}|_{x=1} = 0 \qquad (t > 0) \tag{4.3-15}$$

$$t \le 0, \quad v = 0 \qquad (0 \le y \le 1) \tag{4.3-16}$$

$$y = 0 \quad \frac{\partial v}{\partial y}|_{y=0} = 0 \qquad (t>0) \tag{4.3-17}$$

$$y = 1 \quad \frac{\partial v}{\partial y}|_{y=1} = Bo(u - v|_{y=1}) \qquad (t>0) \tag{4.3-18}$$

The definitions of new variables used in the above equations are as follows:

$$u = \frac{C_b}{C_{in}}, \quad v = \frac{C_r}{C_{in}}, \quad t = \frac{D_e}{R^2}\theta,$$

$$\gamma = \frac{D_e L}{U_z R^2}, \quad \beta = (1-\varepsilon)\gamma, \quad Bo = \frac{K_f R}{D_e}, \quad \lambda(v) = \varepsilon_p + \rho\frac{\partial f}{\partial c}(c_{in}\, v)$$

4.3.7 Numerical solution of the column model equations

The dimensionless PDEs can be solved numerically by the Orthogonal Collocation (OC) method as described by Villadsen and Michelsen (1978). The discretizing equation (4.3-11) at axial collocation points, x_j, are:

$$\sum_{j=1}^{N+1} A_{ij} u_j + \beta(u_i - v_{i,M+1}) = 0, \ (i = 1, N+1) \tag{4.3-19}$$

and the discretizing equation (4.3-12) at radial collocation points, y_{il}, are:

$$\lambda(v_{il})\frac{\partial v_{il}}{\partial t} = \sum_{k=1}^{M+1} BR_{lk} v_{ik}, \qquad (l = 1, M+1) \tag{4.3-20}$$

where i and l are the number of axial and radial collocation points, respectively. U_j and V_{ik} are the approximate values of u and v at the j^{th} axial collocation point and the k^{th} radial collocation point, respectively. $A(i, j)$, $B(i, j)$ and $AR(i, j)$, $BR(i, j)$ are the orthogonal collocation matrices for the first and second order derivatives in axial and radial directions, respectively. Since axial dispersion is neglected, the matrix $B(i, j)$ is not

needed in the situation. The collocation points are fixed at the outset of the calculation and thus the discretizing matrices need be calculated only once because they only depend on the choice of collocation points.

Similarly, the radial boundary condition equations (4.3-16) and (4.3-17) are discretized at collocation points as follows:

$$\sum_{k=1}^{M+1} AR_{1,k} v_{ik} = 0, \qquad (i = 1, N+1) \qquad (4.3\text{-}21)$$

$$\sum_{k=1}^{M+1} AR_{M+1,k} v_{ik} = Bo(u_i - v_{i,M+1}) \qquad (i = 1, N+1) \qquad (4.3\text{-}22)$$

We express the boundary value V_{i1} and $V_{i,M+1}$ by solving the above two equations:

$$v_{i,1} = \frac{-AR_{1,M+1} Bo\, u_i + \sum_{k=2}^{M} [AR_{1,M+1} AR_{M+1,k} - AR_{1,k}(AR_{M+1,M+1} + Bo)] v_{ik}}{[AR_{1,1}(AR_{M+1,M+1} + Bo) - AR_{M+1,1} AR_{1,M+1}]} \qquad (4.3\text{-}23)$$

$$v_{i,M+1} = \frac{AR_{1,1} Bo\, u_i - \sum_{k=2}^{M} (AR_{1,1} AR_{M+1,k} - AR_{M+1,1} AR_{1,k}) v_{ik}}{[AR_{1,1}(AR_{M+1,M+1} + Bo) - AR_{M+1,1} AR_{1,M+1}]} \qquad (4.3\text{-}24)$$

Substituting equations (4.3-23), (4.3-24) into (4.3-20):

$$\frac{dv_{i,l}}{dt} = \frac{1}{\lambda(v_{il})} \{ \sum_{k=2}^{M} \left[BR_{l,k} + \frac{BR_{l,1}[AR_{1,M+1} AR_{M+1,k} - AR_{1,k}(AR_{M+1,M+1} + Bo)]}{AR_{1,1}(AR_{M+1,M+1} + Bo) - AR_{M+1,1} AR_{1,M+1}} - \frac{BR_{l,1}[AR_{1,1} AR_{M+1,k} - AR_{1,k}(AR_{M+1,M+1} + Bi)]}{AR_{1,1}(AR_{M+1,M+1} + Bo) - AR_{M+1,1} AR_{1,M+1}} \right] v_{ik} + \left[\frac{-BR_{1,M+1} + BR_{1,1}}{AR_{1,1}(AR_{M+1,M+1} + Bo) - AR_{M+1,1} AR_{1,M+1}} \right] Bo\, u_i \} \qquad (4.3\text{-}25)$$

$(i = 1, N+1, l = 2, M)$

In order to eliminate U_i from the above equation, the axial boundary equations (4.3-14), (4.3-15) need to be discretized first as follows:

$$u_1 = 1; \tag{4.3-26}$$

$$\sum_{j=1}^{N+1} A_{N+1,j} u_{ij} = 0, \qquad (i = 1, N+1) \tag{4.3-27}$$

Solving U_{N+1}:

$$u_{N+1} = -\frac{A_{N+1,1}}{A_{N+1,N+1}} - \frac{\sum_{j=2}^{N} A_{N+1,j} u_{ij}}{A_{N+1,N+1}} \tag{4.3-28}$$

Then substitute (4.3-24), (4.3-26) and (4.3-28) into axial equation (4.3-19):

$$\sum_{\substack{j=1 \\ i \neq j}}^{N+1} \left((A_{i,j} - \frac{AR_{i,N+1} AR_{N+1,j}}{AR_{N+1,N+1}}) u_j + (A_{i,i} + \beta - \frac{\beta AR_{1,1}\, Bo}{(AR_{1,1}(AR_{M+1,M+1} + Bo) - AR_{M+1,1} AR_{1,M+1})}) u_i \right)$$

$$= -A_{i,1} + \frac{AR_{i,N+1} AR_{N+1,1}}{AR_{N+1,N+1}} - \frac{\beta \sum_{k=2}^{M} (AR_{1,1} AR_{M+1,k} - AR_{M+1,1} AR_{1,k}) v_{i,k}}{(AR_{1,1}(AR_{M+1,M+1} + Bo) - AR_{M+1,1} AR_{1,M+1})}$$

$$(i = 1, N+1; l = 2, M) \tag{4.3-29}$$

Express u_i with $v_{i,k}$:

$$U_i = \sum_{j=1}^{N+1} D_{i,j}^{-1} e_j \tag{4.3-30}$$

where

$$i \neq j: \quad D_{i,j} = A_{i,j} - \frac{AR_{i,N+1} AR_{N+1,j}}{AR_{N+1,N+1}} \tag{4.3-31}$$

$$i = j: \quad D_{i,j} = A_{i,j} - \frac{AR_{i,N+1} AR_{N+1,j}}{AR_{N+1,N+1}} + \beta - \frac{\beta\, Bo}{(AR_{1,1} AR_{M+1,M+1} - AR_{M+1,1} AR_{1,M+1} + Bo)} \tag{4.3-32}$$

$$e_i = -A_{i,1} + \frac{AR_{i,N+1} AR_{N+1,1}}{AR_{N+1,N+1}} - \frac{\beta \sum_{k=2}^{M} (AR_{1,1} AR_{M+1,k} - AR_{M+1,1} AR_{1,k}) v_{i,k}}{(AR_{1,1}(AR_{M+1,M+1} + Bo) - AR_{M+1,1} AR_{1,M+1})} \tag{4.3-33}$$

$(i = 1, N+1; \quad j = 1, N+1)$

By substituting equation (4.3-30) into equation (4.3-25), the latter becomes a series of ODEs with respect to the interior radial concentration $V_{i,l}$. Thus with the initial condition $V_{i,l} = 0$, equation (4.3-25) can be integrated over time by a standard integrating method, such as the 4th order Runge-Kutta algorithm (Lapidus and Pinder, 1982). Once the $V_{i,l}$ s are obtained, the axial concentration U_i can be calculated from equation (4.3-30). A computer program was developed to implement the above numerical algorithm. The source code in FORTRAN is shown in Appendix C.

4.3.8 Determination of model parameters and modelling the experimental data

The intraparticle diffusion coefficient D_e was determined by a batch dynamic study (section 4.2.6). The film coefficient K_f may be regressed from the experimental breakthrough curves. A trial and error procedure was adapted by adjusting the value of K_f until the regression objective function reached its minimum value. The objective function is as follows:

$$\varphi = \sum_{i=1}^{n} \left| \left(\overline{C}^{Model} - \overline{C}^{Experimental} \right) \right|_i \qquad (4.3.26)$$

where i is the i^{th} experimental data point and n is the total number of experimental data points.

Figure 4.3.9 illustrates experimental and model-calculated breakthrough curves for uranium ions sorbed by protonated biomass. During column operation, 22.6 g (dry) of biomass was loaded in to 280 cm^3 of bed volume. A 1.0 mM uranium solution with pH = 2.5 was fed into the column at a flowrate of 340 ml/h. The isotherm parameters at pH 2.5 were determined in section 4.1 and the biomass particle properties are described in section 4.2 for batch system dynamics. The value of the effective intraparticle diffusion coefficient obtained in section 4.2, 6.0×10^{-6} cm^2/s, was applied in this model. The bed porosity was determined by Kratochvil (1997) to be 0.77. The value of the external mass transfer coefficient K_f was therefore regressed and found to be 3.0×10^{-3} cm/s.

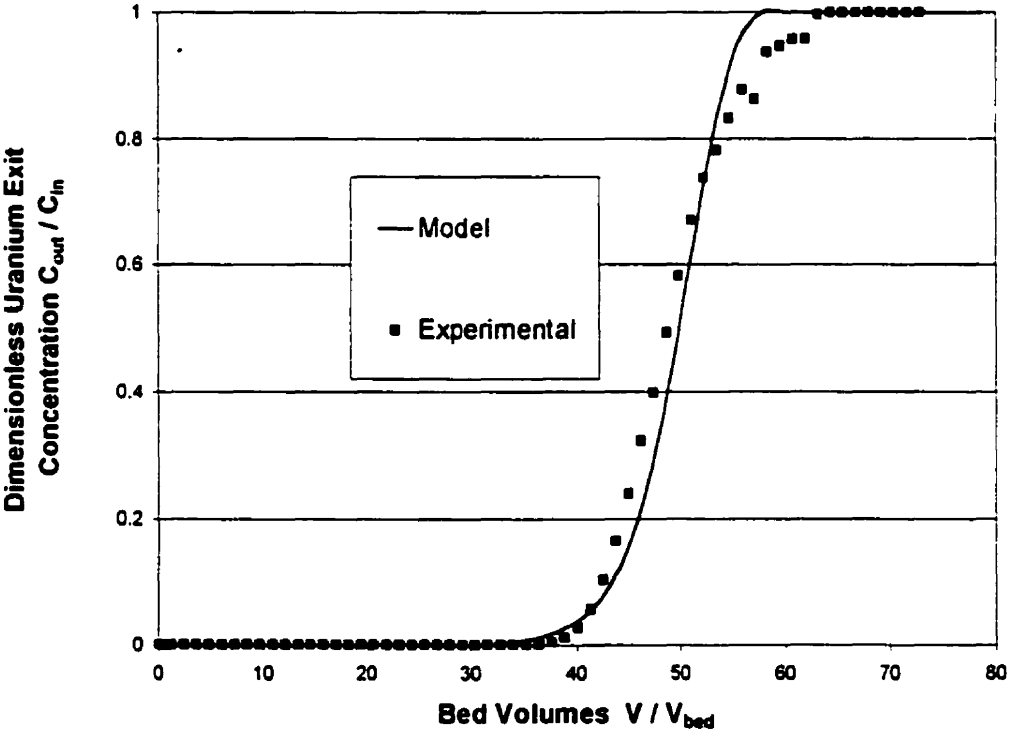

Figure 4.3.9: Comparison of experimental uranium breakthrough curve and the Mass Transfer Model calculated breakthrough curve for the protonated *Sargassum* biomass.

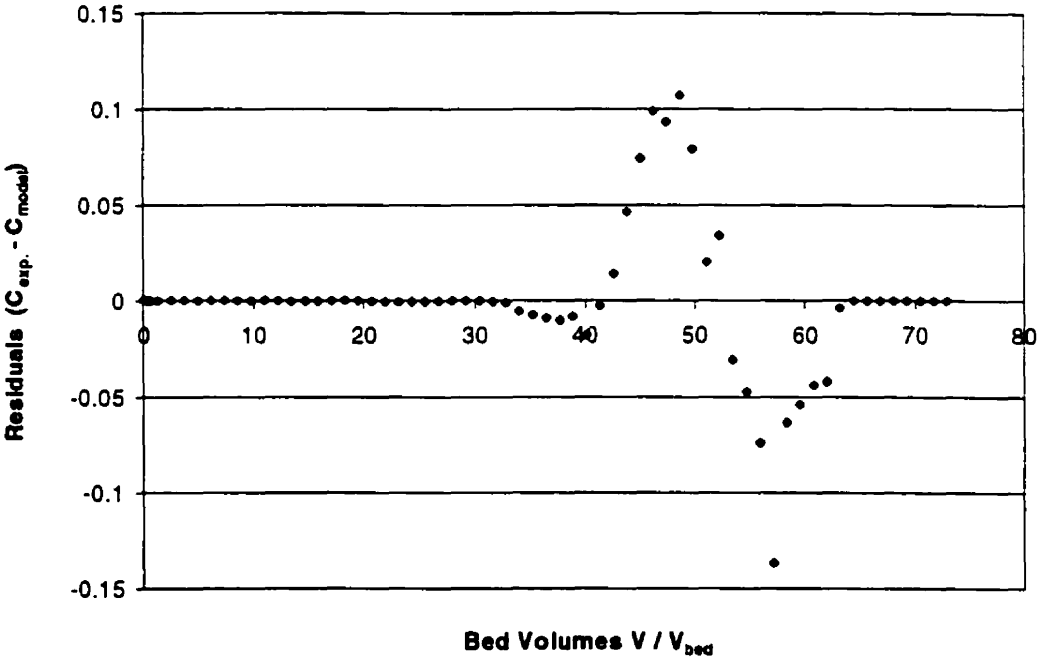

Figure 4.3.10: Residuals of experimental and the Mass Transfer Model calculated uranium breakthrough curve.

The fitting curve was close to the experimental one within an average deviation of 5%. The trend in residual is presented in Figure 4.3.10. The residuals for the "sorption" zone and for the "saturation" zone were minor. During the breakthrough process, the residual increases to a valued of approximately 0.1 and then decreased to -0.08 before returning to zero again. The fact that the residuals in the breakthrough zone of the breakthrough curve are not randomly distributed suggests that the model does not statistically represent the experimental data well for this part of the curve. However, the trend of the fitted curve agrees well with the experimental breakthrough data. Although K_f is correlated with hydraulic conditions, such as the Reynolds number and the kinematic viscosity of the fluid (Karberry, 1960: Williamson, et al., 1963: Kataoka, et al., 1972: Furusawa and Smith, 1973), it is more convenient to numerically regress K_f from column experimental data. Weber and Liu (1980) obtained a range of K_f values from 2.0 to 5.0×10^{-3} cm/sec using a "micro-column" technique. The model regressed value of K_f

($3.0x10^{-3}$ cm/s) agrees well with Weber and Liu's results. However, the model curve was not very sensitive to the external mass transfer diffusion coefficient. This implies that the external mass transfer may not play as important a role as compared to the intraparticle diffusion coefficient. The model simulation results can be applied to the biosorption process design and to optimize the operation of biosorption columns. However, the loading of brown algal biomass to a large-scale column in industry may be quite different from the process of filling a small column in the lab. Many factors including channeling and wall effects may raise serious problems in large-scale applications and therefore affect the validity of the mathematical model. A series of pilot experiments may be required to modify the mathematical model during the scaling-up design.

4.3.9 Section summary

The biosorption of uranium by *Sargassum* seaweed biomass in a continuous flow column was established to be a highly efficient process even under acidic feed conditions. For feed pH 2.5, the average column binding capacity for uranium before the breakthrough time was as high as 105 mg/g biomass. The uranium uptake increased more than two-fold when a higher feed pH (4.0) was used. The saturated column was regenerated effectively by elution with a dilute hydrochloric acid (0.1 N). The average uranium concentration in the eluant HCl solution was approximately 6000 mg/L which yields an overall uranium process concentration factor of approximately 25-30. The column can operate for a prolonged time, e.g. 30 days, over multiple biosorption-elution-rinse process cycles. No visible structural damage to the biomass was observed during these multiple operation cycles. Operation at a higher pH level can be maintained by using calcium pre-treated biomass. For instance, when the feed pH was 4.5, a pH value ranging from pH 4.0 to 4.3 was detected at the column outlet. As a result, the breakthrough time increased two-fold compared with the protonated biomass.

A mass transfer model based on external and intraparticle diffusion was applied to quantitatively describe the operation of a continuous flow biosorption column. The effective diffusion coefficient obtained from batch biosorption studies was incorporated into the column model. The Orthogonal Collocation method was employed to

numerically solve the non-linear model PDEs. The film diffusion coefficient was regressed by fitting the model equations to the experimental breakthrough curves and the obtained value was $3.0x10^{-3}$ cm/sec. The model-calculated breakthrough curve agrees approximately with the experimental data and the column service time was successfully fitted by the model. However, a more thorough investigation of model simulation must be performed under different experimental conditions before the process can be applied to broader process simulations.

5 Summary, Original Contributions and Suggestions for Future Research

5.1 Summary

Ion exchange was established to be the dominant mechanism for the biosorption of uranium and cadmium by the marine brown algae *Sargassum fluitans*. The solution pH affected metal sorption significantly, and increased with rising pH. The proton concentration was incorporated into an explicit isotherm model as an independent variable by Schiewer and Volesky (1995; 1996). For some metals, such as uranium, speciation plays an important role in its sorption on to the biosorbent. Various complexes participate in the ion exchange with protons of the seaweed binding sites and this affects the ion exchange stoichiometry. For instance, the divalent $(UO_2)_2(OH)_2^{2+}$ specie makes a significant contribution to the total uranium uptake because it contains two uranium atoms. Whereas two biomass binding sites are required to bind one divalent UO_2^{2+} ion, they can accommodate two of the monovalent specie UO_2OH^+ or one of the divalent specie $(UO_2)_2(OH)_2^{2+}$. At pH 4.0, the hydrolyzed forms are more abundant and the maximum uranium uptake was affected and reached as high as 480 mg/g or 2.08 mmol/g. This corresponds closely to the total number biomass binding sites.

The novel Hydrolyzed Ion Exchange Model (HIEM) is based on ion exchange between hydrolyzed uranium ions and protons which were originally bound to the biomass. The model incorporates the proton concentration, the hydrolysis equilibrium constants for uranium, and the total uranium concentration. The four model parameters were determined by regression using a two-step multivariable regression technique. Either the uranium biosorption or acid desorption equilibrium state may be predicted

from the initial conditions. The influence of pH on uranium biosorption under acidic conditions was well described by the model-calculated curves with an acceptable deviation. The HIEM model equation reduces to Schiewer-Volesky's one-site model formula for non-hydrolyzable metal cations such as cadmium

Biosorption of heavy metals was accompanied by proton release from the protonated biosorbent. The resulting pH decrease of the batch sorption system would negatively affect biosorption uptake had no base been added to maintain it. The end-point titration method was used for the experimental determination of uranium and cadmium biosorption rates by *Sargassum fluitans* biomass at constant pH values ranging from pH 2.5 – 4.0. Intraparticle diffusion was assumed to be the main rate controlling step for the sorption of ionic species. The dynamics of *desorption* differ only at the initial condition from that which occurs during biosorption. The geometry of the *Sargassum* biomass particle approximate flat chips whereby its thickness can be used as the controlling dimension for diffusion. This provides a basis by which a one-dimensional intraparticle diffusion model may be applied to simulate the biosorption and desorption rates. The Galerkin Finite-Element Method (GFEM) numerical technique was applied to solve the non-linear model partial differential equations. The biosorption rates of uranium and cadmium at various solution pH values were quantified by the model and the effective diffusion coefficients for the metals were regressed using the end-point titration data set.

Biosorption of uranium in a continuous flow column was shown to be highly efficient even under acidic feed pH values, such as pH 2.5. The average biosorption column capacity for uranium before breakthrough occurred was 105 mg/g biomass. The uranium saturated column was regenerated efficiently by rinsing with dilute hydrochloric acid. The overall process uranium concentration factor was approximately 25-30. Column operation was maintained for a prolonged period and comprised multiple process cycles. Higher feed pH values and lower flowrates yielded the best biosorption performance. No pH decrease was observed when calcium pre-treated biomass was used, a doubling in biosorption performance occurred at higher feed pH values. However, regeneration of calcium pre-treated biomass was more difficult.

A mass transfer model based on external and intraparticle diffusion was developed which incorporated an isotherm relationship, the intraparticle diffusion

coefficient and fluid flow in to a continuous flow biosorption column model. Using the Langmuir sorption isotherm equation and the effective diffusion coefficient obtained in this work, the model regressed the film diffusion coefficient by fitting the model equations to the experimental breakthrough curves. The model-calculated breakthrough curve agrees well with the experimental data set. This model simulation constitutes a powerful tool for biosorption process design and optimization.

5.2 Original Contributions

Biosorption Isotherm

- It has been demonstrated that the brown algae *Sargassum fluitans* can sorb uranium and cadmium effectively. The uptake of uranium was found to be 60 – 70% higher than one would predict based on an assumption of ion exchange involving solely the uranyl ion.
- The role uranium hydrolysis plays in the biosorption of total uranium was found to be crucial.
- A new uranium equilibrium isotherm model (HIEM) which is based on the ion exchange of the hydrolyzed uranium complexes was developed.
- Model parameters were determined by multivariable parameter regression for uranium biosorption.
- The influence of solution pH on uranium biosorption performance was quantified.

Biosorption Rate

- The end-point titration method typically used in enzyme kinetics was introduced to determine the biosorption rate for *Sargassum fluitans* at constant solution pH values.
- A one-dimensional intraparticle mass transfer model was introduced to quantify the biosorption rate.
- A method for determining the effective intraparticle diffusion coefficient was developed and applied to uranium and cadmium biosorption and desorption processes successfully.

Biosorption column

- The biosorption of uranium in a continuous flow column was established to be highly efficient even at acidic pH values.
- Protonated *Sargassum fluitans* biomass was found to be stable in multiple biosorption-acid elution cycles over prolonged operation periods.
- A mass transfer model which included the biosorption isotherm, mass transfer diffusion coefficient and fluid flow conditions was developed for continuous flow biosorption columns.
- The mass transfer model parameters including the column service time were fitted successfully to the experimental breakthrough curve which was obtained from the operation of a uranium biosorption column.

5.3 Suggestions for Further Research

- Physically confirm the presence of the uranium complexes on the biomass phase.
- Investigate the extent to which fucoidan plays a role in the binding uranium complexes.
- Apply the HIEM model to the intraparticle diffusion model for batch biosorption dynamics and to the column mass transfer model.
- Investigate the potential interference of other metals, especially iron, on uranium equilibrium biosorption, dynamics and column operation.

6 REFERENCES

Adams, B.A. and Holmes, E.L. (1935) Adsorptive properties of synthetic resins. I. *J. Soc. Chem. Ind.* **54**, 1-6.

Aldor, I., Fourest, E. and Volesky, B. (1995) Desorption of cadmium from algal biosorbent. *Can. J. Chem. Eng.* **73**, 516-522.

Allen, S., Brown, P., McKay, G. and Flynn, O. (1992) An evaluation of single resistance transfer models in the sorption of metal ions by peat. *J. Chem. Technol. Biotechnol.* **54**, 271-276.

Amundson, N.R. (1956) Solid-fluid interaction in fixed and moving beds. *Ind. Eng. Chem.* **48**, 26-35.

Apel, M.L. and Torma, A.E. (1993) Determination of kinetics and diffusion coefficients of metal sorption on Ca-alginate beads. *Can. J. Chem. Eng.* **71**, 652-656.

Ashley, N.V. and Roach, D.J.W. (1990) Review of biotechnology application to nuclear waste treatment. *J. Chem. Technol. Biotechnol.* **49**, 381-394.

Baes, C.F.J. and Mesmer, R.E. (1976a) The Hydrolysis of Cations. John Wiley & Sons, New York, p. 181.

Baes, C.F.J. and Mesmer, R.E. (1976b) The Hydrolysis of Cations. John Wiley & Sons, New York, pp. 178.

Baes, C.F.J. and Mesmer, R.E. (1976c) The Hydrolysis of Cations. John Wiley & Sons, New York, pp. 397-419.

Benedict, B., Pigford, T.H. and Levi, H.W. (1981) Nuclear Chemical Engineering. McGraw-Hill, New York, pp.

Bohart, G.S. and Adams, E.Q. (1920) Some aspects of the behavior of charcoal with respect to chlorine. *J. Am. Chem. Soc.* **42**, 523-544.

Bold, H.C. and Wynne, M.J. (1985) Introduction to the Algae. Prentice-Hall, Englewood Cliffs, N.J., pp. 389-391.

Brassard, P., Macedo, E. and Fish, S. (1996) Diffusion and binding of protons in sediments. *Environ. Sci. Technol.* **30,** 3216-3222.

Brierley, C.L. (1990) Bioremediation of metal contaminated surfaces and ground waters. *Geomicrobiol. J.* **8,** 201-223.

Brooks, C. S. (1991). Metal Recovery from Industrial Waste. Chelsea, MI. Lewis Publishers.

Buffle, J. (1988) Complexation Reactions in Aquatic Systems: An Analytical Approach. Ellis Horwood Ltd., Chichester, U.K., pp. 156-157, 280-283, 323.

Buffle, J. and Altmann, R.S. (1987) Interpretation of metal complexation by heterogeneous complexants, in Aquatic Surface Chemistry (Stumm, W., ed.) John Wiley & Sons, New York, pp. 351-383.

Byerley, J.J., Scharer, J.M. and Charles, A.M. (1987) U(VI) Bioadsorption from process solutions. *Chem. Eng. Journal* **36,** B49-B59.

Chapman, V.J. (1963) Fucales, in The Marine Algae of Jamaica (Chapman, V.J., ed.) The Institute of Jamaica Science Series, No 12, Kingston, Jamaica, pp. 38-41.

Chapman, V.J. (1980) Seaweeds and Their Uses. Chapman and Hall, London, UK, pp. 194-240.

Chen, D., Lewandowski, Z., Roe, F. and Surapaneni, P. (1993) Diffusivity of Cu^{2+} in calcium alginate beads. *Biotechnol. Bioeng.* **41,** 755-760.

Collins, Y.E. and Stotzky, G. (1992) Heavy metals alter the electrokinetic properties of bacteria, yeasts and clay minerals. *Appl. Environ. Microbiol.* **58,** 1592-1600.

Crank, J. (1975) Mathematics of Diffusion, 2nd ed. Clarendon Press, London, UK, pp. 94.

Crist, D.R., Crist, R.H., Martin, J.R. and Watson, J. (1993) Ion exchange system in proton-metal reactions with algal cell walls, in Metals-Microorganisms Relationships and Applications, FEMS Symposium Abstracts, Metz, France, May 5-7. (Bauda, P., ed.) Societe Francaise de Microbiologie, Paris, France, pp. 13.

Crist, R.H., Martin, J.R., Carr, D., Watson, J.R., Clarke, H.J. and Crist, D.R. (1994) Interaction of metals and protons with algae. 4. Ion exchange *versus* adsorption models and a reassessment of Scatchard plots; ion-exchange rates and equilibria compared with calcium alginate. *Environ. Sci. Technol.* **28,** 1859-1866.

Crist, R.H., Martin, J.R., Chonko, J. and Crist, D.R. (1996) Uptake of metals on peat moss: an ion-exchange process. *Environ. Sci. Technol.* **30,** 2456-2461.

Crist, R.H., Martin, J.R., Guptill, P.W., Eslinger, J.M. and Crist, D.R. (1990) Interactions of metals and protons with algae. 2. Ion exchange in adsorption and metal displacement by protons. *Environ. Sci. Technol.* **24,** 337-342.

Crist, R.H., Oberholser, K., Schwartz, D., Marzoff, J., Ryder, D. and Crist, D.R. (1988) Interactions of metals and protons with algae. *Environ. Sci. Technol.* **22,** 755-760.

Crist, R.H., Oberholser, K., Wong, B. and Crist, D.R. (1992) Amine-algae interactions: Cation exchange and possible hydrogen binding. *Environ. Sci. Technol.* **26,** 1523-1526.

Crittenden, J.C., Asce, A.M. and Weber, W.J., Jr. (1978a) Predictive model for design of fixed-bed adsorber: parameter estimation and model development. *J. Envir. Eng. Div.* **104,** 185-197.

Crittenden, J.C., Asce, A.M. and Weber, W.J., Jr. (1978b) Predictive model for design of fixed-bed adsorber: single-component model verification. *J. Envir. Eng. Div.* **104,** 433-443.

Crittenden, J.C. and Weber, W.J.J. (1978) Model for design of multicomponent adsorption systems. *J. Envir. Eng. Div. ASCE* **104,** 1175-1195.

Darnall, D.W., Greene, B., Henzl, M.T., Hosea, J.M., McPherson, R.A., Sneddon, J. and Alexander, M.D. (1986) Selective recovery of gold and other metal ions from an algal biomass. *Environ. Sci. Technol.* **20,** 206-208.

Dobos, D. (1994) A Handbook for Electrochemists in Industry and Universities. Elsevier Scientific, Amsterdam, The Netherlands, pp. 88.

Dodge, J.D. (1973) The Fine Structure of Algal Cells. Academic Press, London, U.K., pp. 14-45.

Edgington, D.N., Gorden, S.A., Thommes, M.M. and Almodovar, L.R. (1970) The concentration of radium, thorium and uranium by tropical marine algae. *Limnol. Ocean.* **15**, 945-955.

EPS (1987) Metal Finishing Liquid Effluent Guidelines, Report EPS 1-WP-77-5. Water Pollution Control Directorate, Environmental Protection Service, Fisheries and Environment Canada. Ottawa, Canada, pp. 5958-5960.

Faust, S.D. and Aly, O.M. (1987) Adsorption Processes for Water Treatment. Butterworths Publishers, Stoneham, UK, pp. 143-165.

Ferguson, J. and Bubela, B. (1974) The concentration of Cu (II), Pb (II), and Zn (II) from aqueous solutions by particulate algal matter. *Chem. Geol.* **13**, 163-186.

Figueira, M. M. (1998) Biosorption of Metals by brown Seaweeds. PhD Thesis, Federal University of Minas Gerais, Belo Horizonte , Brazil.

Filion, M.P., Sirois, L.L. and Ferguson, K. (1990) Acid mine drainage research in Canada. *CIM Bull.* **83**, 33-44.

Fleck, R.D., Jr. (1973) Mixed resistance diffusion kinetics in fixed-bed adsorption under constant pattern conditions. *Ind. Eng. Chem. Fundam.* **12**, 95-99.

Fourest, E., Serre, A. and Roux, J.-C. (1996) Contribution of carboxyl groups to heavy metal binding sites in fungal wall. *Toxicol. Environ. Chem.* **54**, 1-10.

Fourest, E. and Volesky, B. (1997) Alginate properties and heavy metal biosorption by marine algae. *Appl. Biochem. Biotechnol.* **67**, 33-44.

Freundlich, H. (1926) Colloid and capillary chemistry. Methuen, London, U.K.

Furnas, C.C. (1932) Heat transfer from a gas stream to a bed of broken solids. *U.S. Bur. Mines. Bull.* **361**, 88.

Furusawa, T. and Smith, J.M. (1973) Fluid-particle and intraparticle mass transport in slurries. *Ind. Eng. Chem. Fundam.* **12**, 197-203.

Gazea, B., Adam, K. and Kontopoulos, A. (1996) A review of passive systems for the treatment of acid mine drainage. *Minerals Engineering* **9**, 23-42.

Goldstein, S. (1953a) The mathematics of exchange process in fixed columns: I. Mathematical solution and asymptotic expansion. *Proc. Roy. Soc. (London)* **A219**, 151-170.

Goldstein, S. (1953b) The mathematics of exchange process in fixed columns: II. The equilibrium theory as the limit of the kinetics theory. *Pro. Roy. Soc. (London)* **A219,** 171-185.

Goto, A., S. Morooka, et al. (1993). "The sorption of uranium from amodoxime fiber adsorbent." Sep. Sci. Technol. 28: 2229-2235.

Grant, G.T., Morris, E.R., Rees, D.A., Smith, J.C. and Thom, D. (1973,) Biological interactions between polysaccharides and divalent cations: The egg-box model. *FEBS Lett.* 32, pp.195-198.

Greene, B., Henzl, M.T., Hosea, J.M. and Darnall, D.W. (1986a) Elimination of bicarbonate interference in the binding of U(VI) in mill-waters to freeze-dried *Chlorella vulgaris*. *Biotechnol. Bioeng.* **28,** 764.

Greene, B., Hosea, M., McPherson, R., Henzl, M., Alexander, M.D. and Darnall, D.W. (1986b) Interaction of Gold(I) and Gold(III) complexes with algal biomass. *Environ. Sci. Technol.* **20,** 627-632.

Greene, B., McPherson, R. and Darnall, D. (1987) Algal sorbents for selective metal ion recovery, in Metals Speciation, Separation and Recovery (Patterson, J.W. and Pasino, R., eds.) Lewis, Chelsea, MI, pp. 315-338.

Guibal, E., Roulph, C. and Le Cloirec, P. (1992) Uranium biosorption by a filamentous fungus *Mucor meihei* : pH effect on the mechanisms and performances of uptake. *Water Res.* **26,** 1139-45.

Hall, K.R., Eagleton, L.C., Acrivos, A. and Vermeulen, T. (1966) Pore- and solid-diffusion kinetics in fixed-bed adsorption under constant-pattern conditions. *Ing. Eng. Chem. Fundam.* **5,** 212-223.

Hand, D.W., Crittenden, J.C., Asce, A.M. and Thacker, W.E. (1984) Simplified models for design of fixed-bed adsorber systems. *J. Envir. Eng.* **110,** 441-455.

Harland, C.E. (1994) Ion Ecchange: theory and practice. The Royal Society Chemistry, Cambridge, UK, pp. 40.

Hashimoto, K., Mioura, K. and Nagata, S. (1975) Intraparticle Diffusivities in Liquid Phase Adsorption with Nonlinear Isotherms. *J. Chem. Eng. Japan* **8,** 367-373.

Haug, A., Larsen, B. and Smidsrod, O. (1974) Uronic acid sequence in alginate from different sources. *Carbohyd. Res.* **32,** 217-225.

Heister, N.K. and Vermeulen, H. (1952) Saturation performance of ion-exchange and adsorption columns. *Chem. Eng. Prog.* **48,** 505-516.

Helfferich, F. (1962) Ion Exchange. McGraw-Hill, New York, pp. 299-319.

Hill, C.G.J. (1977) An Introduction to Chemical Engineering Kinetics and Reactor Design. John Wiley & Sons, New York, pp. 167-204.

Himmelblau D. M. (1970) Process analysis by statistical methods. Sterling Swift, Austin, Texas, pp 208 – 229.

Ho, Y.S., Wase, D.A.J. and Forster, C.F. (1995) Batch nickel removal from aqueous solution by sphagnum moss peat. *Wat. Res.* **29,** 1327-1332.

Holan, Z.R., Volesky, B. and Prasetyo, I. (1993) Biosorption of cadmium by biomass of marine algae. *Biotechnol. Bioeng.* **41,** 819-825.

Holan, Z.R. and Volesky, B. (1994) Biosorption of lead and nickel by biomass of marine algae. *Biotechnol. Bioeng.* **43,** 1001-1009.

Horikoshi, T., Nakajima, A. and Sakaguchi, T. (1979) Uptake of uranium by *Chlorella regularis*. *Agric. Biol. Chem.* **332,** 617.

Horvath, A.L. (1985) Handbook of Aqueous Electrolyte Solutions. Ellis Horwood, West Sussex, UK, pp. 289.

Hu, M.Z.-C., Norman, J.M., Faison, N.B. and Reeves, M. (1996) Biosorption of uranium by *Pseudomonas aeruginosa* Strain CSU: characterization and comparison studies. *Biotechnol. Bioeng.* **51,** 237-247.

Huang, C., Huang, C.P. and Morehart, A.L. (1991) Proton competition in Cu (II) adsorption by fungal mycelia. *Wat. Res.* **25,** 1365-1375.

Jang, L.K., Brand, W., Resong, M., Mainieri, W. and Geesey, G.G. (1990) Feasibility of using alginate to absorb dissolved copper from aqueous media. *Environ. Prog.* **9,** 269-274.

Jansson-Charrier, M., Guibal, E., Roussy, J., Surjous, R. and LeCloirec, P. (1996) Dynamic removal of uranium by chitosan: influence of operating parameters. *Water Sci. Tech.* **34,** 169-177.

Karberry, H. (1960) A boundary-layer model of fluid-particle mass transfer in fixed beds. *A. I. Ch. E. J.* **6,** 460-462.

Kataoka, T., Yoshida, H. and Ueyama, K. (1972) Mass transfer in laminar regions between liquid and packing material surface in the packed bed. *J. Chem. Eng. Japan* **5**, 132-136.

Keinath, T.M. and Weber, W.J.J. (1968) Predictive model for the design of fluid-bed adsorbers. *J. Water Pollut. Cont. Fed.* **40**, 741-765.

Klein, G., Tondeur, D. and Vermeulen, T. (1967) Multicomponent ion-exchange in fixed beds. *Ind. Eng. Chem. Fundam.* **6**, 339-350.

Klinkenberg, A. (1954) Heat transfer in cross-flow heat exchanges and packed beds. *Ind. Eng. Chem.* **46**, 2285-2289.

Kratochvil, D., Fourest, E. and Volesky, B. (1995) Biosorption of copper by *Sargassum fluitans* biomass in fixed-bed column. *Biotechnol. Lett.* **17**, 777-782.

Kratochvil, D. (1997) A Study of the Metal Biosorption Process Utilizing *Sargassum* Seaweed Biomass. PhD Thesis, McGill University, Montreal.

Kreger, D.R. (1962) Cell Walls, in Physiology and Biochemistry of Algae (Lewin, R.A., ed.) Academic Press, New York, pp. 315-335.

Ku, Y.P., R. W. (1987) Innovative uses for carbon adsorption of heavy metals from plating waster waters: 1. Activated carbon polishing treatment. *Environmental Progress.* **6**, 119-124.

Kuyucak, N. and Volesky, B. (1989a) Accumulation of cobalt by marine alga. *Biotechnol. Bioeng.* **33**, 809-814.

Kuyucak, N. and Volesky, B. (1989b) Accumulation of gold by algal biosorbent. *Biorecovery* **1**, 189-204.

Kuyucak, N. and Volesky, B. (1990) Biosorption by algal biomass, in Biosorption of Heavy Metals (Volesky, B., ed.) CRC Press, Boca Raton, FL, pp. 173-198.

Langmuir, I. (1918) The adsorption of gases on plane surfaces of glass, mica and platinum. *J. Am. Chem. Soc.* **40**, 1361-1403.

Lapidus, L. and Pinder, G.E. (1982) Numerical Solution of Partial Differential Equations in Science and Engineering. Wiley, New York.

Laul, J.C. (1992) Natural radionuclides in ground water. *Radioanal. Nucl. Chem. Articles* **156**, 235.

Lee, R.E. (1989a) Phycology. Cambridge University Press, Cambridge, UK, pp. 10-13, 34-37, 534-539, 584-599.

Lee, R.E. (1989b) Phycology. Cambridge University Press, Cambridge, UK, pp. 10, 115, 338, 418, 467, 507.

Leusch, A., Holan, Z.R. and Volesky, B. (1995) Biosorption of heavy metals (Cd, Cu, Ni, Pb, Zn) by chemically-reinforced biomass of marine algae. *J. Chem. Tech. Biotechnol.* **62,** 279-288.

Leusch, A. and Volesky, B. (1995) The influence of film diffusion on cadmium biosorption by marine biomass. *J. Biotechnol.* **43,** 1-10.

Levenspiel, O. (1972) Chemical Reaction Engineering. J. Wiley & Sons, New York, NY, pp. 282-284.

Lewin, R.A. (1974) Biochemical Taxonomy, in Algal Physiology and Biochemistry (Stewart, W.D.P., ed.) Blackwell Scientific Publications, Oxford, UK, pp. 1-25.

Liu, K.T. and Weber, W.J. (1981) Characterization of mass transfer parameters for adsorber modeling and design. *J. Water Poll. Control. Fed.* **53,** 1541-1550.

Lo, K.S.L. and Leckie, J.O. (1993) Kinetics of adsorption-desorption of Cd and Zn onto Al_2O_3/solution interfaces. *Wat. Sci. Technol.* **28,** 39-45.

Lobban, C.S., Harrison, P.J. and Duncan, M.J. (1985) The Physiological Ecology of Seaweeds. Cambridge University Press, Cambridge, UK, pp. 123-131.

Macaskie, L.E. (1991) The application of biotechnology to the treatment of wastes produced by the nuclear fuel cycle: biodegradation and bioaccumulation as a means of treating radionuclide-containing streams. *CRC Crit. Rev. Biotechnol.* **11,** 41-112.

Macaskie, L.E., Empson, R.M., Cheetham, A.K., Grey, C.P. and Skarnulis, A.J. (1992) Uranium bioaccumulation by a *Citrobacter* sp. as a result of enzymatically mediated growth of polycrystalline HUO_2PO_4. *Science* **257,** 782-784.

Mackie, W. and Preston, R.D. (1974a) Cell wall and intercellular region polysaccharides, in Algal Physiology and Biochemistry (Stewart, W.D.P., ed.) Blackwell Scientific Publications, Oxford, UK, pp. 40-85.

Mackie, W. and Preston, R.D. (1974b) Cell wall and intercellular region polysaccharides, in Algal Physiology and Biochemistry (Stewart, W.D.P., ed.) Blackwell Scientific Publications, Oxford, UK, pp. 58-64.

Mann, H. (1990) Biosorption of heavy metals by bacterial biomass, in Biosorption of Heavy Metals (Volesky, B., ed.) CRC Press, Boca Raton, FL, pp. 93-137.

Marinsky, J.A. (1987) A two-phase model for the interpretation of proton and metal ion interaction with charged polyelectrolyte gels and their linear analogs, in Aquatic Surface Chemistry (Stumm, W., ed.) John Wiley & Sons, New York, pp. 49-81.

Masamune, S. and Smith, J.M. (1965) Adsorption rate studies - interaction of diffusion and surface process. *A. I. Ch. E. J.* **11,** 34-40.

Mathworks, I. (1993) MATLAB Version 4.0 for Microsoft Windows. MathWorks, Inc., Natick, MA.

Mehablia M.A., Shallcross D.C. and Stevens G.W. (1994) Prediction of multicomponent ion exchange equilibria. Chem. Eng. Sci., 49, 2277-2286

Morris, E.R., Rees, D.A. and Thom, D. (1978) Chiroptical and stoichiometric evdence of a specific, primary dimerization process in alginate gelation. *Carbohyd. Res.* 66, pp.145 – 154.

Morris, E. R., D. A. Rees, et al. (1980). "Characterisation of alginate composition and block-structure by circular dichroism." Carbohydr. Res. 81: 305-314.

Munroe, N.D.H., Bonner, J.D., Williams, R., Pattison, K.F., Norman, J.M. and Faison, B.D. (1993) Binding of dissolved uranium by *Pseudomonas aeruginosa* CSU. In 15th Symposium on Biotechnology for Fuels and Chemicals, Oak Ridge, TN.

Muraleedharan, T.R., Lyengar, L. and Venkobachar, C. (1994) Further insight into the mechanism of biosorption of heavy metals by *Ganoderma lucidum. Environ. Technol.* **15,** 1015-27.

Muzzarelli, R.A.A., Tanfani, F., Emanuelli, M. and Gentile, S. (1980) The chelation of cupric ions by chitosan membranes. *J. Appl. Biochem.* **2,** 380-389.

O'Colla, P.S. (1962) Mucilages, in Physiology and Biochemistry of Algae (Lewin, R.A., ed.) Academic Press, New York, pp. 348-351.

Percival, E. and McDowell, R.H. (1967c) Chemistry and Enzymology of Marine Algal Polysaccharides. Academic Press, London, U.K., pp. 83-98, 99-104, 127-156, 157-164.

Percival, E. and McDowell, R.H. (1967a) Chemistry and Enzymology of Marine Algal Polysaccharides. Academic Press, London, U.K., pp. 53-72.

Percival, E. and McDowell, R.H. (1967b) Chemistry and Enzymology of Marine Algal Polysaccharides. Academic Press, London, U.K., pp. 99-126.

Periasamy, K. and Namasivayam, C. (1994) Process development for removal and recovery of cadmium from waste water by a low-cost adsorbent: Adsorption rate and equilibrium studies. *Industrial and Engineering Chemistry Research* **33,** 317-320.

Prasetyo, I. (1992) Removal of Toxic Metals from Aqueous Solutions by Biosorption. M. Eng. thesis, McGill University, Montreal, Canada.

Ramelow, G.J., Fralick, D. and Zhao, Y. (1992) Factors affecting the uptake of aqueous metal ions by dried seaweed biomass. *Microbios* **72,** 81-93.

Reed, M. and Berg, M. (1993) Investigation of regeneration schemes for granular activated carbon (GAC) columns loaded with lead. In Hazardous and industrial wastes - Proceedings of the Mid-Atlantic Industrial waste conference, Technomic Publ. Co. Inc., Lancaster, PA. pp. 283-292.

Rees, D. A. (1981). Polysaccharide shapes and their interactions – some recent advances Pure Appl. Chem., 53: 1-14.

Rigo, H.G. and Chandler, A.J. (1994) Metals in MSW - where are they and where do they go in an incinerator. In Proceedings of National Waste Processing Conference, ASME, New York, NY. pp. 49-63.

Rosen, J.B. (1952) Kinetics of a fixed bed system for solid diffusion into spherical particles. *J. Chem. Phys.* **20,** 387-394.

Rosen, J.B. (1954) General numerical solution for solid diffusion in fixed-bed. *Ing. Eng. Chem* **46,** 1590-1594.

Schecher, W.D. (1991) MINEQL+ : A Chemical Equilibrium Program for Personal Computers, Users Manual Version 2.22. Environmental Research Software, Inc., Hallowell, ME.

Schiewer, S., Fourest, E., Chong, K.H. and Volesky, B. (1995) Ion exchange in metal biosorption by dried seaweed: Experiments and model predictions, in Biohydrometallurgical Processing: Proceedings of the International Biohydrometallurgy Symposium (Jerez, C.A., Vargas, T., Toledo, H. and Wiertz, J.V., eds.) University of Chile, Santiago, pp. 219-228.

Schiewer, S. and Volesky, B. (1995) Modeling of the proton-metal ion exchange in biosorption. *Environ. Sci. Technol.* **29,** 3049-3058.

Schiewer, S. and Volesky, B. (1996) Modeling of multi-metal ion exchange in biosorption. *Environ. Sci. Technol.* **30,** 2921-2927.

Shallcross D.C., Herrmann, C.C. and McCoy B.J. (1988) An improved model for the prediction of multicomponent ion exchange equilibria. Chem. Eng. Sci., 43, 279-289

Sharma, D.C. and Forster, C.F. (1994) A preliminary examination into the adsorption of hexavalent chromium using low-cost adsorbents. *Biores. Technol.* **47,** 257-264.

South, G.R. and Whittick, A. (1987) Introduction to Phycology. Blackwell Scientific Publications, Oxford, UK, pp. 27-28, 46-63, 104-115, 176-177, 268-271.

Stenzel, M.H. (1993) Remove organics by activated carbon adsorption. *Chem. Eng. Prog.* **April,** 36-43.

Smidsrod, O. and K. I. Draget (1996). Chemistry and physical properties of alginates. Carbohydrates in Europe. Vol. 14 pp 6 – 13.

Stumn, W. and Morgan, J. (1996) Aquatic Chemistry. John Wiley & Sons. New York, pp 238-299, 445-513

Stumn, W. and Morgan, J. (1996) Aquatic Chemistry. John Wiley & Sons, New York, p 103

Tan, H.K.S. and Spinner, I.H. (1994) Multicomponent ion exchange column dynamics. *Can. J. Chem. Eng.* **72,** 330-341.

Taylor, W.R. (1960) Marine Algae of the Eastern Tropical and Subtropical Coasts of the Americas. University of Michigan Press, Ann Arbor, MI, pp. 736.

Thomas, H.C. (1944) Heterogeneous ion exchange in a flowing system. *J. Am. Chem. Soc.* **66,** 1644.

Thomas, H.C. (1951) Solid diffusion in chromatography. *J. Chem. Phys.* **19,** 1213-1214.

Tien, C. (1994) Adsorption Calculations and Modeling. Butterworth-Heinemann, Boston, MA. pp 3-4.

Tobin, J.M., Cooper, D.G. and Neufeld, R.J. (1984) Uptake of metal ions by *Rhizopus arrhizus* biomass. *Appl. Envir. Microbiol.* **47,** 821-824.

Tondeur, D. and Klein, G. (1967) Multicomponent ion exchange in fixed beds. *Ind. Eng. Chem. Fundam.* **6,** 351-361.

Treen-Sears, M.E., Volesky, B. and Neufeld, R.J. (1984) Ion exchange / complexation of the uranyl ion by *Rhizopus* biosorbent. *Biotechnol. Bioeng.* **26,** 1323-1329.

Trujillo, E.M., Jeffers, T.H., Ferguson, C. and Stevenson, H.Q. (1991) Mathematically modeling the removal of heavy metals from waste water using immobilized biomass. *Environ. Sci. Technol.* **25,** 1559-1565.

Tsezos, M. (1980) Biosorption of Uranium and Thorium. Ph.D. thesis, McGill University, Montreal, Canada.

Tsezos, M., Noh, S.H. and Baird, M.H.I. (1988) A batch reactor mass transfer kinetic model. *Biotechnol. Bioeng.* **32,** 545-553.

Tsezos, M. and Volesky, B. (1981) Biosorption of Uranium and Thorium. *Biotechnol.Bioeng.* **23,** 583-604.

Vermeulen, T. (1958) Separation by adsorption methods. *Adv. Chem. Eng.* **2,** 147-208.

Veroy, R.L., Montano, N., Guzman, M.L.B., Laserna, E.C. and Cajipe, G.J.B. (1980) Studies of the binding of heavy metals to algal polysaccharides from Phillipine seaweeds. I. Carrageenan and the binding of lead and cadmium. *Bot. Marina* **23,** 59-62.

Villadsen, J. and Michelsen, M. (1978) Solution of differential equation models by polynomial approximation. Prentice-Hall, Englewood Cliffs, NJ, pp. 111-143.

Volesky, B. (1970) Algal Products, in Properties and Products of Algae (Zajic, J.E., ed.) Plenum Press, New York, pp. 49-82.

Volesky, B. (1990) Removal and recovery of heavy metals by biosorption, in Biosorption of Heavy Metals (Volesky, B., ed.) CRC Press, Boca Raton, FL, pp. 7-43.

Volesky, B. and Holan, Z.R. (1995) Biosorption of heavy metals. *Biotechnol. Prog.* **11,** 235-250.

Volesky, B. and Schiewer, S. (1999) Biosorption of metals, in Encyclopedia of Bioprocess Technology (Flickinger, M. and Drew, S.W., eds.) Wiley & Sons, NY, pp. 433 - 453.

Volesky, B. and Tsezos, M. (1981) Separation of Uranium by Biosorption. U.S. Patent 4 320 093 ; Canadian Patent 1 143 007 (1983)

Weber, W.J. and Liu, K.T. (1980) Determination of mass transport parameters for fixed-bed adsorbers. *Chem. Eng. Commun.* **6,** 49-60.

Weber, W.J.J. and Crittenden, J.C. (1975) MADAM I - A numeric method for design of adsorption systems. *J. Water Poll. Control Fed.* **47,** 924-940.

Westall, J.C., Zachary, J.L. and Morel, F.M.M. (1986) MINEQL: a computer program for the calculation of the chemical equilibrium composition of aqueous systems, in Oregon State university Report No. 86-01 Version 1 eds.) Oregon State University, Eugene, Oregon.

Westrin, B. and Axelsson, A. (1991) Diffusion in gels containing immobilized cells: A critical review. *Biotechnol. Bioeng.* **38,** 439-446.

White, S.K. (1983) Removing uranium by current municipal water treatment process. *J. Am. Water Works Assoc.* **75,** 374.

Williamson, J.E., Bazaire, K.E. and Geankoplis, C.J. (1963) Liquid phase mass transfer at low Reynolds numbers. *Ind. Eng. Chem. Fundam.* **2,** 126-129.

Xue, H.B. and Sigg, L. (1990) Binding Cu(II) to algae in a metal buffer. *Wat. Res.* **24,** 1129-1136.

Appendix A. MATLAB Program for HIEM Isotherm Model

1. **u25main.m**: main program for pH 2.5 uranium isotherm
2. **u25fit.m**: error function for pH 2.5 isotherm
3. **u40main.m**: main program for pH 4.0 uranium isotherm
4. **u40fit.m**: main program for pH 4.0 uranium isotherm
5. **u2540.m**: program for plotting isotherms at pH 2.5 - 4.0

```
%       U25main.m: main program for pH 2.5 uranium isotherm
global H U qu1;
global key kez ct;
global qu;
load data25.txt
data = data25;
H = data(:, 1);
U = data(:, 2)/238/1000;
qu1 = data(:, 3)/238/1000;
alfa = 1.1849;
key = 10^(-5.62)/ alfa;
kez = 10^(-5.8) /alfa;
ct = 2.25e-3;
p = 1e3*[1, 1];
p = fmins( 'u25fit', p );
u25fit(p)
[U*1000 qu*1000 qu1*1000 (qu./qu1-1)]
plot(U*1000,qu*1000, '-', U*1000, qu1*1000, 'o')
xlabel('U (mM)')
ylabel('qU (mmol/g)')
```

```
% u25fit.m :    error function for pH 2.5 isotherm
function err=fit(p)
global H U qu1;
global key kez ct kh;
global qu;
```

```
kx = p;
ky = 0;
kz = 0;
a = key./H;
b = kez./H;
c =  U./H;
xH = ( sqrt( (1+b).^2 + 8*a.*c ) - (1+b) )./ (4*a);
x = xH .* H ;
y = xH .^2 * key;
z = xH .* kez;
denom = (1 + kh*H + sqrt(kx*x) + sqrt(ky*y) + kz*z );
qu = ct*(0.5*sqrt(kx*x) + sqrt(ky*y) + kz*z ) ./ denom ;
qh = ct*kh*H ./ denom ;
e = qu1-qu;
err=sum( abs(e) )

%u40main.m: main program for pH 3.0  uranium isotherm
global H U qu1;
global key kez ct;
global qu qh;
load data40.txt
data = data40;
H = data(:, 1);
U = data(:, 2)/238/1000;
qu1 = data(:, 3)/238/1000;
alfa = 1.1849;
key = 10^(-5.62) /alfa;
kez = 10^(-5.8) /alfa;
ct = 2.250e-3;
p = 1e3*[1, 1];
p = fmins( 'u30fit', p );
u40fit(p)
[U*1000*238 qu*1000 qu1*1000 (qu./qu1-1)]
plot(U*1000,qu*1000, '-', U*1000, qu1*1000, 'o')
xlabel('U (mM)')
ylabel('qU (mmol/g)')


% u40fit.m:    error function for pH 3.0 isotherm
function err=fit(p)
global H U qu1:
global key kez ct:
global qu;
kh = 2.322e2;          % from pH 2.5 fitting
kx = 1.0864e3;         % from pH 2.5 fitting
ky = abs( p(1));
```

```
kz = abs( p(2) );
a = key./H;
b = kez./H;
c =  U./H;
xH = ( sqrt( (1+b).^2 + 8*a.*c ) - (1+b) )./ (4*a);
x = xH .* H ;
y = xH .^2 * key;
z = xH .* kez;
denom = (1 + kh*H + sqrt(kx*x) + sqrt(ky*y) + kz*z );
qu = ct*(0.5*sqrt(kx*x) + sqrt(ky*y) + kz*z ) ./ denom ;
qh = ct*kh*H ./ denom ;
e = qu1-qu;
err=sum( abs(e) )

% u2540.m : Program for isotherms at pH 2.5 - 4.0
load data2540.txt
data = data2540;
H = data(:, 1);
U = data(:, 2)/238/1000;
qu1 = data(:, 3)/238/1000;
alfa = 1.1849;
key = 10^(-5.62) /alfa;
kez = 10^(-5.8) /alfa;
ct = 2.250e-3;
kh = 2.322e2;          % from pH 2.5 fitting
kx = 1.0864e3;         % from pH 2.5 fitting
ky = 1.9318e4;         % obtain from u30main:  p0 = 1e3*[1, 1]
kz = 1.2542e4;         % and set kh, kx to the above values
a = key./H;
b = kez./H;
c =  U./H;
xH = ( sqrt( (1+b).^2 + 8*a.*c ) - (1+b) )./ (4*a);
x = xH .* H ;
y = xH .^2 * key;
z = xH .* kez;
denom = (1 + kh*H + sqrt(kx*x) + sqrt(ky*y) + kz*z );
qu = ct*(0.5*sqrt(kx*x) + sqrt(ky*y) + kz*z ) ./ denom ;
qh = ct*kh*H ./ denom ;
[U*1000*238 qu*1000 qu1*1000 (qu./qu1-1)]
plot(U*1000, qu*1000, '-', U*1000, qu1*1000, 'o')
xlabel('u (mM)')
ylabel('qU (mmol/g)')
grid
```

Appendix B. Program for Batch Dynamics Model

```
C       BATCH DYNAMICS                                  August,1999
C
C       1. LANGMUIR ADSORPTION STR DIFFUSION MODEL, RECTANGAL
C          PARTICLES.
C       2. GALERKIN FINIT ELEMENT METHOD, LINEAR BASIS FUNCTIONS.
C       3. CALCULATE THE MASS MATRIX AND STIFF MATRIX C
C          SEPARATLY.
C       4. EULER BACKWARD TIME DIFFERENCE, FIXED TIME STEP.
C       5. THE LINEAR MATRIX EQUATION SOLVER IS IN TDMA METHOD.

        IMPLICIT REAL*8 (A-H, O-Z)
        DIMENSION SM(122,122), SK(122,122), SJ(122,122), ESJ(122,122)
        DIMENSION  X(122), E(122)
        DIMENSION  W(3),  GP(3),  PHI(2),  PHIX(2)
        DIMENSION  CT(122), CT0(122), CT1(122)
        DATA  W/0.27778D0,0.44444444444D0,0.277777778D0/
        DATA  GP/0.11270D0,0.50D0,0.8873D0/
        OPEN(5,FILE='LANDE1.DAT')
        OPEN(6,FILE='LANDE1.OUT')
C       PARAMETERS
        READ(5,*) DE, CRI, CBI, C0, MESH, DT, ENDTIME, TIMESTEP
        READ(5,*) V,  Vp, THICK
        READ(5,*) PK, QM, VOIDP, DENSITY
        CLOSE(5)
        T=0.0
        R=THICK / 2.0
        ALFA=DE / R**2
        BETA=V / Vp
        GAMA1=PK*QM*DENSITY/C0**2
        GAMA2=PK/C0
        SURFACE=Vp/R
C(1)    Define mesh
        NE=MESH
        NP=NE+1
        H=(1.0-0.0)/FLOAT(NE)
        DO 10 I=1,NP
10      X(I)=FLOAT(I-1)*H
C(2)    initial conditions
```

```
      DO 20 I=1,NP
20    CT(I) =CRI/C0
      CT(NP)=CBI/C0
C     Output parameters
      write(6,*) '                    LANDE1.F90'
      WRITE(6,5010) NE, DT
      WRITE(6,5020) DE, CRI, CBI, C0
      WRITE(6,5030) PK, QM, VOIDP, DENSITY
      WRITE(6,5040) V, Vp, THICK, SURFACE
      WRITE(6,5050) ALFA, BETA
      RMAT(5X,'NE=',I3, ',  DT=',F7.4)
5010  FORMAT(5X,'DE=', D8.2, ', CRI=', F5.2, ', CBI=',
     $F6.2, ', C0=',F6.2)
5030  FORMAT(5X, 'PK=',F6.2, ', QM=', F7.2, ', VOID=',
     $F4.2, ', DENSITY=', F8.2)
5040  FORMAT(5X, 'V=',F8.2, ', Vp=', F5.2, ', THICK=',
     $F6.3, ', SURFACE=',F8.2)
5050  FORMAT(5X, 'ALFA=', F8.4, ', BETA=',F8.2)
C     Output title
      IF (NE .LT. 10) THEN
      NO=1
      ELSE
      NO=NE/10
      ENDIF
      WRITE(6,5060)       ( X( NO*(I-1)+1 ),I=1,11 )
      WRITE(6,5000)T/60,(CT( NO*(I-1)+1 ),I=1.11 ) , T/60
5060  FORMAT(/1X,'Results:'/1X 't\X(I)', 11F6.3/)
C(3)  time marching forward
30    CONTINUE
C     Varing time step
C     IF(T .GT. 600.0) DT=1.0
      T=T+DT
      DO 40 I=1, NP
40    CT0(I)=CT(I)
C(4)  N-R iteration
      JK=0
50    CONTINUE
      JK=JK+1
C     Calcualte coefficient matraces
      DO 60 I=1,NP
      DO 60 I1=1,NP
      SM(I,I1)=0.0
60    SK(I,I1)=0.0
C     Master Loop over elements
      DO 100 I=1, NE
      DX=X(2)-X(1)
```

```
C       Gauss Integration
        DO 100 J=1,3
        CALL TFUNCT(GP(J),DX,PHI,PHIX)
        CON=0.0
        DO 90 LL=1,2
        LL1=LL+(I-1)
90      CON= CON + CT(LL1)* PHI(LL)
        F1=VOIDP+ GAMA1/(CON+GAMA2)**2
C       SM: Mass matrix
C       Sk: Stiffness matrix
C       SJ: Jacobin (coefficient matrix) SJ=SM+DT*SK
        DO 100 L=1,2
        DO 100 M=1,2
        L1=L+(I-1)
        M1=M+(I-1)
        SM(L1,M1)=SM(L1,M1) + W(J)*DX*( PHI(L)*PHI(M)*F1 )
        SK(L1,M1)=SK(L1,M1) + W(J)*DX*(
     $ALFA*PHIX(L)*PHIX(M) )
100     CONTINUE
C       coefficient matrix:(SM+DT*SK).*CT =
C        SM.*CT(OLD)+DELT(i,NP)*DT*(B.T.)
        DO 110 I=1, NP
        DO 110 J=1, NP
110     SJ(I,J)=SM(I,J)+DT*SK(I,J)
C       right hand side
        DO 120 I=1, NP
        CT1(I)=0.0
        DO 120 L=1, NP
120     CT1(I)=CT1(I)+SM(I,L)*CT0(L)
C       Apply boundary conditions
C       CT1(NP)=CT1(NP)-BETA*(CT(NP)-CT0(NP)): do not work!
        SJ(NP,NP)=SJ(NP,NP)+BETA
        CT1(NP)=CT1(NP)+BETA*CT0(NP)
C       Form the exteded matrix for solving the linear
C       equations: SJ*CT=CT1
        DO 130 I=1,NP
        ESJ(I,NP+1)=CT1(I)
        DO 130 J=1,NP
130     ESJ(I,J) = SJ(I,J)
C       Store the old iteration solution vector
        DO 140 I=1,NP
140     CT1(I)=CT(I)
              solving the linear equations: SJ*CT=CT1 by TDMA method
        CALL TDMA(ESJ, NP, CT)
        DO 200 I=1,NP
200     E(I)=CT(I)-CT1(I)
```

```
      ERROR1=0.0
      DO 220 I=1,NP
220   ERROR1=ERROR1+E(I)**2
      ERROR=DSQRT(ERROR1)
      IF(JK .GT. 100) THEN
      WRITE(6,*) 'JK > 100, PROGRAM STOPPED.'
      STOP
      ENDIF
      IF (ERROR .GT. 1.0D-6) GO TO 50
C     (N-R iteration not converged, back to the next iteration.)
C     Output the solution when N-R iteration converged.
      IF(T .GT. 60.0) THEN
      TIMESTEP=60.0
      ENDIF
      IF(T .GT. 600.0) THEN
      TIMESTEP=600.0
      ENDIF
      TT= MOD(T,TIMESTEP)
      IF( DABS(TT) .LT. 1.0D-4) THEN
      WRITE(6,5000)T/60,( CT( NO*(I-1)+1 ),I=1,11 ), T/60
      WRITE(*,5000)T/60,( CT( NO*(I-1)+1 ),I=1,11 ), T/60
      ELSE IF (DABS(TT-TIMESTEP) .LT. 1.0D-4) THEN
      WRITE(6,5000)T/60,( CT( NO*(I-1)+1 ),I=1,11 ), T/60
      WRITE(*,5000)T/60,( CT( NO*(I-1)+1 ),I=1,11 ), T/60
      ENDIF
C(7)  time control
      IF( (CT(NP)-CT(1)) .LT. 1.0D-3) GO TO 9999
      IF(T .LT. ENDTIME+1.0D-3) GO TO 30
C     (go to time forward)
9999  CONTINUE
      WRITE(6,5000)T/60,( CT( NO*(I-1)+1 ),I=1,11 ), T/60
      WRITE(*,5000)T/60,( CT( NO*(I-1)+1 ),I=1,11 ), T/60
5000  FORMAT(1X, F6.2, 11F6.3, 1X, F6.2)
      Cf=C0*( CT(NP) + CT(1) )/2
      WP=DENSITY*Vp
      NEP=2*NE
      qL=QM*Cf/( Cf+PK)
      q1=V*(C0-Cf)/WP
      q2=q1*NEP/(NEP-1)
      q3=( Vp/NEP/1000.0*C0 + QM*C0/( C0+PK)*WP/NEP  + q1*WP )/WP
      WRITE (6, 5100) Cf, qL, q1, q2, q3, q1/qL, q2/qL, q3/qL
5100  format(1x, 9F8.3)
C     pause '1'
      STOP
      END
```

```
      SUBROUTINE TFUNCT(GP, DX, PHI, PHIX)
      IMPLICIT REAL *8 (A-H, O-Z)
      DIMENSION  PHI(2), PHIX(2)
      PHI(1) = 1 - GP
      PHI(2) = GP
      PHIX(1) = -1.0/DX
      PHIX(2) =  1.0/DX
      RETURN
      END

      SUBROUTINE TDMA(A,N,X)
      IMPLICIT REAL *8 (A-H, O-Z)
      DIMENSION A(122,122),B(122,4),P(122),Q(122), X(122)
C     Subroutine for solving tridiangnal matrix equation.
C     A(N,N+1): extended matrix containing right hand  side vector.
C     B(N,4): Non-zero items in A(N,N+1); 2nd column:  diangnal line,
C     4nd column: right hand side, 1st column: under  dianganal line.
C     X(N): the solution vectors.
C     Mapping the non-zero items in matrix A to matrix B.
      DO 10 I=1, N
      DO 10 J=1, 4
      L=(I-2)+ J
      IF (J .EQ. 4)  L=N+1
      IF(I+L .LT. 1) L=1
10    B(I,J)=A(I,L)
      B(1,1)=0.0
      B(N,3)=0.0
C     Forward substitute
      P(1)= - B(1,3)/B(1,2)
      Q(1)=  B(1,4)/B(1,2)
      DO 20 I=2, N
      R= B(I,2) + B(I,1)*P(I-1)
      P(I)= -B(I,3)/R
20    Q(I)= ( B(I,4) - B(I,1)*Q(I-1) )/R
C     Back substitute
      X(N)=Q(N)
      DO 30 I= N-1, 1, -1
30    X(I)=P(I)*X(I+1) + Q(I)
      RETURN
      END
```

Appendix C. Program for Column Model

```
C            COLUMN.FOR            August, 1999
C
C     SIMULATION OF FIXED-BED COLUMN FOR URANIUM BIOSORPTION
C     PROCESS, BASED ON FILM AND (INTRAPARTICLE DIFFUSSION.
C      SOLVED BY ORTHOGONAL COLLOCATION METHOD
C
      IMPLICIT REAL*8 (A-H,O-Z)
      REAL INTERVAL
      DIMENSION ROOT(10),DIF1(10),DIF2(10), DIF3(10)
      DIMENSION VECT1(10),VECT2(10), D(10,10), D1(10,10), RD1(10,10)
C     DIMENSION U(10)
      COMMON/PAR/N,M,A(10,10),B(10,10),AR(10,10),BR(10,10),RD(10,10)
      COMMON/CON/ Y(100), TF, STEP
      COMMON/CON2/ U(10)
      COMMON/CON3/ V(10,10)
      COMMON/PAR4/FLAG
      COMMON/PAR2/ALFA,BETA,GAMA,EP,BI,CIN,QREF
      COMMON/PAR3/DKL, Qm, DL1, DL2
      COMMON/POUT/R, Dp
      OPEN(2,FILE='DATA.TXT')
      OPEN(3,FILE='OUT.TXT')
      OPEN(4,FILE='BREAKS.TXT')
      OPEN(6,FILE='BREAKS0.TXT')
      WRITE(3,499)
      WRITE(*,500)
      READ(*,*) TIME
      WRITE(*,501)
      READ(*,*) INTERVAL
      WRITE(3,502) TIME
      WRITE(3,503) INTERVAL
499   FORMAT(1X,2X,
     $ 'OUT.TXT:  OUTPUT OF COLUMN.FOR CORRESPONDING DATA.TXT',
     $ 3X,'NOV.7, 1994'/)
500   FORMAT(1X, 'INTEGRATING TIME  = ? Minutes')
501   FORMAT(1X, 'OUTPUT TIME INTERVAL = ? Minutes')
502   FORMAT(1X, 'INTEGRATING TIME       =', F9.5)
503   FORMAT(1X  'OUTPUT TIME INTERVAL =', F9.5,'  Minutes'/)
      READ(2,*) NC
      READ(2,*) MC
```

```
      N = NC + 1
      M = MC + 1
      NT = NC + 2
      MT = MC + 2
      AL = 1.0
      BET = 1.0
      READ(2,*) Cin
      READ(2,*) L
      READ(2,*) R
      READ(2,*) Dp
      READ(2,*) DKf
      READ(2,*) ROU
      READ(2,*) EP
      READ(2,*) DKL
      READ(2,*) Qm
      READ(2,*) Us
      READ(2,*) STEP
      READ(2,*) TOL
C     Calculate dimensionless parameters
      GAMA = L*Dp/(Us*R*R)
      Qref = Qm*Cin /(DKL + Cin)
      ALFA = ROU*Qref/Cin
C     BETA = (1-0.5)*GAMA*BI
      EBED = 0.5
      BETA = (1 - EBED)*L*DKf/(Us*R)
      BI = DKf*R/Dp
      DL1 = DKL / Cin
      DL2 = ROU * Qm / Cin
      WRITE(*,400) NC, MC, AL. BET, TOL
400   FORMAT(1X,
     $ 'NC  =', I4/1X,'MC  =',I4/1X, 'AL  =',F9.4/1X,'BET =',F9.4/1X,
     $ 'TOL =', E9.3/)
      WRITE(3,*) 'Cin = ', Cin
      WRITE(3,*) 'Us = ', Us
      WRITE(3,*) 'L = ', L
      WRITE(3,*) 'R = ', R
      WRITE(3,*) 'Dp = ', Dp
      WRITE(3,*) 'DKf = ',DKf
      WRITE(3,*) 'DL1 = ', DL1
      WRITE(3,*) 'DL2 = ', DL2
      WRITE(3,*) 'BETA = ', BETA
      WRITE(3,*) 'GAMA = ', GAMA
      WRITE(3,*) 'BI = ',  BI
C     CALCULATON OF AXIAL COLOCATION CONSTANTS
      CALL JACOBI(NC,1,1,AL,BET,DIF1,DIF2,DIF3,ROOT)
      WRITE(*,100) (ROOT(I), I=1,NT)
```

```
      WRITE(3,100) (ROOT(I), I=1,NT)
100   FORMAT(1X,'AXIAL COLLOCATION POINTS:'//1X,10F8.4/)
C     EVALUATION OF AXIAL MATRICES
      DO 1 I=1,NT
      CALL DFOPR(NC,1,1,I,1,DIF1,DIF2,DIF3,ROOT,VECT1)
      CALL DFOPR(NC,1,1,I,2,DIF1,DIF2,DIF3,ROOT,VECT2)
      DO 2 J=1,NT
      A(I,J)=VECT1(J)
      B(I,J)=VECT2(J)
2     CONTINUE
1     CONTINUE
C     CALCULATION OF RADIAL CONLOCATION POINTS
      CALL JACOBI(MC,1,1,AL,BET,DIF1,DIF2,DIF3,ROOT)
      WRITE(*,101) (ROOT(I), I=1,MT)
      WRITE(3,101) (ROOT(I), I=1,MT)
101    FORMAT(1X,'RADIAL COLLOCATION POINTS:'//1X,10F8.4//)
C     EVALUATION OF RADIAL MATRICES
      DO 3 I=1,MT
      CALL DFOPR(MC,1,1,I,1,DIF1,DIF2,DIF3,ROOT,VECT1)
      CALL DFOPR(MC,1,1,I,2,DIF1,DIF2,DIF3,ROOT,VECT2)
      DO 4 J=1,MT
      AR(I,J)=VECT1(J)
      BR(I,J)=VECT2(J)
4     CONTINUE
3     CONTINUE
C     CALCULATE MATRIX FOR U(I) CALCULATION  EQ(175)
      DENOM  = AR(MT,MT)+BI
      DENOM2 = AR(1,1)*DENOM - AR(MT,1)*AR(1,MT)
      DO 13 I=2,N
      DO 14 J=2,N
      D(I,J) = A(I,J) - A(I, NT)*A(NT,J)/A(NT,NT)
      IF( I .EQ. J ) THEN
      D(I,J) = D(I,J) + BETA * ( 1 - AR(1,1)*BI / DENOM2 )
      ENDIF
      D1(I-1, J-1) = D(I, J)
14     CONTINUE
13    CONTINUE
      WRITE(3,*) 'Matrix D1(i,j)'
      WRITE(*,*) 'Matrix D1(i,j)'
      DO 16 I=1,N
      WRITE(3,17) (D1(I,J), J=1, N)
16    WRITE(*,17) (D1(I,J), J=1, N)
17    FORMAT(1X,10F8.3,/)
C     Inverse of matrix D
      CALL REV(D1,N-1,RD1,DET)
      IF( DABS(DET) .LT. 1D-16 ) THEN
```

```
      WRITE(3, *) 'Inverse failed! EXIT'
      WRITE(*, *) 'Inverse failed! EXIT'
      STOP
      ENDIF
      DO 18 I = 2, N
      DO 18 J = 2, N
18    RD(I, J) = RD1(I-1, J-1)
C     print THE MATRICES
      CALL MAT
C     INITIAL VALUE FOR THE DEPENDENT VARIALES
      DO 5 I=1,NT
      U(I) = 0.0
      DO 5 J=1,MT
      V(I,J)=0.0
5     CONTINUE
C      Initial value from (172)
      DO 6 I = 1, NT
      DO 6 L = 2, M
      IL = L-1 + (I-1) * (M-1)
      Y(IL) = V(I, L)
6     CONTINUE
      NROV = (M-1) * NT
      TF=0.0
      IN=TIME/STEP
C     print initial value
      call out
      ICON = 1
      FLAG = 0
      CALL ODE(NROV,TB,TF,Y,TOL)
      CALL GETU(Y,U)
      FLAG = 1
C     MASTER LOOP
      DO 10 II = 1, IN
      TB = TF
      TF = TB + STEP
      CALL ODE(NROV,TB,TF,Y,TOL)
      CALL GETU(Y, U)
      IF( ICON .GE. INTERVAL ) THEN
      CALL OUT
      ICON = 1
      ELSE
      ICON = ICON + 1
      ENDIF
10    CONTINUE
C     forward a time step
      STOP
```

```
      END

      SUBROUTINE OUT
      IMPLICIT REAL*8 (A-H,O-Z)
      COMMON/PAR/N,M,A(10,10),B(10,10),AR(10,10),BR(10,10),RD(10,10)
      COMMON/CON/ Y(100), TF, STEP
      COMMON/CON2/ U(10)
      COMMON/CON3/ V(10,10)
      COMMON/POUT/R, Dp
      COMMON/PAR2/ALFA,BETA,GAMA,EP,BI,CIN,QREF
      WRITE(*,85)
      WRITE(3,85)
85    FORMAT( 79('-') )
      WRITE(*,102) TF
      WRITE(3,102) TF
      WRITE(*,*) 'INTRAPARTICLE CONCENTRATION:'
      WRITE(3,*) 'INTRAPARTICLE CONCENTRATION:'
      DO 22 I = 1, N+1
      WRITE(*,105) (V(I,J),J=1,M+1),U(I)
      WRITE(3,105) (V(I,J),J=1,M+1),U(I)
C     WRITE(*,*) ( Y(J+(I-1)*M ), J=1,M), V(I, M), U(I)
C     WRITE(3,*) ( Y(J+(I-1)*M ), J=1,M), V(I, M), U(I)
22    CONTINUE
      WRITE(6,106) TF*R*R/Dp/3600, U(N+1)*Cin
      IF( U(N+1) .gt. 1 ) then
      U(N+1) = 1
      ENDIF
      WRITE(4,106) TF*R*R/Dp/3600, U(N+1)*Cin
102   FORMAT(/1X 'INTEGRATED TIME  TF = ',F10.4,'  Minutes')
105   FORMAT(11F7.4/)
106   FORMAT(2F10.4)
      RETURN
      END

      SUBROUTINE MAT
      IMPLICIT REAL*8 (A-H,O-Z)
      COMMON/PAR/N,M,A(10,10),B(10,10),AR(10,10),BR(10,10),RD(10, 10)
      WRITE(3,*) 'MATRIX A'
      WRITE(*,*) 'MATRIX A'
      DO 2000 I=1,N+1
      WRITE(3,2001) (A(I,J), J=1,N+1)
2000  WRITE(*,2001) (A(I,J), J=1,N+1)
C     WRITE(3,*) 'MATRIX B'
C     WRITE(*,*) 'MATRIX B'
C     DO 2100 I=1,N+1
C     WRITE(3,2001) (B(I,J), J=1,N+1)
```

```
      WRITE(3,*) 'MATRIX AR '
      WRITE(*,*) 'MATRIX AR '
      DO 2200 I=1,M+1
      WRITE(3,2002) (AR(I,J), J=1,M+1)
2200  WRITE(*,2002) (AR(I,J), J=1,M+1)
      WRITE(3, *) 'MATRIX BR'
      WRITE(*, *) 'MATRIX BR'
      DO 2300 I=1,M+1
      WRITE(3,2002) (BR(I,J), J=1,M+1)
2300  WRITE(*,2002) (BR(I,J), J=1,M+1)
      WRITE(3,*) 'MATRIX RD'
      WRITE(*,*) 'MATRIX RD'
      DO 2400 I=1,N+1
      WRITE(3,2003) (RD(I,J), J=1,N)
2400  WRITE(*,2003) (RD(I,J), J=1,N)
2001  FORMAT(1X,10F8.3,/)
2002  FORMAT(1X,10F8.3,/)
2003  FORMAT(1X,10F8.3,/)
      RETURN
      END

      SUBROUTINE JACOBI(N,N0,N1,AL,BE,DIF1,DIF2,DIF3,ROOT)
      IMPLICIT REAL*8 (A-H,O-Z)
      DIMENSION ROOT(10),DIF1(10),DIF2(10), DIF3(10)  .
      AB=AL+BE
      AD=BE-AL
      AP=BE*AL
      DIF1(1)=(AD/(AB+2.)+1.)/2.
      DIF2(1)=0.
      IF(N.LT.2) GO TO 15
      DO 10 I=2,N
      Z1=I-1
      Z=AB+2.*Z1
      DIF1(I)=(AB*AD/Z/(Z+2.)+1.)/2.
      IF(I.NE.2) GO TO 11
      DIF2(I)=(AB+AP+Z1)/Z/Z/(Z+1.)
      GO TO 10
11    Z=Z*Z
      Y=Z1*(AB+Z1)
      Y=Y*(AP+Y)
      DIF2(I)=Y/Z/(Z-1.)
10    CONTINUE
15    X=0.
      DO 20 I=1,N
25    XD=0.
      XN=1.
```

```
      XD1=0.
      XN1=0.
      DO 30 J=1,N
      XP=(DIF1(J)-X)*XN-DIF2(J)*XD
      XP1=(DIF1(J)-X)*XN1-DIF2(J)*XD1-XN
      XD=XN
      XD1=XN1
      XN=XP
30    XN1=XP1
      ZC=1.
      Z=XN/XN1
      IF(I.EQ.1) GO TO 21
      DO 22 J=2,I
22    ZC= ZC-Z/(X-ROOT(J-1))
21    Z=Z/ZC
      X=X-Z
      IF(DABS(Z).GT.1.D-9) GO TO 25
      ROOT(I)=X
      X=X+0.0001
20    CONTINUE
      NT=N+N0+N1
      IF(N0.EQ.0) GO TO 35
      DO 31 I=1,N
      J=N+1-I
31    ROOT(J+1)=ROOT(J)
      ROOT(1)=0.
35    IF(N1.EQ.1) ROOT(NT)=1.
      DO 40 I=1,NT
      X=ROOT(I)
      DIF1(I)=1.
      DIF2(I)=0.
      DIF3(I)=0.
      DO 40 J=1,NT
      IF(J.EQ.I) GO TO 40
      Y=X-ROOT(J)
      DIF3(I)=Y*DIF3(I)+3.*DIF2(I)
      DIF2(I)=Y*DIF2(I)+2.*DIF1(I)
      DIF1(I)=Y*DIF1(I)
40    CONTINUE
      RETURN
      END

      SUBROUTINE DFOPR(N,N0,N1,I,ID,DIF1,DIF2,DIF3,ROOT,VECT)
      IMPLICIT REAL*8 (A-H,O-Z)
      DIMENSION ROOT(10),DIF1(10),DIF2(10), DIF3(10),VECT(10)
      NT=N0+N1+N
```

```
      IF(ID.EQ.3) GO TO 10
      DO 20 J=1,NT
      IF(J.NE.I) GO TO 21
      IF(ID.NE.1) GO TO 5
      VECT(I)=DIF2(I)/DIF1(I)/2.
      GO TO 20
5     VECT(I)=DIF3(I)/DIF1(I)/3
      GO TO 20
21    Y=ROOT(I)-ROOT(J)
      VECT(J)=DIF1(I)/DIF1(J)/Y
      IF(ID.EQ.2) VECT(J)=VECT(J)*(DIF2(I)/DIF1(I)-2./Y)
20    CONTINUE
      GO TO 50
10    Y=0.0
      DO 25 J=1,NT
      X=ROOT(J)
      AX=X*(1.-X)
      IF(N0.EQ.0) AX=AX/X/X
      IF(N1.EQ.0) AX=AX/(1.-X)/(1.-X)
      VECT(J)=AX/DIF1(J)**2
25    Y=Y+VECT(J)
      DO 60 J=1,NT
60    VECT(J)=VECT(J)/Y
50    RETURN
      END

      SUBROUTINE ODE(N,XB,XE,Y,EPS)
      IMPLICIT REAL*8 (A-H,O-Z)
      DIMENSION Y1(100),Y2(100),Y3(100),Y(100)
      X=XB
      H=(XE-X)/10.
C     ADOPTED FROM ALGORITHM 8 C ACM (1960) VOL.3 P.312
C     BY J.VOTRUBA  INST.MICROBIOL. PRAGUE CZECHOSLOVAKIA
      IS=0
      IOUT=0
100   IF((X+2.01*H-XE).LT.0.) GO TO 1
      IOUT=1
      H=(XE-X)/2.
1     CALL RK4(N,X,Y,2.*H,X1,Y1)
101   CALL RK4(N,X,Y,H,X2,Y2)
      CALL RK4(N,X2,Y2,H,X3,Y3)
      ERR=0.0
      DO 2 K=1,N
      Q1=DMAX1(1.D-6,DABS(Y3(K)))
      P=DABS(Y1(K)-Y3(K))/Q1
2     ERR=DMAX1(P,ERR)
```

```
      IF(ERR.GT.EPS) GO TO 103
      X=X3
      IF(IOUT.EQ.1) GO TO 104
      DO 3 K=1,N
3     Y(K)=Y3(K)
      IF(IS.LT.5) GO TO 4
      H=2.*H
      IS=0
4      IS=IS+1
      GO TO 100
103   H=0.5*H
      IOUT=0
      X1=X2
      DO 5 K=1,N
5     Y1(K)=Y2(K)
      GO TO 101
104   DO 6 K=1,N
6     Y(K)=Y3(K)
      RETURN
      END

      SUBROUTINE RK4(N,X,Y,H,XE,YE)
      IMPLICIT REAL*8 (A-H,O-Z)
      DIMENSION Y(100),YE(100),Z(100),W(100),A(5)
      DATA A /0.5,0.5,1.0,1.0,0.5/
      XE=X
      DO 1 K=1,N
      YE(K)=Y(K)
1     W(K)=Y(K)
      DO 2 J=1,4
      CALL RHS(W,Z)
      XE=A(J)*H+X
      DO 3 K=1,N
      W(K)=Y(K)+A(J)*H*Z(K)
3     YE(K)=YE(K)+A(J+1)*H*Z(K)/3.
2     CONTINUE
      RETURN
      END

      SUBROUTINE REV(A,N,RA,DETA)
      IMPLICIT REAL *8 (A-H, O-Z)
      DIMENSION  A(10,10),  RA(10,10)
C     A(N,N)=IMPUT MATRIX;  RA(N,N)= REVERSE OF A(N,N)
      DETA=1.0
      DO 10 K=1, N
      IF (A(K,K)) 20, 30, 20
```

```
30    DETA=0.0
      RETURN
20    DETA=DETA*A(K,K)
      DO 40 J=1,N
      IF(J-K) 50, 40, 50
50    A(K,J)=A(K,J)/A(K,K)
40    CONTINUE
      A(K,K)=1.0/A(K,K)
      DO 10 I=1, N
      IF (I-K) 60, 10, 60
60    DO 70 J=1, N
      IF (J-K) 80,70,80
80    A(I,J)=A(I,J)-A(I,K)*A(K,J)
70    CONTINUE
      A(I,K)= -A(I,K)*A(K,K)
10    CONTINUE
      DO 100 I=1,N
      DO 100 J=1,N
100   RA(I,J)=A(I,J)
      RETURN
      END

      SUBROUTINE RHS(Y,F)
      IMPLICIT REAL*8 (A-H,O-Z)
      DIMENSION F(100), Y(100), U(10)
      COMMON/PAR/N,M,A(10,10),B(10,10),AR(10,10),BR(10,10),RD(10,10)
      COMMON/CON3/ V(10,10)
      COMMON/PAR2/ALFA,BETA,GAMA,EP,BI,CIN,QREF
      COMMON/PAR3/DKL, Qm, DL1, DL2
      COMMON/PAR4/FLAG
C     CONSTRUCTION OF INTEGRATED FUNCTION
      MT = M + 1
      NT = N + 1
C     Initial value from (172)
      DO 50 I = 1, NT
      DO 50 L = 2, M
      IL = L-1 + (I-1) * (M-1)
      V(I, L) = Y(IL)
50    CONTINUE
      IF( FLAG .EQ. 0 ) THEN
      DO 55 I = 1, NT
55    U(I) = 0
      U(1) = 1
      FLAG = 1
      ELSE
      CALL GETU(Y,U)
```

```
      ENDIF
      DENOM  = AR(MT,MT)+BI
      DENOM2 = AR(1,1)*DENOM - AR(MT,1)*AR(1,MT)
      DO 60 I = 1, NT
      SUM = 0.0
      DO 61 K = 2, M
61    SUM = SUM + ( AR(1,MT)*AR(MT,K) - DENOM*AR(1,K) ) * V(I,K)
60    V(I,1) = - AR(1,MT)*BI/DENOM2*U(I) + SUM/DENOM2
      DO 70 I = 1, NT
      SUM = 0.0
      DO 71 K = 2, M
71    SUM = SUM + ( AR(1,1)*AR(MT,K) - AR(MT,1)*AR(1,K) ) * V(I,K)
70    V(I,MT) = AR(1,1)*BI/DENOM2*U(I) - SUM/DENOM2
      DO 900 I = 1, NT
      DO 900 L = 2, M
      IL = L-1 + (I-1) * (M-1)
      FNAMDA = EP + DL1*DL2 /( DL1 + V(I,L) )/( DL1 + V(I,L) )
      SUM = 0.0
      DO 901 K = 2, M
901   SUM = SUM + BR(L,K) * V(I,K)
      F(IL) = ( SUM + BR(L,1)*V(I,1) + BR(L,MT)*V(I,MT) )/FNAMDA
900   CONTINUE
       RETURN
      END

      SUBROUTINE GETU(Y, U)
      IMPLICIT REAL*8 (A-H,O-Z)
      DIMENSION Y(100), E(10), U(10)
      COMMON/PAR/N,M,A(10,10),B(10,10),AR(10,10),BR(10,10),RD(10,10)
C      COMMON/CON2/ U(10)
      COMMON/CON3/ V(10,10)
      COMMON/PAR2/ALFA,BETA,GAMA,EP,BI,CIN,QREF
      COMMON/PAR3/DKL, Qm, DL1, DL2
C     CONSTRUCTION OF INTEGRATED FUNCTION
      MT = M + 1
      NT = N + 1
      DO 11 I = 1, NT
      DO 11 L = 2, M
      IL = L-1 + (I-1) * (M-1)
      V(I, L) = Y(IL)
11    CONTINUE
C     Calculate U(I)  FROM EQ(176)
      DENOM  = AR(MT,MT)+BI
      DENOM2 = AR(1,1)*DENOM - AR(MT,1)*AR(1,MT)
      DO 500 I = 2, N
      SUM  = 0.0
```

```
      DO 501 K =2, M
501   SUM = SUM + ( AR(1,1)*AR(MT,K)-AR(MT,1)*AR(1,K) ) * V(I,K)
      E(I) = -A(I,1) + A(I,NT)*A(NT,1)/A(NT,NT) - BETA/DENOM2 * SUM
500   CONTINUE
      DO 600 I = 2, N
       U(I) = 0.0
       DO 601 J = 2, N
601   U(I) = U(I) + RD(I,J) * E(J)
600    CONTINUE
      U(1) = 1
      SUM2 = 0
      DO 602 J = 2, N
602   SUM2 = SUM2 + A(NT,J)/A(NT, NT) * U(J)
      U(NT) = -A(NT,1)/A(NT,NT) - SUM2
      RETURN
END
```